FOREST BIOMETRIC CHARACTERIZATION THROUGH REMOTE SENSING APPLICATIONS

DIOGO NEPOMUCENO COSENZA

SCIENTIFIC ADVISORS:

Doutora Maria Margarida Branco de Brito Tavares Tomé, Professora Catedrática do Instituto Superior de Agronomia da Universidade de Lisboa;

Doutora Ana Paula Soares Marques de Carvalho, Professora Auxiliar do Instituto Superior de Agronomia da Universidade de Lisboa

THESIS PRESENTED TO OBTAIN THE DOCTOR DEGREE IN
FORESTRY ENGINEERING AND NATURAL RESOURCES

2021

FOREST BIOMETRIC CHARACTERIZATION THROUGH REMOTE SENSING APPLICATIONS

DIOGO NEPOMUCENO COSENZA

SCIENTIFIC ADVISORS:

Doutora Maria Margarida Branco de Brito Tavares Tomé, Professora Catedrática do Instituto Superior de Agronomia da Universidade de Lisboa;

Doutora Ana Paula Soares Marques de Carvalho, Professora Auxiliar do Instituto Superior de Agronomia da Universidade de Lisboa

THESIS PRESENTED TO OBTAIN THE DOCTOR DEGREE IN FORESTRY ENGINEERING AND NATURAL RESOURCES

Jury:

President: Doutora Manuela Rodrigues Branco Simões, Professora Associada com Agregação do Instituto Superior de Agronomia da Universidade de Lisboa.

Members: Doutor Felipe Bravo Oviedo, Catedrático de Universidad, UVA - Instituto Universitario de Investigación en Gestión Forestal Sostenible, Universidad de Valladolid, Espanha;

Doutora Maria Margarida Branco de Brito Tavares Tomé, Professora Catedrática do Instituto Superior de Agronomia da Universidade de Lisboa;

Doutor José Miguel Oliveira Cardoso Pereira, Professor Catedrático do Instituto Superior de Agronomia da Universidade de Lisboa;

Doutor Domingos Manuel Mendes Lopes, Professor Auxiliar com Agregação da Escola de Ciências Agrárias e Veterinárias da Universidade de Trás-os-Montes e Alto Douro;

Doutor Gil Rito Gonçalves, Professor Auxiliar da Faculdade de Ciências e Tecnologia da Universidade de Coimbra.

2021

À minha incrível família.

To my amazing family

ACKNOWLEDGMENTS

ABSTRACT

The general objective of this thesis was to step forward in the application of aerial 3D-data in the forest characterization context. To meet this goal, the thesis focused on four cutting-edge research topics related to the forestry applications of 3D data collected by airborne laser scanning (ALS) and digital aerial photogrammetry (DAP).

Four common algorithms were deeply investigated to filter ALS ground points. The results showed that performing exhaustive filter calibration is not mandatory to derive accurate digital terrain models (DTM), that the applications of software defaults can derive accurate DTM as well, and that filter calibration has a significant but low practical improvement on the prediction of forest attributes using area-based approach (ABA).

The application of the high-flexible Johnson's S_B probability density function (PDF) was adapted to the ALS data and compared with the Weibull PDF to estimate diameter distributions in two forest stands, an eucalyptus stand and a radiate pine stand. Johnsons S_B was highly sensitive to the prediction of the inputs used to fit the parameters, reasons why this function was just slightly better than Weibull.

The ALS data from five different forest sites were used to compare three common modeling approaches used to estimate growing stock volume, ordinary least squares (OLS), random forest (RF), and k-nearest neighbor (kNN). The estimation was more accurate with OLS and RF. The kNN-based models had the worst prediction accuracy and may result in overfitting.

The point clouds derived from ALS and DAP presented comparable results when it comes to detect and estimate individual tree volumes in eucalyptus plantations. This result benefits the DAP since it is an inexpensive approach to collect 3D forest data, especially when associated with unmanned aerial vehicles.

Keywords: lidar, point cloud, forest modelling, forest inventory; remote sensing

RESUMO

A tese teve como objetivo geral explorar e analisar a aplicação das nuvens de pontos provenientes de varredura a laser aerotransportado (VLA) e aerofotogrametria digital (AFD) para modelação de atributos florestais. Quatro trabalhos foram então conduzidos com especial atenção ao método VLA dada a sua importância global.

O primeiro trabalho analisou quatro algoritmos populares para filtrar pontos de terreno de dados do VLA. Estes foram calibrados e os efeitos foram observados na qualidade dos modelos digitais de terreno (MDT) e nas estimativas de volume e altura dominante através do método baseado em área (ABA). A calibração dos algoritmos melhorou a qualidade do MDT e das estimativas florestais, mas bons resultados são também obtidos usando os algoritmos com sua parametrização padrão.

O segundo trabalho testou o modelo S_B de Johnson em comparação ao Weibull para simular distribuição diamétrica em plantios homogêneos utilizando VLA e ABA. O modelo S_B se mostrou ligeiramente melhor que o modelo Weibull para simular distribuição diamétricas. Tal resultado se justifica pela alta sensibilidade do modelo S_B aos erros de estimativa dos parâmetros usados no seu ajustamento.

O terceiro trabalho comparou três técnicas de modelação: k-vizinhos mais próximos (kVMP), floresta aleatória (FA) e regressão por mínimos quadrados ordinários (MQO). A técnica kVMP é menos eficiente que as demais, sendo mais propensa ao superajustamento. Já os modelos baseados em MQO e FA tiveram resultados semelhantes.

O quarto e último trabalho comparou as técnicas VLA e AFD na estimativa de atributos de árvores individuais. Ambas as tecnologias apresentaram resultados semelhantes tanto para a deteção das árvores quanto nas estimativas de seus atributos. Este facto é vantajoso para a AFD por se tratar de uma técnica mais acessível que a VLA, especialmente quando associada a veículos aéreos não tripulados.

Palavras chave: nuvem de pontos; lidar; modelação florestal; inventário florestal; deteção remota

RESUMO EXTENDIDO

Os métodos tradicionais de inventário florestal vêm sendo substituídos aos poucos pelas técnicas de deteção remota baseadas em nuvem de pontos, nomeadamente a varredura a laser aerotransportada (VLA) e a aerofotogrametria digital (AFD). Tais tecnologias se tornaram populares pela capacidade de recolher dados tridimensionais de alta precisão e por permitir examinar áreas extensas com eficiência. Entretanto, a implementação dessas tecnologias é onerosa e complexa, pois requerem equipamentos sofisticados. Além disso elas demandarem ajustes do fluxo de processamento dos dados para as diferentes situações. Nas últimas décadas, diversas pesquisas foram desenvolvidas para avaliar e desenvolver metodologias de modelação florestal baseadas em nuvem de pontos, porém ainda há muitas lacunas científicas a serem investigadas.

Portanto, esta tese teve como objetivo geral explorar e analisar a aplicação das nuvens de pontos provenientes de VLA e AFD para modelação de atributos florestais. Especial atenção foi dada à técnica VLA devido a sua maior relevância no cenário mundial. Nesse sentido, quatro linhas de investigação foram traçadas: *i*) calibrar algoritmos para filtrar pontos do terreno provenientes de VLA e avaliar seus impactos na qualidade dos modelos digitais de terreno (MDT) e na estimativa de atributos florestais através da abordagem baseada em área (ABA); *ii*) avaliar a função de densidade de probabilidade (FDP) S_B de Johnson para simular a distribuição diamétrica de povoamentos florestais; *iii*) comparar eficiência da modelação do estoque de emadeira via ABA utilizando três técnicas de aprendizagem automática, nomeadamente, k-vizinhos mais próximos (kVMP), floresta aleatória (FA) e regressão por mínimos quadrados ordinários (MQO); *iv*) comparar as técnicas VLA e AFD na estimativa de atributos de árvores individuais.

No primeiro trabalho foram estudados quatro algoritmos popularmente utilizados para filtrar dados de terreno, sendo eles a rede irregular de triângulos progressiva (RITP), interpolação linear por mínimos quadrados ponderados (ILMQP), classificação de curvatura por múltiplas escalas (CME) e o filtro morfológico progressivo (FMP). Os filtros calibrados foram comparados com a parametrização padrão. Foram utilizados milhares de pontos recolhidos com GPS de alta precisão para aferir a qualidade dos MDTs produzidos. Além disso, dados provenientes de um povoamento de eucalipto foram utilizados para analisar o impacto da calibração dos algoritmos de filtragem na estimativa do estoque de madeira e da altura dominante via ABA. Como conclusão, foi demonstrado que *i*) a calibração dos filtros melhora a qualidade do MDT, embora bons resultados também podem ser produzidos usando a parametrização padrão; *ii*) a calibração dos algoritmos ILMQP, CME e FMP possibilita obter melhores estimativas dos atributos florestais, enquanto que a calibração do RITP não resultou em melhorias significativas.

No segundo trabalho a FDP S_B de Johnson foi adaptada pela primeira vez na literatura para estimar distribuição diamétrica de povoamentos florestais utilizando dados derivados de VLA. Foram testadas diferentes técnicas de ajustamento dos parâmetros da FDP aos dados de povoamentos de eucalipto e de pinheiro bravo localizados na Península Ibérica. A FDP Weibull de dois parâmetros

foi utilizada para efeito de comparação. Apesar de altamente flexível, a FDP S$_B$ de Johnson mostrou ser de difícil ajustamento devido à alta sensibilidade aos erros de estimativa do atributes florestais. Uma vez que o ajustamento da FDP requer diferentes equações (de 3 a 5), os erros acumulados por elas podem gerar fortes alterações na forma da distribuição. Entretanto, a FDP S$_B$ de Johnson teve eficiência semelhante ou melhor que a da Weibull, de modo que a sua aplicação pode ser vista como promissora para simulação de distribuição diamétrica de povoamentos florestais.

No terceiro trabalho, três técnicas de modelação (MQO, kVMP e FA) foram comparadas entre si sendo aplicadas com diferentes esquemas de seleção de variáveis preditoras para a estimativa do volume do povoamento via ABA. Todos as três técnicas foram testadas utilizando cinco variáveis preditoras, as quais foram selecionadas por meio de metaheurísticas. Outro método de seleção de variáveis foi também aplicado ao MQO; neste caso foi aplicada uma busca exaustiva para selecionar três melhores variáveis preditoras. Como alternativa à seleção de variáveis, a técnica FA foi também aplicada utilizando todas as variáveis disponíveis. Os dados utilizados nessa análise envolveram florestas localizadas na América do Sul e do Norte, e três florestas boreais do norte da Europa. Os modelos foram comparados através de validação cruzada. Adicionalmente, os modelos foram validados com dados independentes em duas áreas de florestas boreais. Os resultados demonstraram que a técnica kVMP é menos eficiente que as demais, sendo mais propensa ao superajustamento. Já os modelos baseados em MQO e FA tiveram resultados semelhantes. As técnicas de seleção empregadas para o MQO não apresentaram diferenças significativas. Já a seleção de variáveis para FA não oferece muitos benefícios e, portanto, tal modelo deve ser empregada com todas as variáveis disponíveis.

O último trabalho comparou as tecnologias VLA e AFD na obtenção de dados de árvores individuais em plantações puras e equiâneas de eucalipto. O filtro de máximo local foi aplicado na deteção das copas sendo em seguida extraídas as alturas das árvores para estimação dos diâmetros e seus volumes individuais. Ambas as tecnologias apresentaram resultados semelhantes tanto para a deteção das árvores quanto nas estimativas de seus atributos. Este facto é vantajoso para a AFD por se tratar de uma técnica mais acessível que a VLA, especialmente quando associada a veículos aéreos não tripulados. Além disso, ambas as abordagens são promissoras para futuras aplicações em plantios eucalipto equiâneo.

Todas as conclusões descritas acima compreendem avanços significativos no emprego de deteção remota para caracterização de povoamentos florestais. Após 50 anos de esforços da comunidade científica a VLA se tornou uma tecnologia madura e se transformou numa alternativa confiável para obtenção de dados florestais. Além das informações contidas nesta tese há ainda uma vasta coleção de metodologias que podem ser empregadas para o melhor aproveitamento desta técnica, razão pela qual ela já está a ser aplicada por companhias públicas e privadas em diversos países. Já a tecnologia FAD é mais recente e estar a ganhar espaço no panorama científico mundial dado ao seu baixo custo de implementação.

Entretanto a carência de profissionais especializados para lidar com estes dados e os custos operacionais (especialmente do VLA) ainda são fatores que dificultam a difusão destas tecnologias. Neste caso, mesmo com um número crescente de adeptos pelo mundo, há ainda a oportunidade para o desenvolvimento de novas tecnologias mais acessíveis e aplicações mais amigáveis para

atrair usuários iniciantes. Além disso, há ainda muitas dúvidas relacionadas ao VLA e AFD que necessitam esclarecimento, especialmente aquelas que interferem nos custos dos inventários.

Por fim, o desenvolvimento das metodologias de medição florestal é imperativo para permitir diagnosticar as florestas e definir diretrizes de gestão. Longe de ser um fim em si mesmo, a ciência do inventário conjuntamente com a deteção remota objetiva oferecer informações de qualidade para o planeamento florestal, portanto cada contribuição científica anunciada significa um passo adiante em direção à sustentabilidade.

Palavras chave: nuvem de pontos; lidar; modelação florestal; inventário florestal; deteção remota

CONTENT

1   General Introduction

The pressure for improving forestry practices in private and public forest management has been increasing in the last decades due to the socio-environmental concerns and the high demand for quality in the production process. This paradigm has pushed practitioners worldwide to seek novel approaches able to provide more detailed information of the forest stands and better control the production. As consequence, there were an increasing development of remote sensing techniques to collect aerial three-dimensional (3D) data from forest, with light detection and ranging (LiDAR) technology receiving special attention.

Differently from the traditional forest inventory, LiDAR surveys allow predicting forest attributes at pixel- or tree-level so it is possible to generate high-quality maps of the predictions (Reutebuch et al. 2005). These characteristics are crucial in the context of precision forestry as they allow optimizing practices according to the spatial distribution of the forest attributes (Holopainen et al. 2014; Dash et al. 2016). When adapted to aerial platforms, called then as airborne laser scanning (ALS), a large forest area can be quickly scanned so the inventories become more efficient and less laborious (Vauhkonen et al. 2014). Furthermore, ALS allows deriving high-detailed digital terrain models (DTM) which are extremely valuable for topography studies and forest operation planning (Hollaus 2015). For these reasons, LiDAR application using ALS has conquered a notorious space in remote sensing and forest science.

However, the application of LiDAR in forestry is not straightforward. In the case of the ALS, the flight must be carefully planned considering the properties of the platform, the LiDAR system, the characteristics of the target area, and the goals of the survey (Goodwin et al. 2006; Wulder et al. 2008). The produced point cloud must be pre-processed to derive the desired dataset. For topography studies, the main product of the survey is the DTM since all desired information is derived directly from it. Thus, the ground points must be filtered from the point cloud and interpolated to derive the DTM (Liu 2008; Chen et al. 2017). In the forest assessments, the DTM is used to normalize point clouds by scaling point heights to ground level so the above-ground points can be processed. The survey must also be followed by a forest inventory, which will provide data to build the regression models (Lefsky et al. 2002). The user must choose an approach to estimate the forest attributes. The plot-level estimation through the area-based approach (ABA) (see Næsset 2002, 2004) is the most used, but the tree-level estimation using individual tree detection (ITD) (see Lindberg and Holmgren 2017) is also common. Therefore, working with LiDAR is a multidisciplinary task that demands knowledge related to remote sensing, geoprocessing, data analysis, and forestry.

Many researchers concentrated their efforts on the development of LiDAR techniques for different situations, where each work gives special attention to one of the above-mentioned processes of the LiDAR workflow. Considering the forestry context, forest characterization is a general goal and different approaches have been tested to improve the predictions of forest attributes or to better understand the factors involved in the modeling. The forest growing stock is the most modeled attribute in the related literature, but others are also approached such as those related to tree height and diameter. The prediction of growing stock volume and biomass have direct implication in forest management as they allow assessing current production and carbon storage (McRoberts et

al. 2013). The tree-height-based attributes such as dominant height are important to assess the quality of forest sites (Tesfamichael et al. 2010; Nord-Larsen and Riis-Nielsen 2010). The tree diameter attributes such as basal area or quadratic mean diameter are also useful to assess forest stands, whereas the prediction of the diameter distribution is important to study the horizontal structure of the forest (Maltamo and Gobakken 2014).

Another 3D-scanning technique that has been gaining space among practitioners is digital aerial photogrammetry (DAP). While LiDAR system is based on laser beams emission and backscattering (Wehr and Lohr 1999), DAP uses passive sensors to collect high-detailed photographs of the area so they can be matched to produce multispectral point cloud (Baltsavias 1999; Iglhaut et al. 2019). This technique has also been increasingly applied in the last decade due to its low costs involved and the popularization of unmanned aerial vehicles (UAV) (Nex and Remondino 2014; Colomina and Molina 2014; Guimarães et al. 2020). The workflow to process DAP point clouds is similar to one of ALS and their results are also promising (Goodbody et al. 2019).

In summary, 3D scanning is a cutting-edge technology that is changing the way to perform forest inventory worldwide. However, even with the increasing number of published works, its application is not thoroughly understood given the complexity involved in its workflows and the different forest ecosystems.

1.1 Objectives of the thesis

This thesis aimed to analyze the application of aerial 3D data in the forest characterization context by expanding its use and understandings to better support forest inventory. The focus was given to the ALS approach for its greater relevance in the global scenario.

Following this general goal, four research lines were proposed to explore the use of 3D data in different respects:

i) To analyze the impact of calibrating ground point filtering algorithms on the DTM accuracy and ABA-based estimation.

ii) To test the high-flexible probability density function Johnson's S_B to simulate diameter distributions of homogeneous forest plantations.

iii) To benchmark three popular modeling techniques, namely, ordinary least square, k-nearest neighbor, and random forest for predicting growing stock volume using ABA.

iv) Benchmark ALS and DAP point clouds for estimating three individual attributes through ITD.

The following sections of this chapter bring a brief historical contextualization of aerial 3D scanning in forestry and the state of the art related to each research topic. The researches are then presented in the following chapters by their respective published papers, where each one has its specific literature review, discussion, and conclusions. Finally, the general conclusions of this thesis are given so as the final considerations and future perspectives.

1.2 State of the art

1.2.1 Historical contextualization

The comprehensive review of Nelson (2013) pointed out that the firsts forest-oriented studies with airborne laser scanning (ALS) were developed in the late 1970s in Russia (part of the Soviet Union at the time) and early 1980s in North America. The available technology imposed strong limitations in this period, and the works approached the vertical measurements or density of the forest content using laser perfilograms (e.g., Aldred and Bonnor 1985). In the late 1980s, the studies related to photogrammetry inspired researchers to extend the estimations to stand-level attributes, such as growing stock volume and biomass, achieving promising results (Maclean and Krabill 1986; Nelson et al. 1988). Then, with the technological advances, the approaches continued expanding in the 1990s and more possibilities were opened to ALS (Dubayah and Drake 2000; Lefsky et al. 2002; Lim et al. 2003). Given the success of the pioneer works, the popularity of the ALS spread worldwide in the 2000s and upwards inviting more researchers to explore it in the different fields of the forest science so that it is now a consolidated approach to provide high-quality data for companies and governments (Hudak et al. 2009; Wulder et al. 2012; Eitel et al. 2016)

The increasing number of related works from the 2000s was pushed especially by the technological advances in the scanning systems and computers, which allowed users to obtain more accurate point clouds, reduce the cost of the flights, and process data with less difficulty. Additionally, software oriented to manipulate ALS-data for forest applications became available, so the users did not need to build their own codes to deal with the point clouds, letting the processing workflow more practical and attractive for beginners. Such evolution brought to the present the futuristic concepts of remote-sensing experts from the '70-'90s, and nowadays the ALS technique achieved such degree of reliability that can be used as a data source for nationwide forest surveys (Næsset 2014; Kotivuori et al. 2016; Nilsson et al. 2017).

The first application of point clouds derived by digital aerial photogrammetry (DAP) on forestry, on the other hand, dated from the beginning of the 2010s and had an abrupt increasing number of published works in the second half of the decade (Iglhaut et al. 2019). The technique of combining multiple images follows a principle similar to the traditional stereoscopy, where overlapped images are reproduced in three dimensions (3D). A sequence of images is used in DAP to reconstruct 3D objects through a computational technique called structure from motion (SfM) where a multi-view stereo algorithm is used to match the images and produce the point clouds (Eltner et al. 2016). The great advantage of the SfM is that the images can be taken using simple digital cameras from different orientations, which allows practitioners to implement it in relatively simple platforms such as recreative unmanned aerial vehicles (UAV) (Eltner et al. 2016).

Because it is passive sensing, DAP is highly dependent on the quality of the images, which is related to the environmental conditions and structure of the forest. In the case of UAV-based DAP, the point clouds can be affected by weather conditions such as lightning, clouds, and wind, so they can reduce the number of points and their positioning (Dandois et al. 2015). In dense forests, DAP has a lower ability to collect data of the ground so the derived digital terrain models (DTM) are expected to be less accurate than the ones derived from ALS (Graham et al. 2019). If an ALS-derived DTM is available from previous campaigns, it could be used to assist the DAP point cloud processing

(Iqbal et al. 2019). Therefore, DAP can be considered as a low-cost alternative to provide good 3D data for forest studies.

1.2.2 The ground point filtering

The airborne laser scanning (ALS) survey has great power to collect data of the ground even under dense canopy covers so it is popularly used to derive high-detailed digital terrain models (DTM). To derive DTM, the ground points must be selected from the point clouds in a process known as *filtering* so they can be interpolated. The filtering is one of the most critical and difficult proceedings to derive a DTM from ALS data (Liu 2008). Besides, because the DTM is used in the point cloud normalization, it can directly impact the forest characterization since the ALS-based estimations are derived from normalized point clouds. The existing filtering algorithms usually have many parameters so they require a certain degree of experience from practitioners to be set. The filtering must therefore be carefully conducted to ensure quality in the information produced by ALS data.

Many filtering algorithms are available in the literature. Comparative studies have demonstrated that they perform relatively well in flat terrains, but have less comparable efficiency in steeped slopes (Sithole and Vosselman 2004; Meng et al. 2010). However, despite their efficiency, the popularity of the filters is also related to their availability in the ALS processing software, which demands a good understanding of their calibration and application. Four filtering algorithms are frequently applied in ALS literature when it comes to forest applications: the progressive triangulated irregular network (PTIN, Axelsson 2000), weighted linear least-squares interpolation (WLS, Kraus and Pfeifer 1998), multiscale curvature classification (MCC, Evans and Hudak 2007), and the progressive morphological filter (PMF, Zhang et al. 2003). These filters were developed following different principles so they require special attention when applied. Besides, the practical effect of their parameters over the accuracy of the DTM is unclear, so there is a gap of knowledge in this matter. Additionally, it is important to understand the effect of the filter parametrization over the forest modeling when the point cloud is used assess forest stands.

In this thesis, these four filters were calibrated, and the effects of their parameters were assessed based on DTM accuracy (Chapter 2). The impact of the filter calibration on the forest modeling was also assessed using the growing stock volume and dominant height as target variables. A heterogeneous terrain covered by eucalyptus forest plantation in Portugal was used as a case study dataset.

1.2.3 ALS-derived diameter distribution

Modeling diameter distributions is a traditional proceeding of forest practitioners worldwide that aims to study the horizontal structure of forest stands. It is also particularly important for the initialization of individual tree models. In this process, a probability density function (PDF) is used to model diameter dataset so the tree density and growing stock can be computed for each diameter class (Burkhart and Tomé 2012). Because airborne laser scanning (ALS) cannot collect diameter data, at least directly, the diameter distribution can be estimated indirectly by using ALS metrics computed from the point cloud (Maltamo and Gobakken 2014).

Many attempts have been made to derive diameter distributions from ALS data using traditional PDFs such as the Weibull function (Gobakken and Næsset 2005; Maltamo et al. 2018) or even nonparametric approaches such as percentile-based distribution (Maltamo et al. 2006a; Bollandsås and Næsset 2007). The parametric approaches have the advantage of following statistical principles and providing a smoothed distribution, whereas nonparametric approaches can reproduce unusual distribution shapes. A good alternative is thus to search for a high-flexible PDF to reproduce diameter distributions in different forest conditions. In this context, the Johnson's S_B (Johnson 1949) is a candidate since it has been demonstrated to suit the most to different forest conditions (Parresol 2003; Fonseca et al. 2009; Mateus and Tomé 2011).

Therefore, this thesis assessed the ability of Johnson's S_B to model diameter distributions having the popular Weibull PDF as benchmark (Chapter 3). Datasets from two common forest plantations were used in this assessment, a eucalyptus stand in Portugal and a pine stad in Spain.

1.2.4 ALS-based growing stock models

Collecting data from the forest growing stock can be labor-intensive and time-consuming. For these reasons, the growing stock is one of the most modeled forest attribute in applications of airborne laser scanning (ALS). The area-based approach (ABA) is the technique commonly applied to estimate forest growing stock volume using ALS since it provides high-accurate estimations at pixel-level (Balenović et al. 2013).

The ordinary least squares regression (OLS) is by far the most used approach to fit ABA-models, although nonparametric approaches are also used (Fassnacht et al. 2014). The advantage of nonparametric approaches is the ability to handle high-dimensional datasets without the statistical rigid assumptions that must be assumed in OLS, for instance. Two popular nonparametric methods in ABA are the k-nearest neighbors (kNN, Dudani, 1976) and random forest (RF, Breiman, 2001). They popularity might be justified by their efficiency in making predictions and the relative simplicity when compared to other nonparametric approaches, such as neural networks or support vector machines (see both in Haykin, 2009).

Both kNN and RF are well-known techniques in remote sensing applications as described in the reviews of Chirici et al. (2016) for kNN and Belgiu and Drăgu (2016) for RF. Because kNN can predict multiple responses, it has been used to estimate species-specific growing stock in boreal forests using ALS data (Packalén and Maltamo 2006, 2007; Packalén et al. 2012), although it has been also used for a single response (McRoberts et al. 2015, 2017). However, kNN has proved to overfit the data depending on how it is applied (Packalén et al. 2012). RF on the other hand does not allow multiple responses, but it calls attention from scientific community given its ability to providing robust accurate without overfitting (Shataee et al. 2011; Latifi and Koch 2012). Some studies benchmarked these two modeling approaches and OLS for temperate forest (Latifi et al. 2012; Fassnacht et al. 2014; Tompalski et al. 2019), but a broader study for different site conditions is still not available. Furthermore, the conditions for which kNN overfits are not well-understood nor the effect of using many variables in RF modeling.

Considering the above-mentioned gaps of knowledge, this thesis compared in Chapter 4 the OLS, kNN, and RF to estimate growing stock volume in different forest sites worldwide: boreal forest,

temperate forest, and a forest plantation in a tropical region. Different settings of these approaches were assessed in this benchmark.

1.2.5 Tree characterization through DAP and ALS

One of the remarkable possibilities of working with point cloud data is to estimate forest attributes at tree level based on individual tree detection approach (ITD). In ITD, trees are identified using specific algorithms and biometric attributes are estimated by previously calibrated models (Lindberg and Holmgren 2017). There are many algorithms available to individualize tree canopies from normalized point clouds, such as the ones based on watershed, image segmentation, or local maxima filter, an each approach has its own specificities–see details in the comprehensive benchmarks of Kaartinen et al. (2012), Vauhkonen et al. (2012), and Wang et al. (2016). By identifying trees, practitioners can automatically obtain the stand tree densities, tree heights, and crow measures. However, aerial surveys such as airborne laser scanning (ALS) and digital aerial photogrammetry (DAP) cannot collect diameter data from tree directly, so this variable must be obtained using models based on the tree heigh and crow attributes (e.g., Chen et al., 2007; Cao and Dean, 2013; de Oliveira et al., 2014). Likewise, tree volumes and biomass must be also estimated using other tree variables so the growing stock is computed by summing up the individual tree estimates (e.g., Popescu 2007).

ITD is mostly applied with ALS, although its applications with DAP is becoming more frequent (Bonnet et al. 2017; Mohan et al. 2017; Picos et al. 2020). However, there is a lack of studies comparing both techniques. The exception was the work of Guerra-Hernández et al. (2018), who conducted a study in a eucalyptus plantation applying the local maxima filter. In their work it was showed that more accurate tree detection was achieved with ALS point cloud than with the DAP one, while both techniques had comparable performance in the estimation of tree heights. In this case, further studies must also compare both techniques regarding the tree volume and diameter estimation.

To fill this gap of knowledge this thesis compared ALS and DAP point clouds to obtain individual tree diameters and volumes by using ITD approach (Chapter 5). In this work was used the same dataset of Guerra-Hernández et al. (2018).

1.3 References

Aldred, A., Bonnor, G., 1985. Application of airborne lasers to forest surveys, Information Report PI-X-51. Chalk River, Ontario.

Axelsson, P., 2000. DEM generation from laser scanner data using adaptive TIN models., in: International Archives of Photogrammetry and Remote Sensing. Vol. XXXIII, Part B4. Amsterdam, The Netherlands, pp. 110–117.

Balenović, I., Alberti, G., Marjanović, H., 2013. Airborne laser scanning - the status and perspectives for the application in the South-East European forestry. South-east Eur. For. 4, 59–79. https://doi.org/10.15177/seefor.13-07

Baltsavias, E.P., 1999. A comparison between photogrammetry and laser scanning. ISPRS J. Photogramm. Remote Sens. 54, 83–94. https://doi.org/10.1016/S0924-2716(99)00014-3

Belgiu, M., Drăgu, L., 2016. Random forest in remote sensing: a review of applications and future directions. ISPRS J. Photogramm. Remote Sens. 114, 24–31. https://doi.org/10.1016/j.isprsjprs.2016.01.011

Bollandsås, O.M., Næsset, E., 2007. Estimating percentile-based diameter distributions in uneven-sized Norway spruce stands using airborne laser scanner data. Scand. J. For. Res. 22, 33–47. https://doi.org/10.1080/02827580601138264

Bonnet, S., Lisein, J., Lejeune, P., 2017. Comparison of UAS photogrammetric products for tree detection and characterization of coniferous stands. Int. J. Remote Sens. 38, 5310–5337. https://doi.org/10.1080/01431161.2017.1338839

Breiman, L., 2001. Random Forests. Mach. Learn. 45, 5–32.

Burkhart, H.E., Tomé, M., 2012. Modeling forest trees and stands. Springer Netherlands, Dordrecht. https://doi.org/10.1007/978-90-481-3170-9

Cao, Q. V., Dean, T.J., 2013. State-of-the-art: DTM generation using airborne LIDAR data, in: U.S. Department of Agriculture, Forest Service, S.R.S. (Ed.), Proceedings of the 15th Biennial Southern Silvicultural Research Conference. e-Gen. Tech. Rep. SRS-GTR-175. Asheville, USA, pp. 201–205.

Chen, Q., Gong, P., Baldocchi, D., Tian, Y.Q., 2007. Estimating basal area and stem volume for individual trees from lidar data. Photogramm. Eng. Remote Sens. 73, 1355–1365. https://doi.org/10.14358/PERS.73.12.1355

Chen, Z., Gao, B., Devereux, B., 2017. State-of-the-Art: DTM Generation Using Airborne LIDAR Data. Sensors 17, 150. https://doi.org/10.3390/s17010150

Chirici, G., Mura, M., McInerney, D., Py, N., Tomppo, E.O., Waser, L.T., Travaglini, D., McRoberts, R.E., 2016. A meta-analysis and review of the literature on the k-Nearest Neighbors technique for forestry applications that use remotely sensed data. Remote Sens. Environ. 176, 282–294. https://doi.org/10.1016/j.rse.2016.02.001

Colomina, I., Molina, P., 2014. Unmanned aerial systems for photogrammetry and remote sensing: a review. ISPRS J. Photogramm. Remote Sens. 92, 79–97. https://doi.org/10.1016/j.isprsjprs.2014.02.013

Dandois, J., Olano, M., Ellis, E., 2015. Optimal sltitude, overlap, and weather conditions for computer vision UAV estimates of forest structure. Remote Sens. 7, 13895–13920. https://doi.org/10.3390/rs71013895

Dash, J., Pont, D., Watt, M.S., Dash, J., Pont, D., Brownlie, R., Dunningham, A., Watt, M., Pearse, G., 2016. Remote sensing for precision forestry. NZ J. For. 15–24.

de Oliveira, L.T., Ferreira, M.Z., de Carvalho, L.M.T., Filho, A.C.F., Oliveira, T.C. de A., Silveira, E.M. de O., Junior, F.W.A., 2014. Determining timber volume of eucalyptus stands by airborne laser scanning [In Portuguese]. Pesqui. Agropecu. Bras. 49, 692–700. https://doi.org/10.1590/S0100-204X2014000900005

Dubayah, R.O., Drake, J.B., 2000. Lidar remote sensing for forestry. J. For. 98, 44–46. https://doi.org/10.1093/jof/98.6.44

Dudani, S.A., 1976. The distance-weighted k-nearest-neighbor rule. IEEE Trans. Syst. Man. Cybern. 325–327. https://doi.org/10.1109/TSMC.1976.5408784

Eitel, J.U.H., Höfle, B., Vierling, L.A., Abellán, A., Asner, G.P., Deems, J.S., Glennie, C.L., Joerg, P.C., LeWinter, A.L., Magney, T.S., Mandlburger, G., Morton, D.C., Müller, J., Vierling, K.T., 2016. Beyond 3-D: the new spectrum of lidar applications for earth and ecological sciences. Remote Sens. Environ. 186, 372–392. https://doi.org/10.1016/j.rse.2016.08.018

Eltner, A., Kaiser, A., Castillo, C., Rock, G., Neugirg, F., Abellán, A., 2016. Image-based surface reconstruction in geomorphometry - merits, limits and developments. Earth Surf. Dyn. 4, 359–389. https://doi.org/10.5194/esurf-4-359-2016

Evans, J.S., Hudak, A.T., 2007. A multiscale curvature algorithm for classifying discrete return LiDAR in forested environments. IEEE Trans. Geosci. Remote Sens. 45, 1029–1038. https://doi.org/10.1109/TGRS.2006.890412

Fassnacht, F.E.E., Hartig, F., Latifi, H., Berger, C., Hernández, J., Corvalán, P., Koch, B., 2014. Importance of sample size, data type and prediction method for remote sensing-based estimations of aboveground forest biomass. Remote Sens. Environ. 154, 102–114. https://doi.org/10.1016/j.rse.2014.07.028

Fonseca, T.F., Marques, C.P., Parresol, B.R., 2009. Describing maritime pine diameter distributions with Johnson's SB distribution using a new all-parameter recovery approach. For. Sci. 55, 367–373.

Gobakken, T., Næsset, E., 2005. Weibull and percentile models for lidar-based estimation of basal area distribution. Scand. J. For. Res. 20, 490–502. https://doi.org/10.1080/02827580500373186

Goodbody, T.R.H., Coops, N.C., White, J.C., 2019. Digital aerial photogrammetry for updating area-based forest inventories: a review of opportunities, challenges, and future directions. Curr. For. Reports 5, 55–75. https://doi.org/10.1007/s40725-019-00087-2

Goodwin, N.R., Coops, N.C., Culvenor, D.S., 2006. Assessment of forest structure with airborne LiDAR and the effects of platform altitude. Remote Sens. Environ. 103, 140–152. https://doi.org/10.1016/j.rse.2006.03.003

Graham, A., Coops, N.C., Wilcox, M., Plowright, A., 2019. Evaluation of ground surface models derived from unmanned aerial systems with digital aerial photogrammetry in a disturbed conifer forest. Remote Sens. 11, 1–21. https://doi.org/10.3390/rs11010084

Guerra-Hernández, J., Cosenza, D.N., Rodriguez, L.C.E., Silva, M., Tomé, M., Díaz-Varela, R.A., González-Ferreiro, E., 2018. Comparison of ALS- and UAV(SfM)-derived high-density point clouds for individual tree detection in Eucalyptus plantations. Int. J. Remote Sens. 39, 5211–5235. https://doi.org/10.1080/01431161.2018.1486519

Guimarães, N., Pádua, L., Marques, P., Silva, N., Peres, E., Sousa, J.J., 2020. Forestry remote sensing from unmanned aerial vehicles: a review focusing on the data, processing and potentialities. Remote Sens. 12, 1046. https://doi.org/10.3390/rs12061046

Haykin, S.O., 2009. Neural networks and learning machines, 3rd ed. Pearson education, Inc., Upper Saddle River, USA.

Hollaus, M., 2015. 3D point clouds for forestry applications. Österreichische Z. Vermess. Geoinf. VGI 103, 138–150.

Holopainen, M., Vastaranta, M., Hyyppä, J., 2014. Outlook for the next generation's precision forestry in Finland. Forests 5, 1682–1694. https://doi.org/10.3390/f5071682

Hudak, A.T., Evans, J.S., Stuart Smith, A.M., 2009. LiDAR utility for natural resource managers. Remote Sens. 1, 934–951. https://doi.org/10.3390/rs1040934

Iglhaut, J., Cabo, C., Puliti, S., Piermattei, L., O'Connor, J., Rosette, J., 2019. Structure from motion photogrammetry in forestry: a review. Curr. For. Reports 5, 155–168. https://doi.org/10.1007/s40725-019-00094-3

Iqbal, I.A., Musk, R.A., Osborn, J., Stone, C., Lucieer, A., 2019. A comparison of area-based forest attributes derived from airborne laser scanner, small-format and medium-format digital aerial photography. Int. J. Appl. Earth Obs. Geoinf. 76, 231–241. https://doi.org/10.1016/j.jag.2018.12.002

Johnson, N.L., 1949. Systems of frequency curves generated by methods of translation. Biometrika 36, 149. https://doi.org/10.2307/2332539

Kaartinen, H., Hyyppä, J., Yu, X., Vastaranta, M., Hyyppä, H., Kukko, A., Holopainen, M., Heipke, C., Hirschmugl, M., Morsdorf, F., Næsset, E., Pitkänen, J., Popescu, S., Solberg, S., Wolf, B.M., Wu, J.-C., 2012. An international comparison of individual tree detection and extraction using airborne laser scanning. Remote Sens. 4, 950–974. https://doi.org/10.3390/rs4040950

Kotivuori, E., Korhonen, L., Packalen, P., 2016. Nationwide airborne laser scanning based models for volume, biomass and dominant height in Finland. Silva Fenn. 50, 1–28. https://doi.org/10.14214/sf.1567

Kraus, K., Pfeifer, N., 1998. Determination of terrain models in wooded areas with airborne laser scanner data. ISPRS J. Photogramm. Remote Sens. 53, 193–203. https://doi.org/10.1016/S0924-2716(98)00009-4

Latifi, H., Fassnacht, F., Koch, B., 2012. Forest structure modeling with combined airborne hyperspectral and LiDAR data. Remote Sens. Environ. 121, 10–25. https://doi.org/10.1016/j.rse.2012.01.015

Latifi, H., Koch, B., 2012. Evaluation of most similar neighbour and random forest methods for imputing forest inventory variables using data from target and auxiliary stands. Int. J. Remote Sens. 33, 6668–6694. https://doi.org/10.1080/01431161.2012.693969

Lefsky, M. a., Cohen, W.B., Parker, G.G., Harding, D.J.D., 2002. Lidar remote sensing for ecosystem studies. Bioscience 52, 19. https://doi.org/10.1641/0006-3568(2002)052[0019:LRSFES]2.0.CO;2

Lim, K., Treitz, P., Wulder, M., St-Onge, B., Flood, M., 2003. LiDAR remote sensing of forest structure. Prog. Phys. Geogr. Earth Environ. 27, 88–106. https://doi.org/10.1191/0309133303pp360ra

Lindberg, E., Holmgren, J., 2017. Individual tree crown methods for 3D data from remote sensing. Curr. For. Reports 3, 19–31. https://doi.org/10.1007/s40725-017-0051-6

Liu, X., 2008. Airborne LiDAR for DEM generation: some critical issues. Prog. Phys. Geogr. Earth Environ. 32, 31–49. https://doi.org/10.1177/0309133308089496

Maclean, G.A., Krabill, W.B., 1986. Gross-merchantable timber volume estimation using an airborne lidar system. Can. J. Remote Sens. 12, 7–18. https://doi.org/10.1080/07038992.1986.10855092

Maltamo, M., Eerikäinen, K., Packalén, P., Hyyppä, J., 2006. Estimation of stem volume using laser scanning-based canopy height metrics. For. An Int. J. For. Res. 79, 217–229. https://doi.org/10.1093/forestry/cpl007

Maltamo, M., Gobakken, T., 2014. Predicting tree diameter distributions, in: Maltamo, M., Næsset, E., Vauhkonen, J. (Eds.), Forestry Applycations of Airborne Laser Scanning: Concepts and Case Studies, Managing Forest Ecosystems. Springer Netherlands, Dordrecht, pp. 177–191. https://doi.org/10.1007/978-94-017-8663-8_9

Maltamo, M., Mehtätalo, L., Valbuena, R., Vauhkonen, J., Packalen, P., 2018. Airborne laser scanning for tree diameter distribution modelling: a comparison of different modelling alternatives in a tropical single-species plantation. For. An Int. J. For. Res. 91, 121–131. https://doi.org/10.1093/forestry/cpx041

Mateus, A., Tomé, M., 2011. Modelling the diameter distribution of Eucalyptus plantations with Johnson's SB probability density function: parameters recovery from a compatible system of equations to predict stand variables. Ann. For. Sci. 68, 325–335. https://doi.org/10.1007/s13595-011-0037-7

McRoberts, R.E., Chen, Q., Domke, G.M., Næsset, E., Gobakken, T., Chirici, G., Mura, M., 2017. Optimizing nearest neighbour configurations for airborne laser scanning-assisted estimation of forest volume and biomass. Forestry 90, 99–111. https://doi.org/10.1093/forestry/cpw035

McRoberts, R.E., Næsset, E., Gobakken, T., 2015. Optimizing the k-nearest neighbors technique for estimating forest aboveground biomass using airborne laser scanning data. Remote Sens. Environ. 163, 13–22. https://doi.org/10.1016/j.rse.2015.02.026

McRoberts, R.E., Næsset, E., Gobakken, T., 2013. Inference for lidar-assisted estimation of forest growing stock volume. Remote Sens. Environ. 128, 268–275. https://doi.org/10.1016/j.rse.2012.10.007

Meng, X., Currit, N., Zhao, K., 2010. Ground filtering algorithms for airborne LiDAR data: a review of critical issues. Remote Sens. 2, 833–860. https://doi.org/10.3390/rs2030833

Mohan, M., Silva, C.A., Klauberg, C., Jat, P., Catts, G., Cardil, A., Hudak, A.T., Dia, M., 2017. Individual tree detection from unmanned aerial vehicle (UAV) derived canopy height model in an open canopy mixed conifer forest. Forests 8, 340. https://doi.org/10.3390/f8090340

Næsset, E., 2004. Practical large-scale forest stand inventory using a small-footprint airborne scanning laser. Scand. J. For. Res. 19, 164–179. https://doi.org/10.1080/02827580310019257

Næsset, E., 2002. Predicting forest stand characteristics with airborne scanning laser using a practical two-stage procedure and field data. Remote Sens. Environ. 80, 88–99. https://doi.org/10.1016/S0034-4257(01)00290-5

Næsset, Erik, 2014. Area-based inventory in Norway – from innovation to an operational reality, in: Maltamo, M., Næsset, E, Vauhkonen, J. (Eds.), Forestry Applications of Airborne Laser Scanning. Springer, Dordrecht, pp. 215–240. https://doi.org/10.1007/978-94-017-8663-8_11

Nelson, R., 2013. How did we get here? An early history of forestry lidar 1. Can. J. Remote Sens. 39, S6–S17. https://doi.org/10.5589/m13-011

Nelson, R., Krabill, W., Tonelli, J., 1988. Estimating forest biomass and volume using airborne laser data. Remote Sens. Environ. 267, 247–267. https://doi.org/10.1016/0034-4257(88)90028-4

Nex, F., Remondino, F., 2014. UAV for 3D mapping applications: a review. Appl. Geomatics 6, 1–15. https://doi.org/10.1007/s12518-013-0120-x

Nilsson, M., Nordkvist, K., Jonzén, J., Lindgren, N., Axensten, P., Wallerman, J., Egberth, M., Larsson, S., Nilsson, L., Eriksson, J., Olsson, H., 2017. A nationwide forest attribute map of Sweden predicted using airborne laser scanning data and field data from the National Forest Inventory. Remote Sens. Environ. 194, 447–454. https://doi.org/10.1016/j.rse.2016.10.022

Nord-Larsen, T., Riis-Nielsen, T., 2010. Developing an airborne laser scanning dominant height model from a countrywide scanning survey and national forest inventory data. Scand. J. For. Res. 25, 262–272. https://doi.org/10.1080/02827581.2010.486000

Packalén, P., Maltamo, M., 2007. The k-MSN method for the prediction of species-specific stand attributes using airborne laser scanning and aerial photographs. Remote Sens. Environ. 109, 328–341. https://doi.org/10.1016/j.rse.2007.01.005

Packalén, P., Maltamo, M., 2006. Predicting the plot volume by tree species using airborne laser scanning and aerial photographs. For. Sci. 52, 611–622. https://doi.org/10.109352.6.611

Packalén, P., Temesgen, H., Maltamo, M., 2012. Variable selection strategies for nearest neighbor imputation methods used in remote sensing based forest inventory. Can. J. Remote Sens. 38, 557–569. https://doi.org/10.5589/m12-046

Parresol, B.R., 2003. Recovering parameters of Johnson's SB distribution, Research Paper SRS-31. U.S. Department of Agriculture (USDA) Forest Service, Southern Research Station, Asheville, NC.

Picos, J., Bastos, G., Míguez, D., Alonso, L., Armesto, J., 2020. Individual tree detection in a eucalyptus plantation using unmanned aerial vehicle (UAV)-LiDAR. Remote Sens. 12, 885. https://doi.org/10.3390/rs12050885

Popescu, S.C., 2007. Estimating biomass of individual pine trees using airborne lidar. Biomass and Bioenergy 31, 646–655. https://doi.org/10.1016/j.biombioe.2007.06.022

Reutebuch, S.E., Andersen, H.E., McGaughey, R.J., 2005. Light detection and ranging (LIDAR): an emerging tool for multiple resource inventory. J. For. 103, 286–292. https://doi.org/10.1080/01431160500396493

Shataee, S., Weinaker, H., Babanejad, M., 2011. Plot-level forest volume estimation using airborne laser scanner and TM data, comparison of boosting and random forest tree regression algorithms. Procedia Environ. Sci. 7, 68–73. https://doi.org/10.1016/j.proenv.2011.07.013

Sithole, G., Vosselman, G., 2004. Experimental comparison of filter algorithms for bare-Earth extraction from airborne laser scanning point clouds. ISPRS J. Photogramm. Remote Sens. 59, 85–101. https://doi.org/10.1016/j.isprsjprs.2004.05.004

Tesfamichael, S.G., Ahmed, F.B., van Aardt, J.A.N., 2010. Investigating the impact of discrete-return lidar point density on estimations of mean and dominant plot-level tree height in Eucalyptus grandis plantations. Int. J. Remote Sens. 31, 2925–2940. https://doi.org/10.1080/01431160903144086

Tompalski, P., White, J.C., Coops, N.C., Wulder, M.A., 2019. Demonstrating the transferability of forest inventory attribute models derived using airborne laser scanning data. Remote Sens. Environ. 227, 110–124. https://doi.org/10.1016/j.rse.2019.04.006

Vauhkonen, J., Ene, L., Gupta, S., Heinzel, J., Holmgren, J., Pitkänen, J., Solberg, S., Wang, Y., Weinacker, H., Hauglin, K.M., Lien, V., Packalén, P., Gobakken, T., Koch, B., Næsset, E., Tokola, T., Maltamo, M., 2012. Comparative testing of single-tree detection algorithms under different types of forest. Forestry 85, 27–40. https://doi.org/10.1093/forestry/cpr051

Vauhkonen, J., Maltamo, M., Mcroberts, R.E., Næsset, E., 2014. Forestry applications of airborne laser scanning, Managing Forest Ecosystems. Springer Netherlands, Dordrecht. https://doi.org/10.1007/978-94-017-8663-8

Wang, Y., Hyyppa, J., Liang, X., Kaartinen, H., Yu, X., Lindberg, E., Holmgren, J., Qin, Y., Mallet, C., Ferraz, A., Torabzadeh, H., Morsdorf, F., Zhu, L., Liu, J., Alho, P., 2016. International benchmarking of the individual tree detection methods for modeling 3-D canopy structure for silviculture and forest ecology using airborne laser scanning. IEEE Trans. Geosci. Remote Sens. 54, 5011–5027. https://doi.org/10.1109/TGRS.2016.2543225

Wehr, A., Lohr, U., 1999. Airborne laser scanning—an introduction and overview. ISPRS J. Photogramm. Remote Sens. 54, 68–82. https://doi.org/10.1016/S0924-2716(99)00011-8

Wulder, M.A., Bater, C.W., Coops, N.C., Hilker, T., White, J.C., 2008. The role of LiDAR in sustainable forest management. For. Chron. 84, 807–826. https://doi.org/10.5558/tfc84807-6

Wulder, M.A., White, J.C., Nelson, R.F., Næsset, E., Ørka, H.O., Coops, N.C., Hilker, T., Bater, C.W., Gobakken, T., 2012. Lidar sampling for large-area forest characterization: a review. Remote Sens. Environ. 121, 196–209. https://doi.org/10.1016/j.rse.2012.02.001

Zhang, K., Chen, S.C., Whitman, D., Shyu, M.L., Yan, J., Zhang, C., 2003. A progressive morphological filter for removing nonground measurements from airborne LIDAR data. IEEE Trans. Geosci. Remote Sens. 41, 872–882. https://doi.org/10.1109/TGRS.2003.810682

2   Paper 1: Impact of calibrating filtering algorithms on the quality of LiDAR-derived DTM and on forest attribute estimation through area-based approach

This chapter has been published as an original, **open-access** paper in Remote Sensing:

Impact of Calibrating Filtering Algorithms on the Quality of LiDAR-Derived DTM and on Forest Attribute Estimation through Area-Based Approach

Diogo N. Cosenza [1,*] , **Luísa Gomes Pereira** [2,3] , **Juan Guerra-Hernández** [1,4] ,
Adrián Pascual [1] , **Paula Soares** [1] and **Margarida Tomé** [1]

[1]   Forest Research Centre, School of Agriculture, University of Lisbon, Tapada da Ajuda, 1349-017 Lisboa,
    Portugal; juanguerra@isa.ulisboa.pt (J.G.-H.); apascual@isa.ulisboa.pt (A.P.);
    paulasoares@isa.ulisboa.pt (P.S.); magatome@isa.ulisboa.pt (M.T.)
[2]   Águeda School of Technology and Management (ESTGA), Aveiro University, Apartado 473,
    3754-909 Águeda, Portugal; luisapereira@ua.pt
[3]   Centre for Research in Geospatial Science (CICGE), Porto University, 4099-002 Porto, Portugal
[4]   3edata, Centro de Iniciativas Empresariais, Fundación CEL, 27004 Lugo, Spain
*   Correspondence: dncosenza@isa.ulisboa.pt

Abstract: Ground point filtering of the airborne laser scanning (ALS) returns is crucial to derive digital terrain models (DTMs) and to perform ALS-based forest inventories. However, the filtering calibration requires considerable knowledge from users, who normally perform it by trial and error without knowing the impacts of the calibration on the produced DTM and the forest attribute estimation. Therefore, this work aims at calibrating four popular filtering algorithms and assessing their impact on the quality of the DTM and the estimation of forest attributes through the area-based approach. The analyzed filters were the progressive triangulated irregular network (PTIN), weighted linear least-squares interpolation (WLS) multiscale curvature classification (MCC), and the progressive morphological filter (PMF). The calibration was established by the vertical DTM accuracy, the root mean squared error (RMSE) using 3240 high-accuracy ground control points. The calibrated parameter sets were compared to the default ones regarding the quality of the estimation of the plot growing stock volume and the dominant height through multiple linear regression. The calibrated parameters allowed for producing DTM with RMSE varying from 0.25 to 0.26 m, against a variation from 0.26 to 0.30 m for the default parameters. The PTIN was the least affected by the calibration, while the WLS was the most affected. Compared to the default parameter sets, the calibrated sets resulted in dominant height equations with comparable accuracies for the PTIN, while WLS, MCC, and PFM reduced the models' RMSE by 6.5% to 10.6%. The calibration of PTIN and MCC did not affect the volume estimation accuracy, whereas calibrated WLS and PMF reduced the RMSE by 3.4% to 7.9%. The filter calibration improved the DTM quality for all filters and, excepting PTIN, the filters increased the quality of forest attribute estimation, especially in the case of dominant height.

Keywords: point classification; ALS; forest modeling

---

1. Introduction

The success of airborne laser scanning (ALS) on collecting accurate measurements of forest ecosystems consolidated this technique worldwide as a state-of-the-art approach in forest inventories. The term ALS refers to light detection and ranging system (LiDAR) onboard an aerial platform, aiming to quickly scan large areas to produce detailed three-dimensional point clouds of the surface [1,2]. These characteristics allow the ALS data to be used for many purposes including topographic- and

forest-related studies [3–5]. Among the forest-oriented applications, the area-based approach (ABA) has been widely applied to estimate forest attributes, where the tree dominant height and growing stock volume are commonly targeted [6–8]. However, the interpretation of ALS data requires successive steps to process, filter and re-scale the information. The calibration of the algorithms used on each step during the processes can turn into a prohibitively time-consuming operation for the users. Furthermore, the experience in handling of the ALS data is essential to properly assess the calibration of the algorithms when it comes, for instance, to generate the digital terrain model (DTM).

Despite the many developments related to the ALS data processing, ground point filtering is a critical procedure for deriving DTM [9], and it is necessary to classify raw ALS returns as coming from the ground or non-ground. Once the ground returns are interpolated to build the DTM (see [10]), the point cloud is normalized in a process by which the Z coordinates of all non-ground returns are re-scaled to above-ground elevation. In the case of the ABA, several metrics are extracted from the normalized point cloud and used to estimate the forest attributes (see, for example, [11]). Thus, the DTM has a great influence on the computation of ALS metrics and consequently on the statistical modeling based on ABA, so the filtering process can be regarded as the cornerstone step in the data processing when using ALS in forest inventory.

Great efforts have been made to develop enhanced filtering algorithms [12]. Besides the quality of the filtering, the usability of an algorithm is partially related to its availability on the ALS-oriented processing software. Among the most common filtering algorithms available, good solutions have been reported when using progressive triangulated irregular network (PTIN, [13]), weighted linear least-squares interpolation (WLS, [14]), multiscale curvature classification (MCC, [15]), or the progressive morphological filter (PMF, [16]).

The performance of the above-mentioned methods has been tested in forest areas where the results point to a higher discrepancy among filters as the terrain becomes steep and as the undergrowth increases [17–19]. This fact is common in other benchmarks, which shows the higher difference among the filter efficiencies as the terrain complexity increases [20–25]. As presented by Montealegre et al. [26], the steeped slopes affect the way the filters recognize the returns belonging to the vegetation from ones coming from the ground, causing excessive removal of returns and reducing the details of the ground surfaces. Another source of errors in the filtering process is caused by the border effect, which is the misclassification of returns on the border of the dataset due to the lack of returns outside the boundary [21]. Consequently, many returns in the border are removed causing an erosion in the DTM, so that it cannot extend above all non-ground returns. In this regard, the interpolation process of ground returns located on the edge of the ALS coverage is challenging and can substantially impact the quality of the ALS-based inventory workflow.

The filter calibration is often required to improve the filtering performance, where trial and error are the most common praxis. Using and calibrating a filtering algorithm can involve several parameters that may require considerable knowledge from forest practitioners along a tedious and time-consuming process. Many benchmark studies applied parameters calibration to compare filters [18,26], but the practical effects of the calibration on the accuracy of the DTM and the forest attribute estimation are still unknown. This understanding would be valuable for ALS users by supporting them during the data processing to produce the DTM, especially when the forest characterization is the goal.

The aims of this study are: i) To assess the calibration of four filtering algorithms (PTIN, WLS, MCC, and PMF) commonly used in ALS-based forest inventory; ii) to evaluate the impact of the calibration on the DTM quality and forest modeling, particularly for plot growing stock volume and dominant height estimation. The analysis was oriented to the forest data users or the ones who need to process ALS data of forested areas. We applied alternative combinations of parameter values for each tested algorithm in the software implementation, and the different parameters were calibrated according to the accuracy of the DTM derived from the filtered ground returns. More than 3000 ground control points were used to assess the quality of the produced DTM. The effect of calibrating the

filters was traced from the DTM generation to its impact on the performance of the models, where the multiple linear regression approach and a eucalyptus forest plantation was used as showcase.

2. Material and Methods

2.1. Study Area

The study area is located in Northwest Portugal (40°36′N, 8°25′W), close to the city of Águeda, comprising 9 km^2 of forested landscapes. The terrain presents a heterogenic topography, with altitude varying from 70 to 220 m and slopes ranging from 2.5% to 34.2%. At the time of the forest data collection (July 2008), the forest area was mainly covered by pure even-aged *Eucalyptus globulus* Labill stands, harvested every 10–12 years during three or four rotations, with some stands of *Pinus pinaster* Aiton. The eucalyptus stands had a mean tree density around 1600 trees per hectare, with regular or irregular spacings, and they were composed by stands from seedling (first rotation) and regenerated by coppice (following rotations) for pulp supplying. Many stands were multi-layered, with *E. globulus* in the uppermost layer and suppressed trees, shrubby and herbaceous vegetation in the lowermost layer.

2.2. Field Data Collection

The forest and the topographic surveys occurred between 10 June and 3 July 2008 through 41 circular plots with 400 m^2 of area (11.28 m of radius). The plots were systematically installed over the area (Figure 1a) and covered a large range of terrain slopes (Figure 1b). Within each plot, the diameters at breast height (dbh, at 1.30 m height) were measured from all trees higher than 2 m, together with the height of the dominant and co-dominant trees. For each plot, a concentric subplot of 200 m^2 (7.98 m of radius) was used to collect the heights of all trees higher than 2 m. The missing tree heights of each plot were estimated using the Prodan's model [27] fitted with the respective subplot data. The individual tree volumes with bark were estimated using an equation provided by Tomé et al. [28], and the tree volumes were summed to obtain the ground reference volume for each plot (V, m^3). The 41 plots were used for the filter calibration assessment, from which 25 plots were selected to evaluate the impact of the calibration on the forest modeling. The selection of the 25 plots was needed to remove plots that were located in the transition boundary between two stands, or crossed by roads, that could bias the forest modeling (see [29]). The biometrical description of the forest content within plots is presented in Table 1.

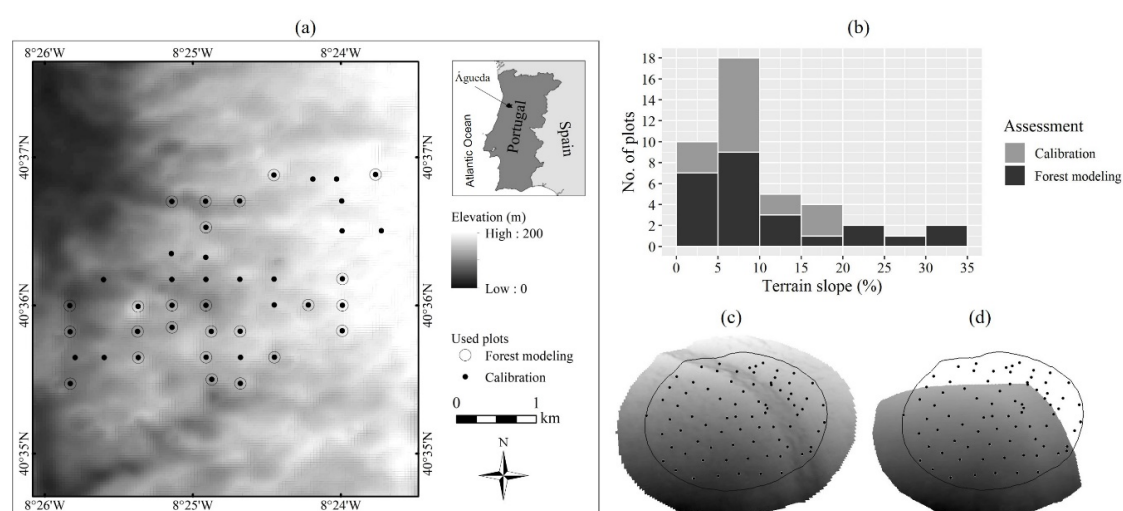**Figure 1.** (**a**) Map of plots distributed over the area. (**b**) Histogram of mean terrain slope within plots used on the filtering calibration assessment (41 plots) and forest modeling assessments (25 plots). (**c**) Exemplification of a digital terrain model (DTM) with their respective control points within a plot. (**d**) A showcase example of an eroded DTM for the plot (**c**).

Table 1. Biometrical description of the forest within plots with their minimum, mean, maximum and standard deviation (σ) values.

Assessment	Plots	* Attribute	Unit	Minimum	Mean	Maximum	σ
Calibration	41	d_g	cm	3.0	11.7	19.3	4.4
		h_d	m	3.67	15.54	26.50	5.79
		V	m^3	0.011	2.937	11.726	2.605
		N	trees ha^{-1}	875	1528	3613	534
Forest modeling	25	d_g	cm	5.6	12.3	18.2	3.6
		h_d	m	6.55	16.74	23.10	4.48
		V	m^3	0.088	3.134	7.891	2.232
		N	trees ha^{-1}	875	1470	2343	361

* V = growing stock volume within plot area; h_d = dominant height; d_g = quadratic mean diameter; N = stand density.

The coordinates of each tree within each plot were recorded as well as the coordinates of prominent terrain points, like breaklines or spot heights (Figure 1c), resulting in 3240 ground control points, a mean of 79 points per plot (σ = 24). The accuracy of the coordinates of points using a geodetic Global Navigation Satellite Systems (GNSS) on land covered with dense vegetation is not reliable; therefore, the devised strategy for measuring the coordinates of ground control points was not straightforward. Firstly, those coordinates were measured in each plot by means of a topographic survey using the radial method [30]. As these coordinates are in a local system, they were converted to that of the LiDAR data by using GNSS receivers. To this end, it was decided to attach to each plot two GNSS-derived points, named GNSS base, whose coordinates were measured with two GNSS receivers. They allow for coordinating the surveyed points directly in the referred coordinate system. Two points are needed to orient the total station. These two points were placed as close as possible to the plot and as much as possible in an open space. The method used to measure the coordinates of the two GNSS-derived points was the relative positioning by using a fixed receiver on a geodetic pillar with known coordinates on the same system as the LiDAR data. This method, in post-processing, is the most precise and may reach levels of precision in the order of centimeters [31].

2.3. ALS Data Collection and Pre-Processing

The ALS survey was carried out in July 2008, a few days after the forest inventory, using a LiteMapper-5600 laser system from RIEGL (www.riegl.com), which has as main components the high-resolution laser scanner LMS-Q560, the positioning system AEROcontrol, and the digital camera DigiCAM (see [32] for more technical details on the system). The airplane flew 600 m above ground with a mean speed of 46.26 m s^{-1}. The parameters of the laser system were: 0.5 mrad of beam divergence, ±45° of scan angle and pulse rate of 150 kHz. The resulted swath was 497 m (60% of overlap) and the returns density was 9.5 returns m^{-2}. More details about the ALS survey is described in [31,33]. The ALS point clouds were inspected for outliers and further clipped using the plot center coordinates with a 15-m radius buffer (706.85 m^2) for each plot. The clipping process was carried out to avoid edge-effect over the ground returns during the filtering process. The FUSION software V3.60 [34] was used for this pre-processing.

2.4. Filtering Calibration

The used filters were chosen based on their recurrent utilization on the related literature [20,26]. We gave preference to those filters implemented into line-code-based software that allows being incorporated into programming routines; in our case the R environment [35] was used. Each filter was applied to the last returns of the point clouds of the 41 plots using different parameter sets. The choice of which parameters to be calibrated was done for each filter since they follow different principles described in the following sections. This work is focused on the filtering process for forest applications, so settings regarding urban terrain or smoothing filters were not considered. The values tested in the

calibration were defined considering the ones close to the software defaults and recommendations (Table 2).

Table 2. The default filtering parameter values and the corresponding set of values for calibration of the progressive triangulated irregular network (PTIN), weighted linear least-squares interpolation (WLS), multiscale curvature classification (MCC), and progressive morphological filter (PMF). The particularities of the parameters are defined in Sections 2.4.1–2.4.4.

Filter	Software	Parameters	Default	Set of Values for Calibration
PTIN	LASground	*Spike*	0.5	0.0, 0.5, 1.0, 1.5, 2.0
		Step size	5	1,3,5,7
		Granularity	*Fine*	*None, coarse, fine, extra fine*
WLS	FUSION	*g*	−2.5	−3.0, −2.5, −2.0, . . . , 0.0
		w	2.5	0.0, 0.5, 1.0, . . . , 3.0
		Iterations	5	3, 5, 7
		Window size	5 *	1, 3, 5
MCC	MCC-LIDAR	*Scale (λ)*	1.5	0.5, 1.0, 1.5, . . . , 5.0
		Tolerance (t)	0.3	0.1, 0.2, 0.3, . . . , 1.0
PMF	lidR	*Threshold*	0.3	0.1, 0.2, 0.3 . . . , 1.5
		Window size	5, 9, 13, 17	1, 3, 5, . . . , 19

* Exemplified value by the software's manual.

2.4.1. Progressive Triangulated Irregular Network (PTIN)

The PTIN is frequently applied in forest studies [36–38]. The algorithm starts with a sparse triangulated irregular network (TIN) created from seed points and then performs the densification of the TIN iteratively. In this process, the densification occurs by including the returns according to their distance to the TIN facets and their angles to the nodes. We used the adaptation of PTIN of the LASground software (rapidlasso.com), which comprises the following three assessed parameters: *Spike*, which is the threshold at which spikes get removed; *step size*, defines the size of the initial search window and it is dependent on the terrain roughness, where values around 5 are suggested for forest or mountain areas; and *granularity,* related to the computational effort invested into finding the initial ground estimate.

2.4.2. Weighted Linear Least-Squares Interpolation (WLS)

The applied WLS filter was the adaptation of the Kraus and Pfeifer's algorithm [14] into the FUSION software [34], which was used in many works [39–41]. This filter averages reiteratively the return heights inside a defined search window, assigning the weights according to their residuals in relation to the mean height. In this case, the weights are recalculated in each iteration according to the weighting function (Equation (1)), so that height values associated with lower residuals receive higher weights, whereas those with higher residuals receive lower weights. The parameter values $a = 1$ and $b = 4$ are commonly used and are recommended by the software developers for most applications so they were kept in the analysis [14,26]. The parameters g, w, *window size* and the number of iterations (*iteration*) are supposed to be defined by the user according to the data, thus they were chosen to be calibrated (Table 2). Among these parameters, the *window size* is the only one without a specified default value, although the software's manual points to 5 m^2. In this case, a *window size* equal to 5 m^2 was considered as a default value.

$$p_i = \begin{cases} 1 & v_i \leq g \\ \frac{1}{1+a(v_i-g)^b} & g < v_i \leq g+w \\ 0 & v_i > g+w \end{cases} , \tag{1}$$

where p_i is the weight for the return $i = 1, \ldots , n$; v_i is the residual point height value from the average height, being $i = 1, \ldots , n$; the parameters a and b determine the steepness of the weight function; g is negative and represents a threshold value after which the weights are set to 1 if $v_i \leq g$ and to 0 if $v_i > g + w$. Note that $w \leq |g|$ for all w values.

2.4.3. Multiscale Curvature Classification (MCC)

The MCC is a filter developed by Evans and Hudak [15] and implemented in MCC-LIDAR software (sourceforge.net/projects/mcclidar). It uses the thin-plate spline interpolation to produce surfaces in different resolutions and uses progressive curvature tolerances to eliminate non-ground returns. The software uses only two parameters that should be set by the user: the initial *scale* (λ), related to the search window size that is used to interpolate the points; and the initial curvature *tolerance* (t), which accounts for slope interaction between the interpolated surface and the returns. During the processing, both parameters are changed through three domains to address variable canopy configurations and their interaction with the terrain slope: the initial value set to λ is multiplied by 0.5, 1, and 1.5, while 0.1 is added to the initial t in each domain. Values for $\lambda = 1.5$ and $t = 0.3$ are claimed by the developers as efficient to filter non-ground returns, so variations around those values were tested in this work (Table 2). Applications of the MCC in forest studies can be found, for example, in [42–44].

2.4.4. The Progressive Morphological Filter (PMF)

The PMF filter was developed by Zhang et al. [16] and uses concepts of object identification in grey-scale images by applying mathematical morphology filters like opening and closing operators. The closing operator removes returns from objects of sizes smaller than the window size, while the opening operator keeps the returns from larger objects. The PMF was applied using the implementation of the lidR package [45], where the filter works at point cloud level without any rasterization process. The PMF has been commonly applied to ALS data [18,26], and the release of the lidR package has also promoted this filter to process photogrammetric point clouds [46]. The package uses two parameters: the sequence of *windows size*, and the sequence of *threshold*, which is the height value below which a return is classified as a ground return. In this study, the PMF was applied using not a sequence but a specific value for each parameter to better isolate the effect of each component in the processing of the ALS datasets (Table 2).

2.5. Filtering Accuracy Assessment

For each combination of filter parameters, the classified ground returns within each plot were interpolated into a DTM (1.0 m of cell size) from a TIN surface using the *grid_terrain* command implemented on the lidR package [45]. The choice of using the TIN interpolation was due to its efficiency and frequent application to generate DTM from ALS data [9,19,47]; thus, eventual errors in the interpolation were not considered in this analysis. Each combination of the filter parameters was assessed using the root mean squared error (RMSE, Equation (2)) computed with the height values interpolated from the derived DTM at the same planimetric positions as the ground control points. Note that the DTM was generated for each plot separately to allow detecting DTM erosion, which was defined here as the non-inclusion of all ground control points within the DTM extension of its respective plot (Figure 1d). The efficiency of a filtering process was then evaluated using the accuracy of the DTM (the lower the RMSE, the better) so as its integrity, where the erosions were not allowed.

$$\text{RMSE} = \sqrt{\frac{\sum_{i=1}^{n}(y_i - \hat{y}_i)^2}{n}} \tag{2}$$

where, y_i and $\hat{y}_i$ are, respectively, the observed and estimated value for the observation $i = 1, \ldots , n$.

2.6. Forest Modeling Assessment

The calibrated parameter values for each filter were further benchmarked against the default values by assessing the impact of the corresponding derived DTM on the estimation of forest attributes through ABA. Each of these DTM was used further into the normalization process, which provided the height of points above ground. The growing-stock volume (V, m^3) and the dominant height (h_d, m) were estimated for each plot using ALS metrics since these attributes are frequently assessed in the ALS applications. The ALS metrics were computed for each plot using its respective normalized point cloud and considering only points higher than 1 m above ground. The normalization and the computation of ALS metrics were performed using the lidR package [45]; the set of metrics (Table 3) were used as candidate predictors in forest modeling.

Table 3. Description of candidate metrics derived from airborne laser scanning (ALS).

Metric Type	Metric	Description
Position	Z_{min}, Z_{mean}, Z_{max}	Minimum (Z_{min}), mean (Z_{mean}) and maximum (Z_{max}) return height
	Z_5, Z_{10}, Z_{15}, Z_{20}, Z_{25}, Z_{30}, Z_{35}, Z_{40}, Z_{45}, Z_{50}, Z_{55}, Z_{60}, Z_{65}, Z_{70}, Z_{75}, Z_{80}, Z_{85}, Z_{90}, Z_{95}	Z_x-th percentile (quantile) of height distribution
	MQ, MC	Quadratic (MQ) and cubic (MC) mean height
Height variability	Z_{cv}, Z_{sd}	Height coefficient of variation (Z_{cv}) and standard deviation (Z_{sd})
	Z_{sqew}, Z_{kurt}	Height skewness (Z_{sqew}) and kurtosis (Z_{kurt})
Density	$PFRZ_{mean}$, $PARZ_{mean}$	Percentage of first ($PFRZ_{mean}$) and all returns ($PARZ_{mean}$) above Z_{mean}
	PFR_{2m}, PAR_{2m}	Percentage of first (PFR_{2m}) and all returns (PAR_{2m}) above 2 m
	C_1, C_2, C_3, C_4, C_5, C_6, C_7, C_8, C_9	Cumulative percentage of returns in the C-th layer, i.e., $C_{10} = 100\%$
Others	CR	Canopy relief ratio: $(Z_{mean} - Z_{min})/(Z_{max} - H_{min})$

Although there are several methodologies to perform a forest attribute modeling [48], the multiple linear regression fitted using ordinary least squares was used as a showcase for its simplicity, efficiency and frequent application to ALS data [49–52]. Thus, the multiple linear model (Equation (3)) was used to estimate each forest attribute (V and h_d), where the two metrics were selected through exhaustive search.

$$\sqrt{Y} = \beta_0 + \beta_1 x_1 + \beta_2 x_2 + \varepsilon \tag{3}$$

where, $\sqrt{Y}$ is the response variable; β_i is the model parameter $i = 0, 1, 2$; x_i is the predictor $i = 1, 2$; and ε is the random error.

Despite this analysis focusing on the estimative efficiency of the models (no inference made), the linear regression assumptions were taken into account. The response variable was square rooted to avoid heteroscedasticity, and the residual variance component was added to the back-transformed response variable when an equation was used to estimate a forest attribute: $\hat{Y} = \left(\hat{\sqrt{Y}} \right)^2 + \sigma^2$ [8,53]. In the exhaustive search, all possible combinations of two candidate metrics were used to fit the models using the above-mentioned dataset with 25 plots. The best model was considered to be the one with the lowest RMSE (Equation (2)), all parameters significantly different from zero (t-test, $\alpha = 5\%$), and with variance inflation factors lower than 10 [54] computed using the *car* package [55]. The RMSE was chosen for this purpose for is has been proven to be a stable and robust measure to assess model performances [52].

Each model was selected and fitted using the data from the 25 plots referred above. The fitted equation was assessed through 5-fold cross-validation. In the cross-validation the dataset is split into five sets ("folds") of equal size to start an iterative process. In each iteration one fold is omitted from the model fitting and has their values estimated by the model; the estimated values of all omitted folds at the end of the process are used to compute the final error. The entire cross-validation was repeated 100 times to reduce the randomness involved in this process [56]. Thus, the resultant RMSE values from the calibrated filter were compared to the ones derived from the default values through the Wilcoxon–Mann–Whitney test [57,58], since preliminary analysis demonstrates that the RMSE values

were not normally distributed. The accuracy of the models was thus represented by the median of the error values (RMSE$_{med}$) as well as its percentage from the observed mean values RMSE%$_{med}$.

3. Results

3.1. Filtering Parameters Calibration

As a general result, the calibration of the filter parameters allowed to produce more accurate DTMs than those produced using the software defaults, with RMSE from 0.25 to 0.26 m when calibrated, against a variation from 0.26 to 0.30 m with the default (Table 4). The accuracy of the DTMs produced with the calibrated PTIN had the smallest improvement when compared to that obtained by using the default parameters (a reduction of 4% in the RMSE). On the other hand, the accuracy of the DTMs produced with calibrated WLS had the highest improvement on accuracy, decreasing 16% in terms of RMSE. Excepting the PMF, the filters have more than one calibrated parameter set, so the set that has less impact on the computational effort was chosen.

Table 4. Root mean square error (RMSE) of the digital terrain models (DTMs) derived by the default and the calibrated parameter values for progressive triangulated irregular network (PTIN), weighted linear least-squares interpolation (WLS), multiscale curvature classification (MCC), and progressive morphological filter (PMF).

Filter	RMSE (m)		Difference *	Calibrated Parameters Values
	Default	Calibration		
PTIN	0.26	0.25	−0.01 (−4%)	*Spike*: 0
				Step size: 5
				Granularity: Fine, extra fine
WLS	0.30	0.25	−0.05 (−16%)	$|g| = w = 0.0, 0.5, 1.0, \ldots, 3.0$
				Iterations: 3
				Window size: 1
MCC	0.29	0.26	−0.03 (−10%)	*Scale*: 1, 1.5, 2, . . . , 4.5
				Tolerance: 0.1
PMF	0.27	0.25	−0.02 (−7%)	*Threshold*: 0.1
				Window size: 5

* Differences between the calibrated parameter values and the default ones.

The tested parameters of PTIN resulted in a small variation in the accuracy of DTMs, with RMSE ranging from 0.25 to 0.29 m (Figure 2). The DTM accuracy was less affected by the *spike* and most influenced by the *step size*—the RMSE decreased continually as the *step size* increased. On the other hand, larger values for *step size* increased the susceptibility of the filter to border effect, producing eroded DTMs. This effect was intensified when the *coarse granularity* was applied so that smaller values of *step size* were needed to derive eroded DTMs. Despite the influence of the border effect, the *granularity* had marginal impact on the accuracy of the DTMs, and the *fine* and *extra fine granularity* had comparable results. Therefore, the *fine granularity* should be preferred since it requires less computational effort during data processing.

The WLS presented high variation in the DTM accuracy among the different parameter settings (RMSE between 0.25 and 0.46 m). It is strongly and similarly affected by the parameters *g* and *w* (Figure 3), where the RMSE decreased with their decreasing in value. Additionally, the RMSE decreased as the differences in the absolute values of these parameters decreased, which means that the filter is more accurate as $|g|$ and *w* values are closer. The tested number of *iterations* and window *cell sizes* did not influence the accuracy of the DTMs, but they were important concerning the border effect. Eroded DTMs occurred when $|g| = w$, except when the *cell size* was set to 1 m^2 and using three or five iterations. By setting $|g| = w$ the filter is forced to consider only the lowest residuals to compute the averages, and positive residuals (*v*) are no longer accepted. Consequently, the WLS becomes less tolerant of

variations in the ground surface within the search window so more points are removed if a higher *cell size* or a higher number of *iterations* are used. Furthermore, there was no difference in the filtering performance when the number of *iterations* was set to either three or five, so the lower value (i.e., three) should be preferred to speed up the computational process.
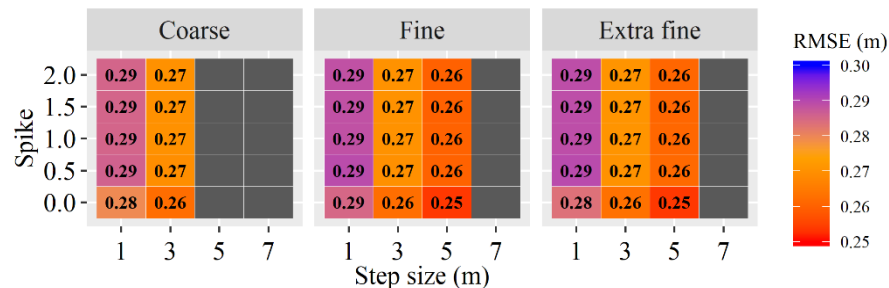

Figure 2. Root mean square error (RMSE) values of the digital terrain models (DTMs) derived from the calibration of the parameters of the progressive triangulated irregular network (PTIN). Grey tiles represent settings that produced eroded DTMs.
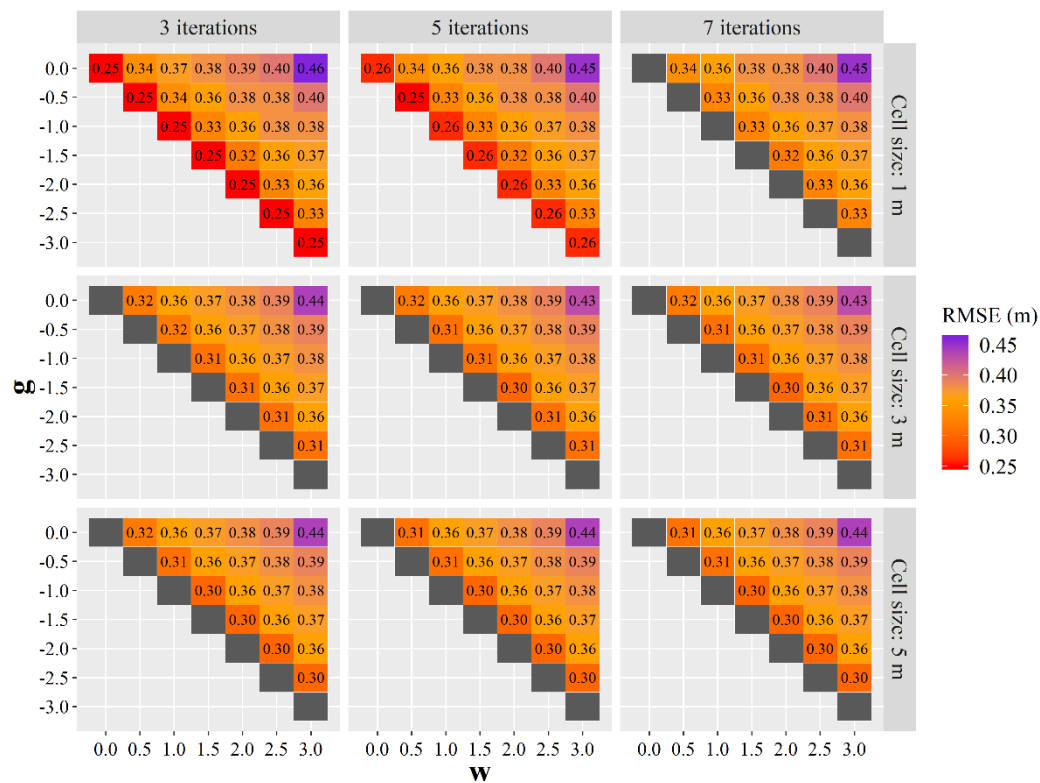

Figure 3. Root mean square error (RMSE) values of the digital terrain models (DTMs) derived from the calibration of the parameters of the weighted linear least-squares interpolation (WLS). Grey tiles represent settings that produced eroded DTMs.

The calibration of the MCC did not produce eroded DTMs, and their accuracy varied between 0.26 and 0.36 m (Figure 4). The *tolerance* had the greatest impact on the filter's performance (i.e., the higher its value, the higher the RMSE and thus the smaller the DTM accuracy). On the other hand, the *scale* appears to have only marginal impact, tending to reduce the RMSE as the values increase. The tested values for *scale* suggested that its effect on the DTM accuracy also depends on the *tolerance*; when the *tolerance* was set to 0.1, the effect of the *scale* on the accuracy was marginal (RMSE between 0.26 and 0.27 m), while a wider range was observed for intermediary *tolerance* values (e.g., RMSE between 0.29 and 0.34 m for *tolerance* value equal to 0.4). Despite the most accurate DTM being produced when

setting *tolerance* to 0.1, many values could be used for the *scale* (0.1–4.5). This parameter controls the cell resolution of the thin-plate spline interpolation (see Section 2.4.3), so setting larger values increases the number of returns to be interpolated. For this reason, using lower values for the *scale* (i.e., between 1 to 2) is advisable to reduce the computational effort.
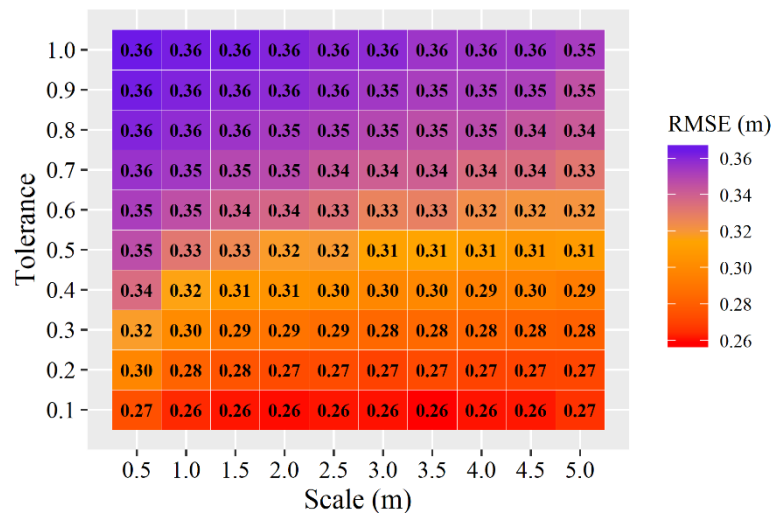

Figure 4. Root mean square error (RMSE) values of the digital terrain models (DTMs) derived from the calibration of the parameters of the multiscale curvature classification (MCC).

The calibration of the PMF parameters resulted in the widest range of DTM accuracies, with RMSE between 0.25 and 0.56 m (Figure 5). Both tested parameters influenced the filtering efficiency. The RMSE of the DTMs increased with the increasing of the *threshold*. The changes in the accuracy due to the *window size* were more highlighted when its values shifted from 1 to 3, but a marginal effect was noted for values higher than three. The eroded DTMs were more frequent as the *threshold* value was lower and the *window size* higher. Since the PMF uses a sequence of *window size* values in the filtering, the use of higher values (i.e., ≥9) showed to be not effective for the filtering efficiency in the studied area.

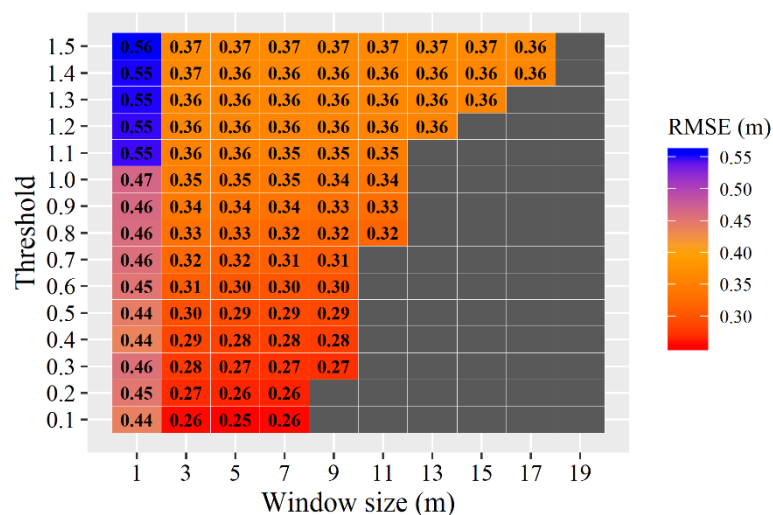

Figure 5. Root mean square error (RMSE) values of the digital terrain models (DTMs) derived from the calibration of the parameters of the progressive morphological filter (PMF). Grey tiles represent settings that produced eroded DTMs.

3.2. Estimation of Forest Attributes

The default and the calibrated parameter values listed in Table 4 were used to estimate the forest attributes through ABA. The parameters with more than one calibrated value were set as follows: *Fine granularity* for PTIN; $g = 0$ and $w = 0$ for WLS; and *scale* = 1.0 for MCC.

The dominant height equations resulted in good accuracy for all filters, with RMSE%$_{med}$ between 4.9% and 5.2% for the calibrated values, and between 5.0% and 5.6% for the default values (Table 5). The calibrated and the default parameters values originated equations with comparable performances for the PTIN considering a confidence level (α) of 5%. The metrics used by the equations derived from PTIN were also similar; the equation derived from the calibrated parameters used Z_{65}, while the one derived from the default parameters used Z_{60}. The calibration of WLS, MCC and PFM resulted in a significant improvement of the estimated dominant height accuracy when compared to that one derived using the default parameter values. The decrease in the RMSE$_{med}$ values due to the calibration was 0.08 m points for WLS, 0.06 m for MCC and 0.10 for PMF, which are equivalent to an improvement of 8.5%, 6.5% and 10.6%, respectively. Although their respective equations used the metric Z_{95}, the ones derived for the calibrated values used Z_{60} instead of C_8 in the equations of the default values, which are metrics computed with different principles (see Table 3).

Table 5. Dominant height equations with their associated variances (σ^2), and the *p*-value for the Wilcoxon–Mann–Whitney test obtained with different settings of the progressive triangulated irregular network (PTIN), weighted linear least-squares interpolation (WLS), multiscale curvature classification (MCC), and progressive morphological filter (PMF).

Filter	Setting	* Equation	σ^2 (m)	** RMSE$_{med}$ (m)	*p*-value
PTIN	Calibrated	$\sqrt{h_d} = 1.922 - 0.037\,Z_{65} + 0.164\,Z_{95}$	0.009	0.829 (4.9%)	0.011
	Default	$\sqrt{h_d} = 1.930 - 0.032\,Z_{60} + 0.159\,Z_{95}$	0.009	0.844 (5.0%)	
WLS	Calibrated	$\sqrt{h_d} = 1.926 - 0.032\,Z_{60} + 0.159\,Z_{95}$	0.010	0.86 (5.2%)	<0.001
	Default	$\sqrt{h_d} = 1.406 + 0.006\,C_8 - 0.139\,Z_{95}$	0.009	0.94 (5.6%)	
MCC	Calibrated	$\sqrt{h_d} = 1.331 - 0.034\,Z_{60} + 0.161\,Z_{95}$	0.009	0.86 (5.1%)	<0.001
	Default	$\sqrt{h_d} = 1.390 + 0.006\,C_8 - 0.139\,Z_{95}$	0.009	0.92 (5.5%)	
PMF	Calibrated	$\sqrt{h_d} = 1.930 - 0.032\,Z_{60} + 0.159\,Z_{95}$	0.009	0.84 (5.0%)	<0.001
	Default	$\sqrt{h_d} = 1.393 + 0.006\,C_8 - 0.139\,Z_{95}$	0.009	0.94 (5.6%)	

* h_d is the dominant height (m); Z_x is the height of the *x*-th percentile of height distribution; C_x is the cumulative percentage of returns in the *x*-thlayer. ** Median of root mean square error (RMSE) values computed through 100 repetitions of five-fold cross-validation. The RMSE%$_{med}$ is shown in parenthesis.

Regarding the volume estimation, the models presented RMSE%$_{med}$ between 16.3% and 16.7% when using the calibrated values and 16.5% and 17.7% when using the default values (Table 6). Although these errors are higher than those encountered in the estimation of the dominant height, they could be considered low in the case of volume modeling when assessed through cross-validation. The estimation efficiency when using the calibrated PTIN and MCC did not differ from those derived with filters using their respective default values. The use of WLS and PMF with calibrated parameters significantly improved the volume estimation when comparing to their respective default values. Despite the related equations used the same metrics, the decrease of the RMSE$_{med}$ values by using the calibrated parameters were 0.018 m^3 for WLS and 0.044 m^3 for PMF, which is equivalent to an improvement of 3.4% and 7.9%, respectively.

Table 6. Volume equations with their associated variances (σ^2), and the *p*-value for the Wilcoxon–Mann–Whitney test obtained with different settings of the progressive triangulated irregular network (PTIN), weighted linear least-squares interpolation (WLS), multiscale curvature classification (MCC), and progressive morphological filter (PMF).

Filter	Setting	* Equation	σ^2 (m^3)	** RMSE_{med} (m^3)	*p*-value
PTIN	Calibrated	$\sqrt{V} = -0.538 + 0.137\,Z_{max} - 0.013\,C_2$	0.021	0.522 (16.7%)	0.554
	Default	$\sqrt{V} = -0.532 + 0.138\,Z_{max} - 0.014\,C_2$	0.020	0.528 (16.8%)	
WLS	Calibrated	$\sqrt{V} = -0.518 + 0.137\,Z_{max} - 0.014\,C_2$	0.019	0.514 (16.4%)	0.007
	Default	$\sqrt{V} = -0.516 + 0.139\,Z_{max} - 0.018\,C_2$	0.019	0.532 (17.0%)	
MCC	Calibrated	$\sqrt{V} = -0.520 + 0.138\,Z_{max} - 0.015\,C_2$	0.019	0.515 (16.4%)	0.267
	Default	$\sqrt{V} = -0.522 + 0.139\,Z_{max} - 0.017\,C_2$	0.018	0.517 (16.5%)	
PMF	Calibrated	$\sqrt{V} = -0.532 + 0.138\,Z_{max} - 0.014\,C_2$	0.020	0.510 (16.3%)	<0.001
	Default	$\sqrt{V} = -0.516 + 0.140\,Z_{max} - 0.021\,C_2$	0.020	0.554 (17.7%)	

* V is the plot growing stock volume (m^3); Z_{max} is the maximum height; C_2 is the cumulative percentage of returns in the 2nd layer. ** Median of root mean square error (RMSE) values computed through 100 repetitions of five-fold cross-validation. The RMSE%$_{\text{med}}$ is shown in parenthesis.

4. Discussion

This study demonstrated that a DTM derived from ALS is more accurate when the parameters of the filtering process are calibrated. The DTM produced with the WLS was the most affected by the calibration, followed by that of the MCC, PMF and of the PTIN (less affected). This fact influenced the estimation of forest attributes, especially for dominant height. Except for PTIN, the estimation of the dominant height derived by using the calibrated parameter values was significantly more accurate than those that are derived with the default ones. In the case of the volume estimation, the calibration of WLS and PFM derived equations with significantly better accuracies, contrary to the PTIN and MCC filters that performed comparably when using calibrated and default parameter values.

The lower effect of the calibration for PTIN is justified by the similarity between the calibrated and the default parameters values, which differs only by 0.5 in the *spike* parameter value (see Tables 2 and 4). The calibrated parameters for the MCC differed the most with respect to the default ones, having a large impact on the dominant height estimation as opposed to the volume estimation. The result shows that a DTM can have different impacts on the modeling of these forest attributes and that the calibration will lead to the best results depending on the filter and on the attribute to be estimated.

Although these two forest attributes are highly correlated, they present different aspects when are estimated through ALS data. Many works have reported good correlations between the tree height attributes with upper-tail percentiles of the height distribution of ALS returns [59,60]. The literature is less consensual for the case of the volume estimation, for which good performances are found based on ALS metrics associated to intermediary percentiles (higher than 50%), density metrics (e.g., C_8) and/or height variability measures (e.g., height kurtosis) [6,44,50]. These characteristics were also observed in our work, where the metric Z_{95} appears in all dominant height equations just as the Z_{max} and C_2 in the volume equations. However, studies focusing on the effect of point density over the metrics demonstrated that those ones related to the tail ends of the return distribution (e.g., C_1 and C_9, or Z_{min} and Z_{max}) are more sensible and, therefore, less stable [61]. Despite the point density remaining constant in our analysis, it is possible that those same metrics are also more sensitive to variations in the normalized point cloud due to errors in the DTM. This fact is important in the case of ordinary least squares regression since the predictors are selected following several rules to match the regression assumptions, so small variations in the metric values have unpredictable effects in the final model.

It should be highlighted that the quality of the estimation of stand attributes is strongly dependent on the applied modeling approach [52]. Nonparametric models, such as k-nearest neighbors or random forest, have the advantage of being distribution-free and are normally used with more predictor variables to improve their accuracy [48,62,63]. In this case, it is reasonable to suspect that using more variables would turn the models less vulnerable against changes in the metrics and, thus, the effect of

the filter calibration could be hidden by an improvement in the performance of the models. However, the non-parametric approaches require a higher amount of field data for the modeling, which is not often available (as is the case of this work). Besides, traditional parametric modeling approaches have shown to be less affected by biased normalized point clouds, for instance, due to co-registration errors, so that alternative combinations of ALS metrics models can result in similar estimative efficiency [51]. The co-registration effect could be ignored in this work given the high-accurate plot positioning throughout the data collection; therefore, it corroborates that DTM quality is the major factor affecting the performances of the model in the benchmark.

The researches focused on calibration of the above tested filters are scarce in the literature and the few examples were oriented to digital aerial photogrammetry (DAP, [64,65]). One of them is the study of Graham et al. [66] who analyzed the PTIN, WLS and the simple morphological filter (SMRF, see [67]), which works similarly to the PMF. Their results share some similarities with ours: the PTIN was mostly affected by the *step size* parameter, while the *spike* had minor or no effects over the accuracy of the derived DTM; the WLS had the best accuracy with the |*g*| close to *w*; and low *threshold* for the SMRF (analogous in PMF). On the other hand, the parameters related to the size of the search windows of these filters (i.e., *window size* and *step size*) were exceptionally higher (≥ 17 m^2). However, we have demonstrated that using larger values for these parameters over ALS point clouds increases the susceptibility of the filters to the border effect, resulting in eroded DTM.

The PTIN was also analyzed by Wallace et al. [68] using DAP-based data, where the calibration was performed for different ecosystems. However, in contrast to the study of Wallace et al. [68], our work did not distinguish the areas regarding the terrain conditions or forest covers due to a lack of data for this discretization, especially in the forest modeling assessment. Instead, the filters were analyzed considering all ALS data available so the results of the calibration can be applied to a wider range of forest conditions. Furthermore, many works have been applied the ABA to mountainous sites with success, demonstrating that the impact of the terrain slope over the forest attribute estimation is not significant as expected [60,69,70], thereby it is unlikely that this effect can also compromise the performances of our forest models.

Most of the ground filtering benchmarks assess the accuracy through visual inspection of the filtered ground returns, which allows accounting for omission and commission errors of the filtering [20,21,26]. Although such analysis produces detailed information about the filtering process, it is highly time-consuming and can be impracticable in terms of the calibration routines like the ones performed in this study. The analysis based on the quality of DTM is thus a good and practical alternative when high-accurate ground control data is available. Additionally, further benchmarks should also account for DTM erosion, since it is prohibitive when the goal is forest modeling.

Although this work did not aim at comparing filters, it should be highlighted that all tested filters had comparable performances after the calibration, considering the accuracy of the derived DTM. This fact suggests that more efforts should be given to calibrate the ground point filters instead of finding a better one. Therefore, the software developers must be encouraged to implement adaptive filters to reduce the number of parameters to be set to process the data (e.g., [24,71,72]).

The improvement in the estimation of dominant height is of great importance for forest management since it ensures a more accurate analysis of forest site productivity [59,73]. Likewise, ALS-based models play a key role in the valuation of growing stock inventory [74,75], so reducing the errors of the estimated attributes by calibrating the filters allows increasing the liability of the assessments. However, ALS-data users must preliminarily consider the potential improvement on the DTM accuracy and forest attribute estimation before deciding to calibrate it instead of using the software's default.

This work did not consider the impact of the errors originating from different interpolation methods on the accuracy of DTM nor on the forest attribute estimation. Previous studies demonstrated the difference among the efficiency of interpolators while deriving DTM from ALS data [19,47]; despite the TIN approach usually performed the best, Stereńczak et al. [19] showed that the differences

among the interpolators were reduced after calibration. Additionally, Graham et al. [76] tested several interpolation methods using DAP-data and showed that they do not have significant differences regarding the accuracy of estimated forest attributes. The same may occur in the case of ALS-data, but proper research is needed to investigate such a hypothesis. Finally, our analysis was based on a massive ground control dataset that was collected using an exhaustive and high-accurate topographic survey, which supports the liability of the DTM accuracy assessment [77]. For this reason, our results can be used as a rule of thumb and the information we provided from the filter calibration can guide the user during the ALS data processing, especially if the estimation of forest attributes is the goal.

5. Conclusions

The calibration of four algorithms to filter ground returns of airborne laser scanning data were assessed, namely, the progressive triangulated irregular network (PTIN), weighted linear least-squares interpolation (WLS), multiscale curvature classification (MCC) and the progressive morphological filter (PMF). The impact of the calibration was assessed on the quality of the digital terrain models (DTM) and on the forest attribute estimation accuracy, where the area-based approach (ABA) was applied. The conclusions of this work are:

- The calibration of the ground filter parameters improved the quality of the DTM.
- The calibrated parameter values for WLS, MCC, and PMF allowed deriving more accurate estimated forest attributes than those obtained when filtering using their default counterparts, with a more highlighted impact on the estimation of dominant height than of growing stock.
- The results derived when using the PTIN filter varied the least with the calibration of the parameters.

References

1. Wehr, A.; Lohr, U. Airborne laser scanning—An introduction and overview. *ISPRS J. Photogramm. Remote Sens.* **1999**, *54*, 68–82. [CrossRef]
2. Vauhkonen, J.; Maltamo, M.; Mcroberts, R.E.; Næsset, E. *Forestry Applications of Airborne Laser Scanning*; Maltamo, M., Næsset, E., Vauhkonen, J., Eds.; Managing Forest Ecosystems; Springer: Dordrecht, The Netherlands, 2014; Volume 27.
3. Eitel, J.U.H.; Höfle, B.; Vierling, L.A.; Abellán, A.; Asner, G.P.; Deems, J.S.; Glennie, C.L.; Joerg, P.C.; LeWinter, A.L.; Magney, T.S.; et al. Beyond 3-D: The new spectrum of lidar applications for earth and ecological sciences. *Remote Sens. Environ.* **2016**, *186*, 372–392. [CrossRef]
4. Nelson, R. How did we get here? An early history of forestry lidar. *Can. J. Remote Sens.* **2013**, *39*, S6–S17. [CrossRef]

5.　　Hyyppä, J.; Hyyppä, H.; Leckie, D.; Gougeon, F.; Yu, X.; Maltamo, M. Review of methods of small-footprint airborne laser scanning for extracting forest inventory data in boreal forests. *Int. J. Remote Sens.* **2008**, *29*, 1339–1366. [CrossRef]

6.　　Nilsson, M.; Nordkvist, K.; Jonzén, J.; Lindgren, N.; Axensten, P.; Wallerman, J.; Egberth, M.; Larsson, S.; Nilsson, L.; Eriksson, J.; et al. A nationwide forest attribute map of Sweden predicted using airborne laser scanning data and field data from the National Forest Inventory. *Remote Sens. Environ.* **2017**, *194*, 447–454. [CrossRef]

7.　　Næsset, E. Area-based inventory in Norway—From innovation to an operational reality. In *Forestry Applications of Airborne Laser Scanning*; Maltamo, M., Næsset, E., Vauhkonen, J., Eds.; Springer: Dordrecht, The Netherlands, 2014; pp. 215–240.

8.　　Kotivuori, E.; Korhonen, L.; Packalen, P. Nationwide airborne laser scanning based models for volume, biomass and dominant height in Finland. *Silva Fenn* **2016**, *50*, 1–28. [CrossRef]

9.　　Liu, X. Airborne LiDAR for DEM generation: Some critical issues. *Prog. Phys. Geogr. Earth Environ.* **2008**, *32*, 31–49.

10.　Chen, Z.; Gao, B.; Devereux, B. State-of-the-art: DTM generation using airborne LIDAR data. *Sensors* **2017**, *17*, 150. [CrossRef]

11.　Næsset, E. Practical large-scale forest stand inventory using a small-footprint airborne scanning laser. *Scand. J. For. Res.* **2004**, *19*, 164–179. [CrossRef]

12.　Meng, X.; Currit, N.; Zhao, K. Ground filtering algorithms for airborne LiDAR data: A review of critical issues. *Remote Sens.* **2010**, *2*, 833–860. [CrossRef]

13.　Axelsson, P. DEM generation from laser scanner data using adaptive TIN models. In Proceedings of the International Archives of Photogrammetry and Remote Sensing. XIXth ISPRS Congress, Amsterdam, The Netherlands, 16–23 July 2000; Schenk, T., Vosselman, G., Eds.; International Society for Photogrammetry and Remote Sensing: Amsterdam, The Netherlands, 2000; Volume XXXIII, pp. 110–117.

14.　Kraus, K.; Pfeifer, N. Determination of terrain models in wooded areas with airborne laser scanner data. *ISPRS J. Photogramm. Remote Sens.* **1998**, *53*, 193–203. [CrossRef]

15.　Evans, J.S.; Hudak, A.T. A multiscale curvature algorithm for classifying discrete return LiDAR in forested environments. *IEEE Trans. Geosci. Remote Sens.* **2007**, *45*, 1029–1038. [CrossRef]

16.　Zhang, K.; Chen, S.C.; Whitman, D.; Shyu, M.L.; Yan, J.; Zhang, C. A progressive morphological filter for removing nonground measurements from airborne LIDAR data. *IEEE Trans. Geosci. Remote Sens.* **2003**, *41*, 872–882. [CrossRef]

17.　Tinkham, W.T.; Huang, H.; Smith, A.M.S.; Shrestha, R.; Falkowski, M.J.; Hudak, A.T.; Link, T.E.; Glenn, N.F.; Marks, D.G. A Comparison of two open source LiDAR surface classification algorithms. *Remote Sens.* **2011**, *3*, 638–649. [CrossRef]

18.　Silva, C.A.; Klauberg, C.; Hentz, Â.M.K.; Corte, A.P.D.; Ribeiro, U.; Liesenberg, V. Comparing the performance of ground filtering algorithms for terrain modeling in a forest environment using airborne LiDAR data. *Floresta E Ambiente* **2018**, *25*, 1–10. [CrossRef]

19.　Stereńczak, K.; Ciesielski, M.; Balazy, R.; Zawiła-Niedźwiecki, T. Comparison of various algorithms for DTM interpolation from LIDAR data in dense mountain forests. *Eur. J. Remote Sens.* **2016**, *49*, 599–621. [CrossRef]

20.　Sithole, G.; Vosselman, G. Experimental comparison of filter algorithms for bare-Earth extraction from airborne laser scanning point clouds. *ISPRS J. Photogramm. Remote Sens.* **2004**, *59*, 85–101. [CrossRef]

21.　Korzeniowska, K.; Pfeifer, N.; Mandlburger, G.; Lugmayr, A. Experimental evaluation of ALS point cloud ground extraction tools over different terrain slope and land-cover types. *Int. J. Remote Sens.* **2014**, *35*, 4673–4697. [CrossRef]

22.　Polat, N.; Uysal, M. Investigating performance of Airborne LiDAR data filtering algorithms for DTM generation. *Measurement* **2015**, *63*, 61–68. [CrossRef]

23.　White, J.C.; Arnett, J.T.T.R.; Wulder, M.A.; Tompalski, P.; Coops, N.C. Evaluating the impact of leaf-on and leaf-off airborne laser scanning data on the estimation of forest inventory attributes with the area-based approach. *Can. J. For. Res.* **2015**, *45*, 1498–1513. [CrossRef]

24.　Hu, H.; Ding, Y.; Zhu, Q.; Wu, B.; Lin, H.; Du, Z.; Zhang, Y.; Zhang, Y. An adaptive surface filter for airborne laser scanning point clouds by means of regularization and bending energy. *ISPRS J. Photogramm. Remote Sens.* **2014**, *92*, 98–111. [CrossRef]

25. Zhang, K.; Whitman, D. Comparison of three algorithms for filtering airborne LiDAR data. *Photogramm. Eng. Remote Sens.* **2005**, *71*, 313–324. [CrossRef]

26. Montealegre, A.L.; Lamelas, M.T.; de la Riva, J. A comparison of open-source LiDAR filtering algorithms in a Mediterranean forest environment. *IEEE J. Sel. Top. Appl. Earth Obs. Remote Sens.* **2015**, *8*, 4072–4085. [CrossRef]

27. Prodan, M. *Holzmesslehre*; Sauerländer's Verlag: Frankfurt, Germany, 1965.

28. Tomé, M.; Tomé, J.; Ribeiro, F.; Faias, S. Equações de volume total, volume percentual e de perfil do tronco para *Eucalyptus globulus* Labill. em Portugal. *Silva Lusitana* **2007**, *15*, 25–39.

29. Gobakken, T.; Næsset, E. Assessing effects of positioning errors and sample plot size on biophysical stand properties derived from airborne laser scanner data. *Can. J. For. Res.* **2009**, *39*, 1036–1052. [CrossRef]

30. Aderson, J.; Mikhail, E. *Surveying: Theory and Practice*, 7th ed.; McGraw-Hill: New York, NY, USA, 1997.

31. Gonçalves, G.R.; Gomes Pereira, L. A thorough accuracy estimation of DTM produced from airborne full-waveform laser scanning data of unmanaged eucalypt plantations. *IEEE Trans. Geosci. Remote Sens.* **2012**, *50*, 3256–3266. [CrossRef]

32. Hug, C.; Ullrich, A.; Grimm, A. Litemapper-5600—A waveform-digitizing LIDAR terrain and vegetation mapping system. In Proceedings of the ISPRS Working Gorunp VIII/2, Freiburg, Germany, 3–6 October 2004; International Archives of Photogrammetry, Remote Sensing and Spatial Information Sciences. volume 36–8/W2, pp. 24–29.

33. Ferraz, A.; Bretar, F.; Jacquemoud, S.; Gonçalves, G.; Pereira, L.; Tomé, M.; Soares, P. 3-D mapping of a multi-layered Mediterranean forest using ALS data. *Remote Sens. Environ.* **2012**, *121*, 210–223. [CrossRef]

34. McGaughey, R. *FUSION/LDV: Software for LIDAR data analysis and visualization, v3.60+*; Pacific Northwest Research Station, United States Department of Agriculture Forest Service: Corvallis, OR, USA, 2016.

35. R Core Team R: A Language and Environment for Statistical Computing. Available online: https://www.r-project.org/ (accessed on 10 January 2020).

36. Maltamo, M.; Bollandsås, O.M.; Næsset, E.; Gobakken, T.; Packalén, P. Different plot selection strategies for field training data in ALS-assisted forest inventory. *Forestry* **2011**, *84*, 23–31. [CrossRef]

37. Lauri, K.; Jussi, P.; Jukka, M.; Aki, S.; Matti, M.; Petteri, P.; Jyrki, K. The use of airborne laser scanning to estimate sawlog volumes. *Forestry* **2008**, *81*, 499–510. [CrossRef]

38. Jakubowski, M.K.; Guo, Q.; Kelly, M. Tradeoffs between lidar pulse density and forest measurement accuracy. *Remote Sens. Environ.* **2013**, *130*, 245–253. [CrossRef]

39. Guerra-Hernández, J.; Görgens, E.B.; García-Gutiérrez, J.; Rodriguez, L.C.E.; Tomé, M.; González-Ferreiro, E. Comparison of ALS based models for estimating aboveground biomass in three types of Mediterranean forest. *Eur. J. Remote Sens.* **2016**, *49*, 185–204. [CrossRef]

40. Arias-Rodil, M.; Diéguez-Aranda, U.; Álvarez-González, J.G.; Pérez-Cruzado, C.; Castedo-Dorado, F.; González-Ferreiro, E. Modeling diameter distributions in radiata pine plantations in Spain with existing countrywide LiDAR data. *Ann. For. Sci.* **2018**, *75*, 36. [CrossRef]

41. Cosenza, D.N.; Soares, P.; Guerra-Hernández, J.; Pereira, L.; González-Ferreiro, E.; Castedo-Dorado, F.; Tomé, M. Comparing Johnson's SB and Weibull functions to model the diameter distribution of forest plantations through ALS data. *Remote Sens.* **2019**, *11*, 2792. [CrossRef]

42. Silva, A.G.P.; Görgens, E.B.; Campoe, O.C.; Alvares, C.A.; Stape, J.L.; Rodriguez, L.C.E. Assessing biomass based on canopy height profiles using airborne laser scanning data in eucalypt plantations. *Sci. Agric.* **2015**, *72*, 504–512. [CrossRef]

43. Falkowski, M.J.; Evans, J.S.; Martinuzzi, S.; Gessler, P.E.; Hudak, A.T. Characterizing forest succession with lidar data: An evaluation for the Inland Northwest, USA. *Remote Sens. Environ.* **2009**, *113*, 946–956. [CrossRef]

44. Montealegre, A.L.; Lamelas, M.T.; de la Riva, J.; García-Martín, A.; Escribano, F. Use of low point density ALS data to estimate stand-level structural variables in Mediterranean Aleppo pine forest. *Forestry* **2016**, *89*, 373–382. [CrossRef]

45. Roussel, J.-R.; Auty, D.; De Boissieu, F.; Meador, A.S. lidR: Airborne LiDAR Data Manipulation and Visualization for Forestry Applications. Available online: https://cran.r-project.org/package=lidR (accessed on 12 September 2019).

46. Fawcett, D.; Azlan, B.; Hill, T.C.; Kho, L.K.; Bennie, J.; Anderson, K. Unmanned aerial vehicle (UAV) derived structure-from-motion photogrammetry point clouds for oil palm (*Elaeis guineensis*) canopy segmentation and height estimation. *Int. J. Remote Sens.* **2019**, *40*, 7538–7560. [CrossRef]

47. Montealegre, A.L.; Lamelas, M.T.; de la Riva, J. Interpolation routines assessment in ALS-derived digital elevation models for forestry applications. *Remote Sens.* **2015**, *7*, 8631–8654. [CrossRef]

48. García-Gutiérrez, J.; Martínez-Álvarez, F.; Troncoso, A.; Riquelme, J.C. A comparison of machine learning regression techniques for LiDAR-derived estimation of forest variables. *Neurocomputing* **2015**, *167*, 24–31. [CrossRef]

49. Gonçalves-Seco, L.; González-Ferreiro, E.; Diéguez-Aranda, U.; Fraga-Bugallo, B.; Crecente, R.; Miranda, D. Assessing the attributes of high-density *Eucalyptus globulus* stands using airborne laser scanner data. *Int. J. Remote Sens.* **2011**, *32*, 9821–9841. [CrossRef]

50. Görgens, E.B.; Packalen, P.; da Silva, A.G.P.; Alvares, C.A.; Campoe, O.C.; Stape, J.L.; Rodriguez, L.C.E. Stand volume models based on stable metrics as from multiple ALS acquisitions in *Eucalyptus plantations*. *Ann. For. Sci.* **2015**, *72*, 489–498. [CrossRef]

51. Pascual, A.; Bravo, F.; Ordoñez, C. Assessing the robustness of variable selection methods when accounting for co-registration errors in the estimation of forest biophysical and ecological attributes. *Ecol. Modell.* **2019**, *403*, 11–19. [CrossRef]

52. Fassnacht, F.E.; Hartig, F.; Latifi, H.; Berger, C.; Hernández, J.; Corvalán, P.; Koch, B. Importance of sample size, data type and prediction method for remote sensing-based estimations of aboveground forest biomass. *Remote Sens. Environ.* **2014**, *154*, 102–114. [CrossRef]

53. Gregoire, T.G.; Lin, Q.F.; Boudreau, J.; Nelson, R. Regression estimation following the square-root transformation of the response. *For. Sci.* **2008**, *54*, 597–606.

54. Myers, R.H. *Classical and Modern Regression with Applications*; Duxbury Press: Boston, MA, USA, 1989.

55. Fox, J.; Weisberg, S. An R Companion to Applied Regression. Available online: https://socialsciences.mcmaster.ca/jfox/Books/Companion/ (accessed on 12 September 2019).

56. Cosenza, D.N.; Lauri, K.; Matti, M.; Petteri, P.; Strunk, J.L.; Næsset, E.; Gobakken, T.; Soares, P.; Tomé, M. Comparison of linear regression, k-nearest neighbor, and random forest methods in airborne laser scanning based prediction of growing stock. *Forestry*. under review.

57. Wilcoxon, F. Individual comparisons by ranking methods. *Biom. Bull.* **1945**, *1*, 80–83. [CrossRef]

58. Mann, H.B.; Whitney, D.R. On a test of whether one of two random variables is stochastically larger than the other. *Ann. Math. Stat.* **1947**, *18*, 50–60. [CrossRef]

59. Nord-Larsen, T.; Riis-Nielsen, T. Developing an airborne laser scanning dominant height model from a countrywide scanning survey and national forest inventory data. *Scand. J. For. Res.* **2010**, *25*, 262–272. [CrossRef]

60. Tompalski, P.; White, J.C.; Coops, N.C.; Wulder, M.A. Demonstrating the transferability of forest inventory attribute models derived using airborne laser scanning data. *Remote Sens. Environ.* **2019**, *227*, 110–124. [CrossRef]

61. Lim, K.; Hopkinson, C.; Treitz, P. Examining the effects of sampling point densities. *For. Chron.* **2008**, *84*, 876–885. [CrossRef]

62. McRoberts, R.E.; Chen, Q.; Domke, G.M.; Næsset, E.; Gobakken, T.; Chirici, G.; Mura, M. Optimizing nearest neighbour configurations for airborne laser scanning-assisted estimation of forest volume and biomass. *Forestry* **2017**, *90*, 99–111. [CrossRef]

63. Görgens, E.B.; Montaghi, A.; Rodriguez, L.C.E. A performance comparison of machine learning methods to estimate the fast-growing forest plantation yield based on laser scanning metrics. *Comput. Electron. Agric.* **2015**, *116*, 221–227. [CrossRef]

64. Colomina, I.; Molina, P. Unmanned aerial systems for photogrammetry and remote sensing: A review. *ISPRS J. Photogramm. Remote Sens.* **2014**, *92*, 79–97. [CrossRef]

65. Goodbody, T.R.H.; Coops, N.C.; Marshall, P.L.; Tompalski, P.; Crawford, P. Unmanned aerial systems for precision forest inventory purposes: A review and case study. *For. Chron.* **2017**, *93*, 71–81. [CrossRef]

66. Graham, A.; Coops, N.; Wilcox, M.; Plowright, A. Evaluation of ground surface models derived from unmanned aerial systems with digital aerial photogrammetry in a disturbed conifer forest. *Remote Sens.* **2019**, *11*, 84. [CrossRef]

67. Pingel, T.J.; Clarke, K.C.; Mcbride, W.A. An improved simple morphological filter for the terrain classification of airborne LIDAR data. *ISPRS J. Photogramm. Remote Sens.* **2013**, *77*, 21–30. [CrossRef]

68. Wallace, L.; Bellman, C.; Hally, B.; Hernandez, J.; Jones, S.; Hillman, S. Assessing the ability of image based point clouds captured from a UAV to measure the terrain in the presence of canopy cover. *Forests* **2019**, *10*, 284. [CrossRef]

69. Hollaus, M.; Wagner, W.; Eberhöfer, C.; Karel, W. Accuracy of large-scale canopy heights derived from LiDAR data under operational constraints in a complex alpine environment. *ISPRS J. Photogramm. Remote Sens.* **2006**, *60*, 323–338. [CrossRef]

70. Hollaus, M.; Wagner, W.; Maier, B.; Schadauer, K. Airborne laser scanning of forest stem volume in a mountainous environment. *Sensors* **2007**, *7*, 1559–1577. [CrossRef]

71. Lee, H.S.; Younan, N.H. DTM extraction of Lidar returns via adaptive processing. *IEEE Trans. Geosci. Remote Sens.* **2003**, *41*, 2063–2069. [CrossRef]

72. Zhang, W.; Qi, J.; Wan, P.; Wang, H.; Xie, D.; Wang, X.; Yan, G. An sasy-to-use airborne LiDAR data filtering method based on cloth simulation. *Remote Sens.* **2016**, *8*, 501. [CrossRef]

73. Tompalski, P.; Coops, N.C.; White, J.C.; Wulder, M.A. Augmenting site index estimation with airborne laser scanning data. *For. Sci.* **2015**, *61*, 861–873. [CrossRef]

74. Gregoire, T.G.; Næsset, E.; McRoberts, R.E.; Ståhl, G.; Andersen, H.E.; Gobakken, T.; Ene, L.; Nelson, R. Statistical rigor in LiDAR-assisted estimation of aboveground forest biomass. *Remote Sens. Environ.* **2016**, *173*, 98–108. [CrossRef]

75. McRoberts, R.E.; Næsset, E.; Gobakken, T. Inference for lidar-assisted estimation of forest growing stock volume. *Remote Sens. Environ.* **2013**, *128*, 268–275. [CrossRef]

76. Graham, A.N.V.; Coops, N.C.; Tompalski, P.; Plowright, A.; Wilcox, M. Effect of ground surface interpolation methods on the accuracy of forest attribute modelling using unmanned aerial systems-based digital aerial photogrammetry. *Int. J. Remote Sens.* **2020**, *41*, 3287–3306. [CrossRef]

77. Simpson, J.E.; Smith, T.E.L.; Wooster, M.J. Assessment of errors caused by forest vegetation structure in airborne LiDAR-derived DTMs. *Remote Sens.* **2017**, *9*, 1101. [CrossRef]

3 Paper 2: Comparing Johnson's SB and Weibull functions to model the diameter distribution of forest plantations through ALS data

Article

Comparing Johnson's S_B and Weibull Functions to Model the Diameter Distribution of Forest Plantations through ALS Data

Diogo Nepomuceno Cosenza [1,*], **Paula Soares** [1], **Juan Guerra-Hernández** [1,2], **Luísa Pereira** [3,4], **Eduardo González-Ferreiro** [5,6], **Fernando Castedo-Dorado** [6] and **Margarida Tomé** [1]

[1] Centro de Estudos Florestais, Instituto Superior de Agronomia (ISA), Universidade de Lisboa, Tapada da Ajuda, 1349-017 Lisboa, Portugal; paulasoares@isa.ulisboa.pt (P.S.); juanguerra@isa.ulisboa.pt (J.G.-H.); magatome@isa.ulisboa.pt (M.T.)

[2] 3edata, Centro de iniciativas empresariais, Fundación CEL, O Palomar s/n, 27004 Lugo, Spain

[3] Escola Superior de Tecnologia e Gestão de Águeda (ESTGA), Universidade de Aveiro, Apartado 473, 3754-909 Águeda, Portugal; luisapereira@ua.pt

[4] Centro de Investigação em Ciências Geoespaciais (CICGE), Universidade do Porto, 4099-002 Porto, Portugal

[5] Escuela Superior y Técnica de Ingenieros de Minas, Universidad de León, Avda. Astorga s/n, 24401 Ponferrada, Spain; egonf@unileon.es

[6] Escuela de Ingeniería Agraria y Forestal, Universidad de León, Avda. Astorga s/n, 24401 Ponferrada, Spain; fcasd@unileon.es

* Correspondence: dncosenza@isa.ulisboa.pt; Tel.: +351-213-653-309

Abstract: The analysis of the diameter distribution is important for forest management since the knowledge of tree density and growing stock by diameter classes is essential to define management plans and to support operational decisions. The modeling of diameter distributions from airborne laser scanning (ALS) data has been performed through the two-parameter Weibull probability density function (PDF), but the more flexible PDF Johnson's S_B has never been tested for this purpose until now. This study evaluated the performance of the Johnson's S_B to predict the diameter distributions based on ALS data from two of the most common forest plantations in the northwest of the Iberian Peninsula (*Eucalyptus globulus* Labill. and *Pinus radiata* D. Don). The Weibull PDF was taken as a benchmark for the diameter distributions prediction and both PDFs were fitted with ALS data. The results show that the S_B presented a comparable performance to the Weibull for both forest types. The S_B presented a slightly better performance for the *E. globulus*, while the Weibull PDF had a small advantage when applied to the *P. radiata* data. The Johnson's S_B PDF is more flexible but also more sensitive to possible errors arising from the higher number of stand variables needed for the estimation of the PDF parameters.

Keywords: probability density function; LiDAR; remote sensing; forest horizontal structure

1. Introduction

Forest inventory is essential in forest management by providing information to diagnose the stands, which supports decision-makers. The inventories are traditionally based on sampling of field plots, in which tree measures are collected in a time consuming and laborious process. However, the forest mensuration has faced a new paradigm with the improvement of light detection and ranging (LiDAR) tools, especially with airborne laser scanning (ALS), which has the ability to quickly record high-accuracy 3D-data in large areas [1].

One of the most common approaches to performing an ALS forest inventory is the area-based approach (ABA), where metrics are extracted from the normalized height of the LiDAR data cloud (NHD) and used to predict the forest variables [2,3]. The growing stock assessment is the most frequent target of the inventories, but effective forest management often requires information of the timber volume distributed through the diameter at the breast height (dbh, 1.30 m) classes [4] (pp. 261–298). In this case, even though the ABA does not allow detecting tree diameters directly, it enables obtaining the forest stand structure indirectly by using the NHD metrics to estimate probability density functions (PDF) that describe diameter distributions [5].

Earlier studies [6,7] succeeded in incorporating NHD metrics to obtain the diameter distribution of boreal forests using the two-parameter Weibull distribution, especially when applying the parameter recovery approach. Other similar applications of this approach were also used by other researchers [8–10]. Non-parametric techniques, such as k-nearest neighbors [11] or percentiles [12], have also been applied to capture the irregularities in the diameter distribution [13–18]. Despite improving the accuracy, those methods usually do not follow biological principles and are focused on reducing the prediction errors so the interpretation of their results is not straightforward.

As suggested by Gobakken and Næsset [6], Johnson's S_B distribution [19] could be tested to ALS data as an alternative to the Weibull distribution. The S_B is recognized by the scientific community as a highly flexible distribution, since it allows the representation of a large region over the plane of the β_1 and β_2 coefficients, being β_1 the squared skewness and β_2 the kurtosis [20]. This distribution has shown remarkable results when fitted using field data [21–30]. Mateus and Tomé [31] also conducted a large-scale study in Portugal and demonstrated through a skewness–kurtosis analysis that the S_B PDF is the most suitable to represent the diametric distribution of *Eucalyptus globulus* Labill. stands. However, to the best of our knowledge, there are no records of its applications to ALS data.

In this context, this study evaluated the ability of the S_B PDF to predict the diameter distribution of forest plantations through ALS data. The hypothesis is that the Johnson's S_B, due to its flexibility, is more efficient than the Weibull distribution. Two datasets from pure even-aged plantations of *Eucalyptus globulus* Labill. and *Pinus radiata* D. Don. were used to support this study.

2. Materials and Methodology

2.1. Study Areas

The eucalyptus dataset was collected from a 9-km^2 forest area located in northwest Portugal, close to the city of Águeda (Figure 1, left). The area presented variability in its topography, with altitude varying from 70 to 220 m and slope of 2.5–34.2%. Pure even-aged eucalyptus plantations felled every 10–12 years during three rotations were dominant at the landscape, where high forest and coppice forest coexisted in the area. Many stands were multi-layered, with eucalyptus in the upper layer and dense understory occupying the lower layer (see [32,33] for more details).
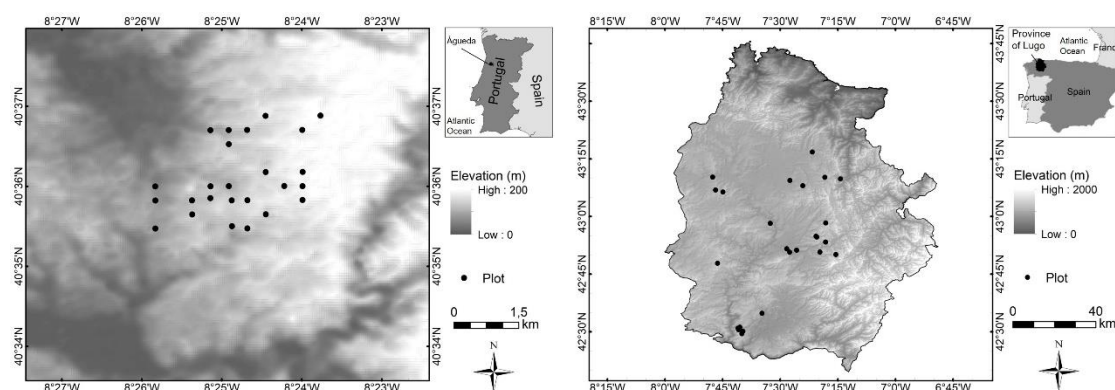

Figure 1. Study areas of: (**left**) eucalyptus stands; and (**right**) pine stands.

The pine dataset was collected over a large area of 9.856 km^2, which represents the main distribution area of *P. radiata* in the province of Lugo (Figure 1, right), located in the Galicia region (northwest Spain). The altitude of most sites ranges 400–750 m and the slopes often exceed 15%. The forests are representative of *P. radiata* stands in NW of the Iberian Peninsula and are thus mainly characterized by high planting-density, low-intensity silvicultural treatments, and the presence of moderate shrub fuel loads (for more details see [34,35]).

2.2. Forest Inventory

The inventory in eucalyptus plantations was carried out between 10 June and 3 July 2008, using 45 circular plots of 400 m^2 that were selected based on systematic sampling, where each plot's center was recorded using a total station and a differential Global Navigation Satellite System (GNSS). All plots covering two different stands or crossed by roads were discarded (20 plots). A total of 25 eucalyptus plots were therefore used in this study (Figure 1, left). All of them were representative of the area regarding the stand composition, structure, and rotation. Field measurements followed the Portuguese National Forest Inventory Field Manual [36]. The dbh was measured for each tree higher than 2 m. In the center of each plot, a 200-m^2 sub-plot was used to measure the heights of all trees higher than 2 m. The missing tree heights of the 400 m^2 plots were estimated using the Prodan's model [37] fitted using the data from their respective subplots. Table 1 presents the summary statistics for the data. More information about the eucalyptus dataset can be found in [33,38].

Table 1. Biometrical descriptions of the field data with their minimum, mean, maximum, and standard deviation (s) values.

Dataset	Variable *	Unit	Minimum	Mean	Maximum	s
Eucalyptus	d_{min}	cm	1.0	2.7	5.0	0.9
	$\overline{d}$	cm	4.8	8.8	13.0	2.3
	d_{max}	cm	10.0	17.5	23.9	4.3
	d_g	cm	5.5	9.6	14.0	2.5
	G	m^2 ha^{-1}	3.9	10.9	21.3	5.2
	N	stems ha^{-1}	875	1454	2343	361
Pine	d_{min}	cm	3.2	8.9	22.8	5.6
	$\overline{d}$	cm	13.5	22.2	38.2	7.6
	d_{max}	cm	25.3	37.9	59.0	10.2
	d_g	cm	14.4	23.3	39.1	7.7
	G	m^2 ha^{-1}	16.7	36.9	68.1	11.0
	N	stems ha^{-1}	393	1009	1820	425

* d_{min}, minimum dbh; $\overline{d}$, mean dbh; d_{max}, maximum dbh; d_g, quadratic mean dbh; G, basal area; N, number of trees per hectare.

The pine field dataset was obtained during the winter of 2009–2010 from two different sources. The first source comprises a network of 10 permanent rectangular plots (600–1000 m^2 area, depending on stand density). The inventory design was focused on obtaining an adequate representation of the existing range of ages, stem densities, and site indices (for details, see [39]). The second source comprises 15 rectangular plots (1000 m^2 area) established for assessing the influence of thinning on crown fire potential. The inventory was designed to represent young and highly stocked stands, as these are usually fire-prone (see [40] for details). For all 25 inventory plots (Figure 1, right), dbh and total tree heights were measured in every tree. In addition, the coordinates of the four corners of each plot were obtained from topographic surveys by using a total station and a differential GNSS.

The individual tree volumes were predicted using allometric equations and summed up to obtain the ground reference value for the plot growing stocks (m^3 ha^{-1}). The equations were provided by Tomé et al. [41] for the eucalyptus dataset and by Diéguez-Aranda et al. [42] for the pine dataset.

All datasets present similar behavior regarding the β_1 and β_2 coefficients computed for the tree dbh within plots (Figure 2). They are mostly spread over the area of the S_B domain, and not over the line of the Weibull distribution. This fact corroborates the higher expectation for S_B over Weibull to obtain diameter distributions for these two species.
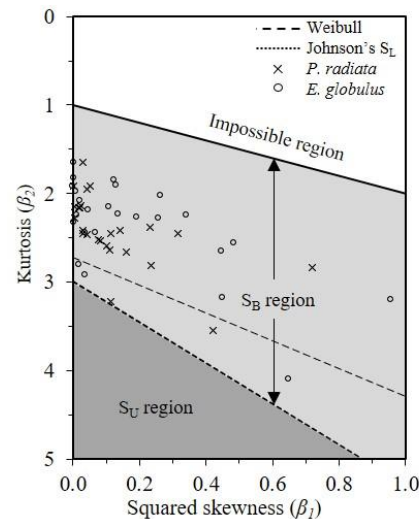

Figure 2. Data dispersion over the β_1 and β_2 coefficients computed for the tree dbh within plots.

2.3. ALS Data Acquisition and Processing

2.3.1. Eucalyptus Data

The LiDAR data covering the *E. globulus* plots were acquired on 14 July 2008, few days after the forest inventory, using a LiteMapper-5600 laser system with the full-waveform hardware RIEGL LMS-Q560. The airplane flew 600 m from the ground at 46.26 m s^{-1}. The parameters of the laser system were 0.5 mrad of beam divergence, ±45° of scan angle, and pulse rate of 150 kHz. The resulted swath was 497 m (60% of overlap) and the point density was 9.5 points m^{-2}. The ALS point clouds were processed using the FUSION software [43]. The ground points were filtered [44] and used to derive a 0.5-m-pixel digital terrain model (DTM) by triangulation. Ground reference measures collected with a differential GNNS were used to assess the vertical accuracy of the DTM (see [33]). The vertical accuracy of the ALS data, given by the root mean squared error (RMSE), was equal to 0.25 m. The DTM was applied to normalize the height data cloud, a process where the points are re-scaled to aboveground elevation. The metrics were computed for each plot considering the points higher than 1 m from the ground. The used metrics are described in Table 2.

2.3.2. Pine Data

The LiDAR data covering the *P. radiata* plots was acquired in a nationwide survey for the PNOA (*Plan Nacional de Ortofotografía de España*) project between 5 September and 29 October 2009, under the direction of the Spanish Ministerio de Fomento (*Dirección General del Instituto Geográfico Nacional* (IGN) and *Centro Nacional de Información Geográfica*–CNIG), using a RIEGL LMS-Q680 sensor operated at 1064 nm. The airplane's average flying height was 1300 m from the ground. The parameters of the laser system were: ±30° of scan angle and pulse rate of 70 kHz. A maximum of 4 returns per pulse was registered, reaching an average point density of 0.47 points m^{-2}. The ALS point clouds were also processed with the FUSION software [43]. The filtered ground points were triangulated to derive a 2 m-pixel DTM, which was used to normalize the point cloud. As reported by the provider (https://pnoa.ign.es/), the vertical accuracy of the ALS data, given by the RMSE, is ≤0.20 m. The set of metrics from the points laid above 1.5 m was extracted for each plot (Table 2).

Table 2. Description of the normalized height data cloud (NHD) metrics.

Metric	Dataset		Description
	Eucal.	**Pine**	
Hmin, Hmean, Hmax	✔	✔	Minimum, mean, and maximum height.
Hmode, Hsd, Hvar, Hcv	✔	✔	Mode, standard deviation, variance height and height's coefficient of variation.
Hiq	✔	✔	Height interquartile amplitude
Hsqew, Hkurt	✔	✔	Height skewness and kurtosis.
Haad	✔	✔	Height average absolute deviation.
Hmad.med, Hmad.mode	✔	✔	Median of the absolute deviations from the overall height median (*Hmad.med*) and mode (*Hmad.mode*).
HL1, HL2, HL3, HL4	✔	✔	Height L moments [45].
HLskew, HLkurt, HLcv	✔	✔	Linear combinations of height L moments (skewness, kurtosis and coefficient of variation).
$h_{01}, h_{05}, h_{10}, h_{20}, h_{25}, h_{30}, h_{40}, h_{50},$ $h_{60}, h_{70}, h_{75}, h_{80}, h_{90}, h_{95}, h_{99}$	✔	✔	Height percentile at 1%, 5%, ... , 99%
Cnp.Ratio	✔	✔	Canopy ratio: (*Hmean* − *Hmin*)/(*Hmax* − *Hmin*).
MeanQuad, MeanCub	✔	✘	Squared and cubic mean.
PercFAT, PercAAT	✔	✔	Percentage of first and all return above the threshold.
PercFAMean, PercAAMode	✔	✔	Percentage of first return above mean and mode.
RatioAAmeanF	✔	✔	Ratio between the first return above mean height and the number of first returns.
RatioAAmodeF	✔	✔	Ratio between the first return above mode height and the number of first returns.
$S_{20}, S_{40}, S_{60}, S_{80}, S_{100}$	✔	✘	S_x is the percentage of points in x layer (e.g., S_{40} is the percentage of points within 20–40% of *Hmax*).

2.4. Fitting of the Distributions

The Johnson's S_B PDF (Equation (1)) originally has four parameters: λ is the scale parameter, responsible for the distribution extension; ε is the location parameter (lower limit); and γ and δ are the shape parameters. Because we are dealing with sampling, a low value for the location parameter is preferable [20,22,46], although the maximum likelihood estimation for this parameter is typically zero or close to zero [28]. For this reason, we set the location parameter to zero ($\varepsilon = 0$).

$$f(x) = \frac{\delta\lambda}{\sqrt{2\pi}(x-\varepsilon)(\varepsilon+\lambda-x)} exp\left\{-\frac{1}{2}\left[\gamma+\delta \ln\left(\frac{x-\varepsilon}{\varepsilon+\lambda-x}\right)\right]^2\right\} \tag{1}$$

$\varepsilon < x < \varepsilon + \lambda, \delta > 0, -\infty < \gamma < \infty, \lambda > 0$, and $\varepsilon \geq 0$; $f(x) = 0$, otherwise.

The adaptation of three approaches were tested to fit this model: (*i*) the method of moments of Scolforo et al. [47] (Table 3); (*ii*) the percentile method of Knoebel and Burkhart [48] (Table 3); and (*iii*) the three-parameter recovery of Parresol [28], described below. These approaches are referred hereafter respectively as "S_B-Moments", "S_B-Percentile", and "S_B-3PR". Other parameter estimation approaches were also considered but previous tests with our dataset showed a poor correlation among the parameters and NHD metrics for our dataset.

Table 3. Johnson's S_B fitting based on methods of moments and percentile.

Method	ε	λ	δ	γ	Inputs
S_B-Moments	0	d_{max}	$\frac{\mu(1-\mu)}{Sd(x)} + \frac{Sd(x)}{4}\left[\frac{1}{\mu(1-\mu)} - 8\right]$	$\delta * \ln\left(\frac{1-\mu}{\mu}\right) + \left(\frac{0.5-\mu}{\delta}\right)$	$d_{max}, d_s, \overline{d}$
S_B-Percentile	0	d_{max}	$\frac{Z_{95\%}}{\ln\left(\frac{d_{95\%}-\varepsilon}{\varepsilon+\lambda-d_{95\%}}\right)-\ln\left(\frac{d_{50\%}-\varepsilon}{\varepsilon+\lambda-d_{50\%}}\right)}$	$-\delta * \ln\left(\frac{d_{50\%}-\varepsilon}{\varepsilon+\lambda-d_{50\%}}\right)$	$d_{max}, d_{95\%}, d_{50\%}$

d_{max}, maximum dbh; $\overline{d}$, mean dbh; $\mu = \frac{\overline{d}-\varepsilon}{\lambda}$; d_s, dbh standard deviation; $Sd(x) = \frac{d_s}{\lambda}$; $Z_{95\%}$, 95% quantile of the standard normal distribution (1.6448); $d_{95\%}$, 95% percentile dbh; $d_{50\%}$, 50% percentile dbh (or median dbh).

The S_B-3PR was performed according to the algorithm of Parresol et al. [49] but adapted in this work to R environment [50] using the *minpack.lm* package [51]. This approach estimates the parameters by solving a system of nonlinear equation using Levenberg–Marquardt optimization. In summary, the 3PR considers d as a particular diameter of the random variable D~SB (λ, ε, γ, δ). Starting from Equation (2), it is possible to establish the property in Equation (3), whose generating function for the r-th non-centered moment $\mu'_r(y)$ is given by Equation (4).

$$y = f(d) = \frac{d - \varepsilon}{\lambda} \tag{2}$$

$$z = \gamma + \delta \ln\left[\frac{y}{1-y}\right] \sim N(0,1) \tag{3}$$

$$\mu'_r(y) = \frac{1}{\sqrt{2\pi}} \int_{-\infty}^{\infty} \left[1 + e^{\frac{\gamma-z}{\delta}}\right]^{-r} e^{-z^2/2}\, dz \tag{4}$$

The PDF parameters are then obtained by solving the system of Equations (5)–(7), where G is basal area (m^2 ha^{-1}), N is tree density (trees ha^{-1}), and $K = \pi/40{,}000$ for the metric system.

$$\gamma = \delta \ln(\lambda/d_{50\%} - 1) \tag{5}$$

$$\bar{d} = \varepsilon + \lambda \mu'_1(y) \tag{6}$$

$$G = KN\left[\varepsilon^2 + 2\,\varepsilon\lambda\mu'_1(y) + \lambda^2\mu'_2(y)\right] \tag{7}$$

The parameter ε is defined a priori; γ is calculated by Equation (5); and λ and δ are obtained iteratively by Equations (6) and (7) from pre-defined values. The starting values for the parameters were $\varepsilon = 0$, $\lambda = d_{max}$, and $\delta = 3$, with 0.8 as lower bound for δ. Note that 3PR uses five inputs defined above: G, N, $d_{50\%}$, $\bar{d}$, and d_{max}.

The two-parameter Weibull (Equation (8)) was applied according to Bailey and Dell [52], where b and c are the shape and scale parameters, respectively, and the fitting was performed through the two-parameter recovered [53,54]. In this process, the inputs $\bar{d}$ and the quadratic mean diameter (d_g) are used to solve Equations (9) and (10) to recover the parameters b and c. Note that this approach uses the two inputs defined above: d_g and $\bar{d}$.

$$f(x) = \left(\frac{c}{b}\right)\left(\frac{x}{b}\right)^{c-1} exp\left(-\left(\frac{x}{b}\right)^c\right) \tag{8}$$

$$\bar{d} = b\,\Gamma\left(1 + \frac{1}{c}\right) \tag{9}$$

$$d_g{}^2 = \frac{\bar{d}^2}{\Gamma^2\left(1 + \frac{1}{c}\right)}\, \Gamma\left(1 + \frac{2}{c}\right) \tag{10}$$

where $\Gamma(.)$ is the Gamma function.

2.5. Estimating the PDF's Inputs

All distributions were fitted using stand variables as inputs in the estimation of the PDF's parameters. These stand variables had to be predicted from the NHD metrics. For each approach, a system of nonlinear models was fitted to provide a consistent prediction of the stand variables for the plots. The variables related to the diameter position were fitted with the following constraints: $d_{max} \geq \bar{d}$ for the S_B-Moment; $d_{max} \geq d_{95\%} \geq d_{50\%}$ for the S_B-Percentile; $d_{max} \geq d_{50\%}$ and $d_{max} \geq \bar{d}$ for the S_B-3PR; and $d_g \geq \bar{d}$ for the Weibull. In the S_B-3PR approach, the additional constraint $N = (40{,}000\,G)/(\pi\,d_g{}^2)$ was added to the system to guarantee the consistency of N and G predictions. All systems are described in Table 4.

Table 4. Equation systems used in the fitting approaches.

Approach	Equation System
S$_B$-Moments	$d_s = exp(XB_1) + \epsilon_1$ $d_{max} = exp(XB_2) + \epsilon_2$ $\bar{d} = d_{max} - exp(XB_3) + \epsilon_3$
S$_B$-Percentile	$d_{max} = exp(XB_1) + \epsilon_1$ $d_{95\%} = d_{max} - exp(XB_2) + \epsilon_2$ $d_{50\%} = d_{95\%} - exp(XB_3) + \epsilon_3$
S$_B$-3PR	$G = exp(XB_1) + \epsilon_1$ $N = exp(XB_2) + \epsilon_2$ $d_{max} = exp(XB_3) + \epsilon_3$ $\bar{d} = d_{max} - exp(XB_4) + \epsilon_4$ $d_{50\%} = d_{max} - exp(XB_5) + \epsilon_5$
Weibull	$d_g = exp(XB_1) + \epsilon_1$ $\bar{d} = d_g - exp(XB_2) + \epsilon_2$

$XB_i = \beta_{i0} + \beta_{i1}x_{i1} + \beta_{i2}x_{i2} + \beta_{i3}x_{i3}$, where x_{ij} and β_{ij} are, respectively, the predictor variables and the parameters j of model i; ϵ_i is the random error of model i.

Each model of the systems uses up to three NHD metrics as predictors, which were selected through an exhaustive search of their respective linearized models. The searching was implemented by fitting all possible combinations of three of the available metrics. The model was chosen following three criteria: (*i*) the lowest value for the relative root mean squared error (RMSE%); (*ii*) all estimated parameters significantly different from zero (*t*-test, α = 5%); and (*iii*) variance inflation factors (VIF) lower than 10 [55]. The VIF, used to avoid collinearity among metrics, was computed with the *car* package [56]. The models that include other stand variables as predictor have their best metrics also found by the exhaustive search using the generic model in Equation (11),

$$\ln(Y_u - Y_l) = \beta_0 + \beta_1 x_1 + \beta_2 x_2 + \beta_3 x_3 + \epsilon \tag{11}$$

where Y_u and Y_l are, respectively, the upper and the lower stand variable, e.g., $Y_u = d_{max}$ and $Y_l = \bar{d}$ for the S$_B$-Moments; β_i is the model parameter $i = 0, \dots, 3$; x_i is the predictor variable $i = 1, \dots 3$; and ϵ is the random error.

After finding the best metrics for the models, each one of the nonlinear systems was fitted simultaneously by the three-stage least-squares method (3SLS, [57]) using the *systemfit* package [58]. The 3SLS combines two-stage least squares (2SLS) and seemingly unrelated regression taking into account the cross-equation errors. Any fitted parameter not significantly different from zero was removed from the model, and the system was refitted.

The system of equations corresponding to the best distribution fitting approach was assessed through the mean deviation (Bias%, 12), the squared Pearson's correlation (r^2) between the observed and predicted values, and the relative root mean squared error (RMSE%, 13) computed through the leave-one-out cross-validation (LOOCV).

$$\text{Bias\%} = 100 \sum_{i=1}^{n} \frac{(y_i - \hat{y}_i)}{n\,\bar{y}} \tag{12}$$

$$\text{RMSE\%} = \frac{100}{\bar{y}} \sqrt{\frac{\sum_{i=1}^{n}(y_i - \hat{y}_i)^2}{n}} \tag{13}$$

where y_i and $\hat{y}_i$ are the observed and estimated value for the plot $i = 1, \dots, n$; and $\bar{y}$ is the observed mean value.

2.6. PDF's Accuracy Assessment

The fitted distributions were assessed using the two-sided Kolmogorov–Smirnov test (KS) under the null hypothesis that the plot data could be a sample from the fitted distribution. However, as the distribution parameters were empirically estimated, the theoretical distribution for each plot is unknown, so that the KS test should be conducted through a Monte Carlo simulation [59]. Therefore, for each plot and fitting approach, we used the fitted parameters to generate 1000 independent and identically pseudo-random samples with a size equal to the number of trees of the corresponding plot. For each sample, we refitted the corresponding distribution to compute the KS statistic. We used the mean of the resultant KS statistics to check (one-sided *t*-test, α = 5%) if it is lower or equal to the critical value of the KS distribution, considering α = 1% due to the small number of trees that could occur inside plots [17,60]. We use the term acceptance hereinafter to refer to not rejecting the null hypothesis of the KS test.

The error index (see [61]) was also applied to verify the accuracy of the fitted diameter distributions to predict the relative frequency in each diameter class (5 cm amplitude). This index is frequently used for this purpose (e.g., [6,10,31]). It was computed through Equation (14) and the values range from 0 to 200, where the fit is more accurate as the index is lower. The index was obtained for each plot (*e*) and averaged for each one of the fitting approaches to obtain the mean index error ($\bar{e}$) for each dataset.

$$e = 100 \sum_{i=1}^{m} \left| f_i - \hat{f}_i \right| \tag{14}$$

where *e* is the plot index error; and f_i and $\hat{f}_i$ are, respectively, the observed and the estimated relative frequency of class *i* = 1, ..., *m*.

The predicted plot growing stock produced by each fitting approach was also compared to the ground reference values using the RMSE%, Bias%, and the paired *t*-test. In this prediction, the respective high-diameter equation fitted by plot (see Section 2.2) was applied to each diameter class, and allometric equations for the individual tree volumes were applied according to the dataset. The fitted probability density functions were used to obtain the number of trees in each class, and then the plot growing stock. However, the tree density (*N*, trees ha^{-1}) was predicted for each plot using an equation fitted with the model $N = \exp(\beta_0 + \beta_1 x_1 + \beta_2 x_2 + \beta_3 x_3) + \epsilon$, where β_i, x_i, and ϵ are defined above. The equation was fitted for each dataset and three metrics were used as a predictor. The metrics were selected through the same exhaustive searching described in Section 2.5 and the model was also assessed by the Bias%, r^2, and RMSE% computed through LOOCV. Finally, a graphical analysis was also conducted over the best PDF fitting approaches to illustrate the previous assessments.

3. Results

As a general result, the S$_B$ presented a comparable performance to the Weibull function in modeling the diameter distributions using ALS data for both forest species. The S$_B$ presented a slightly better performance for the *E. globulus* dataset, especially with the S$_B$-Moments approach, while the Weibull function had a small advantage when applied to the *P. radiata* dataset.

According to the KS test, the S$_B$-Moments was accepted by 72% of the observed plot diameter distributions (Table 5), one plot more than for the Weibull distribution (68%). On the other hand, the Weibull distribution was accepted by 48% of plot distributions in the *P. radiata* dataset, against 36% for the S$_B$-Moments. The S$_B$-3PR had the worst results, with 4% and 8% of acceptance for the *E. globulus* and *P. radiata* datasets, respectively. Another important fact is the higher values of acceptance for the eucalyptus when compared with pine for almost all tested approaches, which suggests that eucalyptus plantations allow for better modeling of the diameter distributions based on ALS data.

The mean error indices (Table 5) showed the lower values for the S$_B$-Percentile on the *E. globulus* dataset ($\bar{e}$ = 26), while the S$_B$-Moments and Weibull presented close values ($\bar{e}$ = 30 and $\bar{e}$ = 31, respectively). In *P. radiata*, however, the lower error occurred for the Weibull distribution ($\bar{e}$ = 42),

followed closely by the S_B-Moments and S_B-Percentile ($\bar{e}$ = 45 for both). The S_B-3PR resulted in the higher mean error indices ($\bar{e}$ = 57 and $\bar{e}$ = 96 for the *E. globulus* and *P. radiata* datasets, respectively). Additionally, as verified for the KS analysis, the error index values were also higher for the *P. radiata* dataset than for *E. globulus* dataset.

Table 5. Acceptances for the KS test (percentage inside the parenthesis) and mean error indices (range inside the parenthesis).

Approach	KS Acceptance				Mean Error Index ($\bar{e}$)			
	E. globulus		*P. radiata*		*E. globulus*		*P. radiata*	
S_B-Moments	18	(72%)	9	(36%)	30	(14–65)	45	(23–96)
S_B-Percentiles	17	(68%)	8	(32%)	26	(2–55)	45	(13–77)
S_B-3PR	1	(4%)	2	(8%)	57	(7–138)	96	(27–163)
Weibull	17	(68%)	12	(48%)	31	(12–53)	42	(12–88)

KS acceptance indicates the null hypothesis of the KS test was not rejected.

The results regarding the growing stock prediction for each distribution followed the previous analysis for the *E. globulus* dataset and slightly different for the *P. radiata* dataset (Table 6). For the eucalyptus, the S_B-Moments was the most accurate and the least biased, with RMSE% and Bias% equal to 21% and −0.8%, respectively. The Weibull approach was slightly less accurate and more biased, with RMSE% equal to 22% and −2% for Bias%, respectively. Besides, the paired *t*-test showed that all tested approaches were able to predict the growing stock without significant difference from the ground reference values, including for the S_B-3PR. In the *P. radiata* dataset, the Weibull was the most accurate approach (RMSE% = 24%) and, differently from the previous analysis, the S_B-3PR was the second most accurate (RMSE% = 28%). However, these two approaches were the most biased (Bias% equal to −16% and −12%, respectively), while the S_B-Moments was the least biased (−7%). Likely, the paired *t*-test did not show a significant difference among observed and predicted values.

Table 6. Accuracy of the growing stock (V, m^3 ha^{-1}) estimation through the fitted distributions.

Approach	*E. globulus* Data			*P. radiata* Data		
	RMSE%	Bias%	t-statistic	RMSE%	Bias%	t-statistic
S_B-Moments	21%	−0.8%	−0.22 [ns]	35%	−7%	−0.95 [ns]
S_B-Percentiles	24%	−2.9%	−0.69 [ns]	43%	−10%	−1.35 [ns]
S_B-3PR	27%	0.9%	0.18 [ns]	28%	−16%	−1.72 [ns]
Weibull	22%	−2.0%	−0.65 [ns]	24%	−12%	−1.81 [ns]

Paired *t*-test, where *ns* means non-significant at α = 5%.

Those facts suggest that possible inefficiencies of an approach in estimating the diameter distribution do not necessarily harm its accuracy for growing stock predictions. One explanation for that is the error related to the *N* prediction (Table 7), which accumulates to the PDF estimation error. Additionally, since the individual tree volume grows exponentially with its diameter, small errors in the distribution could have a lower or higher effect in the growing stock prediction depending on the dbh classes where they occur. For this reason, the S_B-Moments could be considered as a suitable approach for the growing stock analysis in both datasets, since it presented a relatively good accuracy (RMSE% = 21% for *E. globulus* and RMSE% = 35% for *P. radiata*) and the lowest Bias%.

Since the S_B-Moments and Weibull presented good results for most accuracy assessments, their respective systems of equations are presented in Table 7. Both systems presented relatively good accuracy for their equations, with RMSE% lower than 16%, high r^2 (0.77–0.93) and a low Bias% (<3%, in absolute values). Examples of the diameter distributions produced by each of those approaches are

presented in Figures 3 and 4. The distributions over the *E. globulus* dataset showed that the S_B-Moments predictions are close to the observed frequencies for all exemplified plots (Figure 3). This fact is confirmed by their respective error indices, where the lowest values are obtained for the S_B-Moments, reflecting in smaller discrepancies than for the Weibull. As shown for the *P. radiata* dataset (Figure 4), the observed distributions are more complex and less smooth, with abrupt differences between the frequencies of consecutive dbh classes (e.g., Plots 2 and 3 in Figure 4). This fact explains the lower quality of the indicator values when assessing the distribution fittings. Nevertheless, the Weibull and S_B were able to reproduce those distributions satisfactorily, with a small advantage for the Weibull in most cases (e.g., Plots 1, 3, and 4 in Figure 4).

Table 7. Fitted equations with their respective accuracy assessment.

Approach	Variable	E. globulus Dataset					P. radiata Dataset				
		Predictor	b_i	RMSE%	Bias%	r^2	Predictor	b_i	RMSE%	Bias%	r^2
-	N	Constant	9.054	19%	−3%	0.56	Constant	7.210	30%	−9%	0.61
		Hcv	−3.149				h_{90}	−0.030			
		h_{25}	−0.076				$PercAAT$	0.027			
		$PercFAMode$	0.011				$RatioAAmeanF$	−0.034			
S_B-Moments	d_s	Constant	0.865	16%	−3%	0.81	Constant	2.284	16%	−2%	0.77
		$Hmad.mode$	−0.025				$hmean$	0.041			
		$Cnp.Ratio$	−1.347				h_{01}	−0.048			
		$MeanCub$	0.105				$Cnp.Ratio$	−1.421			
	d_{max}	Constant	1.924	12%	−1%	0.83	Constant	2.962	8%	−1%	0.93
		Hsd	0.137				$Hmin$	0.033			
		h_{10}	0.048				$Hmad.med$	0.149			
		S_{60}	0.024				$HL4$	0.585			
	d_{max}			15%	−1%	0.83	d_{max}		18%	−2%	0.82
		Constant	1.731				Constant	2.530			
		$Hmode$	0.028				h_{05}	−0.076			
		$PercAAMode$	0.021				h_{10}	0.047			
		str_{40}	−0.049				$PercAAMode$	0.009			
Weibull		Constant	1.044	10%	<1%	0.89	Constant	2.483	14%	−2%	0.84
		Hsd	0.164				h_{90}	0.037			
		h_{10}	0.060				$PercAAT$	−0.010			
		S_{60}	0.043				$RatioAAmodeF$	0.013			
				11%	<1%	0.86			16%	−2%	0.82
		Constant	−0.304				Constant	1.624			
		$Hsqew$	−0.268				h_{01}	−0.105			
							h_{10}	0.059			
							$Cnp.Ratio$	−2.992			

RMSE% computed through LOOCV (see Section 2.5).

4. Discussion

This work performed a novel study by evaluating the capability of Johnson's S_B to predict diameter distributions based on ALS data from two of the most common species used for forest plantations in the Iberian Peninsula: *E. globulus* and *P. radiata*. The results were different among the datasets, where the distributions resulted in better indicators when fitted over the *E. globulus* dataset. A plausible explanation for this difference is the distinction between the structure of the two forests and the adopted scanning properties. The eucalyptus ALS-data collection aimed at forest inventory while the pine flight was planned to produce high-resolution DTM for general applications in the country. Nationwide data have been applied to many forest-oriented studies, showing promising results in, e.g., Finland [62,63], Sweden [64], and Denmark [65]. Likewise, the Spanish survey proved to be a consistent data source for different forest applications [34,66–70]. However, nationwide ALS surveys are planned to reduce the flight costs so they present non-optimum scanning parameters for forest inventory, generally deriving low-density point clouds [71]. It is known that this characteristic has a negative impact on the forest modeling [72,73], so it is plausible that the models related to pine dataset have been influenced by the characteristics of the point density when compared to the ones derived from eucalyptus dataset.
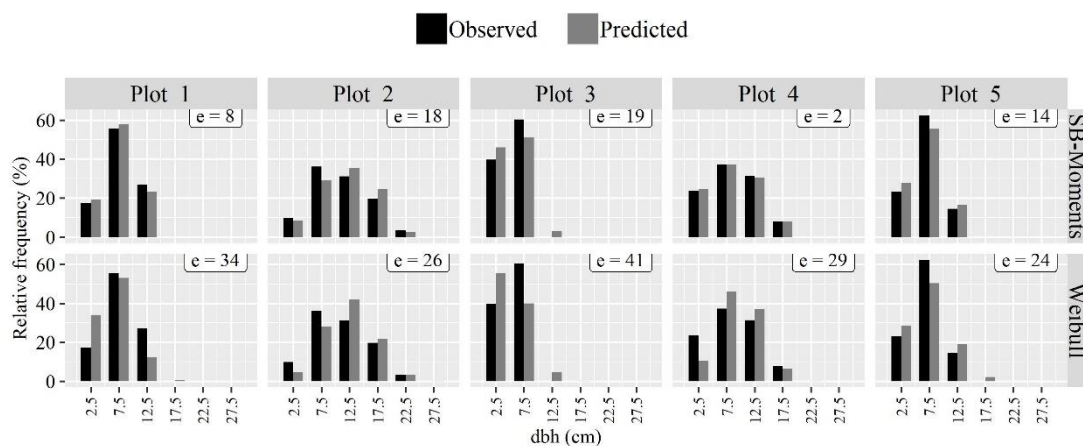
Figure 3. S$_B$-Moments and Weibull distributions and error indices (*e*) for five plots of the eucalyptus dataset.
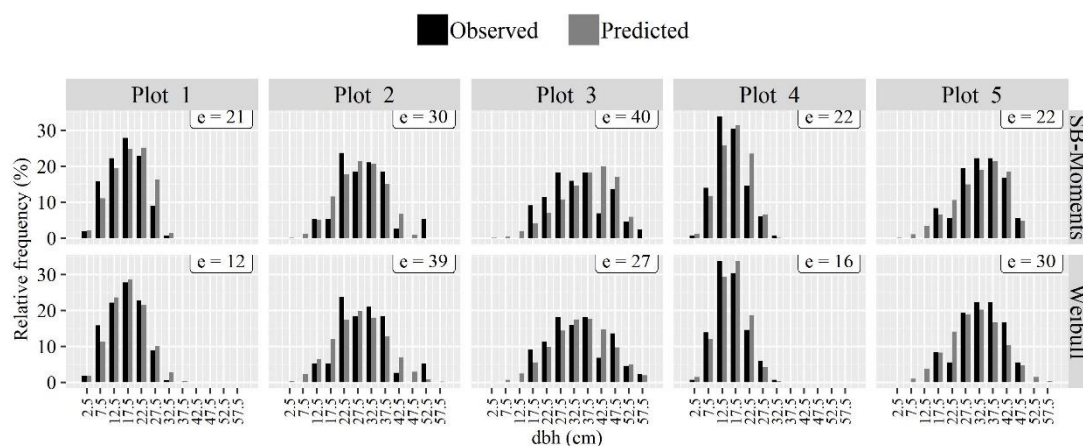

Figure 4. S$_B$-Moments and Weibull diameter and error indices (*e*) for five plots of the pine dataset.

The pine dataset is located in a larger and more complex terrain when compared to the eucalyptus area (see Section 2.1). Thus, it is reasonable to consider this difference as a possible error source for the models since the terrain slope has a well-known influence on the accuracy of the ALS-derived DTM (e.g., [74,75]). However, the ABA has been commonly applied in steeped slopes with success (e.g., [76,77]) so it is not clear that the terrain complexity affects the forest models. Furthermore, the accuracy of the ALS surveys was relatively low (RMSE ≤ 0.25 m) so it is unlikely that the variation in the terrain had caused significant impact in the forest attribute predictions.

The S$_B$ was highly sensitive to the input variables. Because of that, small deviations in the input predictions can result in changes in the parameters of the dbh distribution since they are interdependent in the fitting approaches (see Section 2.6). Therefore, the prediction errors can accumulate and affect the distribution even if the fitted equations have good performance. An example of those facts can be seen for S$_B$-3PR, which uses five stand variables as inputs in the parameter estimation and resulted in the worst performance for almost all assessments. On the other hand, the S$_B$-Moments and the S$_B$-Percentile use three stand variables each, while the Weibull has the advantage of using just two.

Each work involving the prediction of diameter distributions from ALS data has its particularities regarding the forest type, prediction approaches, or assessments, thus the comparative analysis among them is not straightforward. An exception is the work of Arias-Rodil [34], which used the same *P. radiata* dataset and LiDAR flight to estimate the diameter distribution through the two-parameter Weibull fitted also through parameter recovery approach. Our results show considerable improvement in relation to the Weibull distribution fitting; the acceptance by the KS test changes from 28% to 48% among plots. This fact was the result of the better equations to predict the stand variables used as

predictors to estimate the distribution's parameters, which use not two but up to three NHD metrics. If the S_B is taken into account, it is also considered as an improvement in the distribution's prediction since it presented higher acceptance according to Arias-Rodil's baseline, with 36% for the S_B-Moments.

Considering the best approaches of our work (S_B-Moments and Weibull), the mean error indices found could be considered low if compared to the literature. Maltamo et al. [10] found error index values of 50–60 for hybrid eucalyptus (*E. urophilla* x *E. grandis*) in Brazil using the two-parameter Weibull model. Other works involving boreal forests reported average indices varying 75–95 ("*error2*" of Maltamo et al. [18] [Editor1]), 30–45 for diameter and basal area distributions [6], and 49–87 for just basal area distributions [7]. However, it should be highlighted that our dataset consists of homogeneous stands, thus, despite their variable structure, a lower modeling error was already expected.

According to the assessment through the growing stock prediction, the S_B-Moments presented a good indicator for the *E. globulus* data, where it performed slightly better than the Weibull. The Bias% of these estimations ($\leq 2.0\%$, in absolute value) were comparable to the ones found by Gobakken and Næsset [6,7] [Editor2], with values below 4.8%, in absolute value. However, the Bias% values could be considered high in the case of the *P. radiata* data, varying 7–18% (in absolute value) for all approaches, although many of them presented reasonable RMSE% values and no significative differences between the predicted and ground reference values according to the paired *t*-test.

The deviations related to the *N* prediction are another source of error for the growing stock prediction assessment. The *N* is frequently reported as being one of the most difficult forest variables to be modeled from ALS data. In the related literature, it is common to find coefficients of determination (R^2, adjusted or not) of 0.50–0.82 in models with up to six metrics (e.g., [2,3,78]). One of the few studies with *E. globulus* plantations showed a low accuracy for the *N* equation ($R^2 = 0.49$), using 4 points m^{-2} ALS data [79]. Woods et al. [80] suggested that this difficulty in modeling *N* could be bypassed if a high-point-density scanning is used. In our case, the *E. globulus* dataset has a relatively high density (9.5 points m^{-2}) and the equation for the *N* was the least accurate, although its use is no longer discouraged. The *N* fitting for the *P. radiata* data, otherwise, presented a better accuracy even with a low pulse density (0.47 points m^{-2}). In the case of availability of the tree density values of the stands, they could be applied to improve the growing stock prediction. Additionally, the modeling approaches could benefit from multisource data, such as multispectral images or multispectral ALS, which would contribute to improving predictions of the stand variables used as inputs in the estimation of the PDFs' parameters.

The model transferability (see [77]) was not evaluated in this work so our results do not allow us to conclude about the efficiency of the models to predict attributes in stands from other regions. However, the models were developed using heterogeneous datasets in terms of stand age, density, and site index, and were assessed using a robust analysis. These features suggest that the developed models could be applied to *E. globulus* and *P. radiata* stands in the Iberian Peninsula. In the case of the absence of validation datasets to confirm such hypothesis, the replication of our methodology is recommended when the goal is to study different areas. Finally, this work filled the knowledge gap involving the Johnson's S_B distribution and ALS approach and demonstrated that it allows obtaining accurate information about the forest horizontal structure to support decisions in forest management.

5. Conclusions

This work assessed the ability of the Johnson's S_B and Weibull PDFs to model the diameter distributions of *E. globulus* and *P. radiata* plantations. In the studied areas, the S_B-Moments was the best approach to fit the S_B, while the S_B-3PR was the one providing the worse results. The performance of the S_B was comparable to the Weibull, presenting small advantages when applied to *E. globulus* data. S_B is very sensitive to the errors related to the predicted stand variables used to estimate the distribution parameters, so very accurate equations are required for their predictions.

Author Contributions: Conceptualization, D.N.C., P.S., and M.T.; Methodology, D.N.C., P.S., and M.T.; Data Analysis, D.N.C., P.S., M.T., J.G.-H., L.P., E.G.-F., and F.C.-D.; Investigation, D.N.C., P.S., M.T., and J.G.-H.;

References

1.　Wulder, M.A.; White, J.C.; Nelson, R.F.; Næsset, E.; Ørka, H.O.; Coops, N.C.; Hilker, T.; Bater, C.W.; Gobakken, T. Lidar sampling for large-area forest characterization: A review. *Remote. Sens. Environ.* **2012**, *121*, 196–209. [CrossRef]

2.　Næsset, E. Predicting forest stand characteristics with airborne scanning laser using a practical two-stage procedure and field data. *Remote Sens. Environ.* **2002**, *80*, 88–99. [CrossRef]

3.　Næsset, E. Practical large-scale forest stand inventory using a small-footprint airborne scanning laser. *Scand. J. For. Res.* **2004**, *19*, 164–179. [CrossRef]

4.　Burkhart, H.E.; Tomé, M. *Modeling Forest Trees and Stands*; Springer: Dordrecht, The Netherlands, 2012.

5.　Maltamo, M.; Gobakken, T. Predicting tree diameter distributions. In *Forestry Applycations of Airborne Laser Scanning: Concepts and Case Studies*; Maltamo, M., Næsset, E., Vauhkonen, J., Eds.; Managing Forest Ecosystems; Springer: Dordrecht, The Netherlands, 2014; Volume 27, pp. 177–191.

6.　Gobakken, T.; Næsset, E. Estimation of diameter and basal area distributions in coniferous forest by means of airborne laser scanner data. *Scand. J. For. Res.* **2004**, *19*, 529–542. [CrossRef]

7.　Gobakken, T.; Næsset, E. Weibull and percentile models for lidar-based estimation of basal area distribution. *Scand. J. For. Res.* **2005**, *20*, 490–502. [CrossRef]

8.　Maltamo, M.; Suvanto, A.; Packalén, P. Comparison of basal area and stem frequency diameter distribution modelling using airborne laser scanner data and calibration estimation. *For. Ecol. Manag.* **2007**, *247*, 26–34. [CrossRef]

9.　Breidenbach, J.; Gläser, C.; Schmidt, M. Estimation of diameter distributions by means of airborne laser scanner data. *Can. J. For. Res.* **2008**, *38*, 1611–1620. [CrossRef]

10.　Maltamo, M.; Mehtätalo, L.; Valbuena, R.; Vauhkonen, J.; Packalen, P. Airborne laser scanning for tree diameter distribution modelling: A comparison of different modelling alternatives in a tropical single-species plantation. *Forestry* **2018**, *91*, 121–131. [CrossRef]

11.　Dudani, S.A. The distance-weighted k-nearest-neighbor rule. *IEEE Trans. Syst. Man. Cybern.* **1976**, 325–327. [CrossRef]

12.　Borders, B.E.; Souter, R.A.; Bailey, R.L.; Ware, K.D. Percentile-based distributions characterize forest stand tables. *For. Sci.* **1987**, *33*, 570–576.

13.　Bollandsås, O.M.; Næsset, E. Estimating percentile-based diameter distributions in uneven-sized Norway spruce stands using airborne laser scanner data. *Scand. J. For. Res.* **2007**, *22*, 33–47. [CrossRef]

14.　Packalén, P.; Maltamo, M. Estimation of species-specific diameter distributions using airborne laser scanning and aerial photographs. *Can. J. For. Res.* **2008**, *38*, 1750–1760. [CrossRef]

15.　Maltamo, M.; Malinen, J.; Packalén, P.; Suvanto, A.; Kangas, J. Nonparametric estimation of stem volume using airborne laser scanning, aerial photography, and stand-register data. *Can. J. For. Res.* **2006**, *36*, 426–436. [CrossRef]

16.　Xu, Q.; Hou, Z.; Maltamo, M.; Tokola, T. Calibration of area based diameter distribution with individual tree based diameter estimates using airborne laser scanning. *ISPRS J. Photogramm. Remote Sens.* **2014**, *93*, 65–75. [CrossRef]

17. Siipilehto, J.; Lindeman, H.; Vastaranta, M.; Yu, X.; Uusitalo, J. Reliability of the predicted stand structure for clear-cut stands using optional methods: Airborne laser scanning-based methods, smartphone-based forest inventory application Trestima and pre-harvest measurement tool EMO. *Silva Fenn.* **2016**, *50*. [CrossRef]

18. Maltamo, M.; Næsset, E.; Bollandsås, O.M.; Gobakken, T.; Packalén, P. Non-parametric prediction of diameter distributions using airborne laser scanner data. *Scand. J. For. Res.* **2009**, *24*, 541–553. [CrossRef]

19. Johnson, N.L. Systems of frequency curves generated by methods of translation. *Biometrika* **1949**, *36*, 149. [CrossRef]

20. Hafley, W.L.; Schreuder, H.T. Statistical distributions for fitting diameter and height data in even-aged stands. *Can. J. For. Res.* **1977**, *7*, 481–487. [CrossRef]

21. Barra, O.S.V.; Sanquetta, C.R.; Arce, J.E.; do Machado, S.A.; Corte, A.P.D. Proposta metodológica para o ajuste ótimo da distribuição diamétrica SB de Johnson. *Rev. Árvore* **2011**, *35*, 151–156. [CrossRef]

22. Fonseca, T.F.; Marques, C.P.; Parresol, B.R. Describing maritime pine diameter distributions with Johnson's SB distribution using a new all-parameter recovery approach. *For. Sci.* **2009**, *55*, 367–373.

23. Gorgoso, J.J.; Rojo, A.; Cámara-Obregón, A.; Diéguez-Aranda, U. A comparison of estimation methods for fitting Weibull, Johnson's S$_B$ and beta functions to *Pinus pinaster*, *Pinus radiata* and *Pinus sylvestris* stands in northwest Spain. *For. Syst.* **2012**, *21*, 446–459.

24. Kiviste, A.; Nilson, A.; Hordo, M.; Merenäkk, M. Diameter distribution models and height–diameter equations for Estonian forests. In *Modelling Forest System*; Amaro, A., Reed, D., Soares, P., Eds.; CABI: Wallingford, UK, 2003; p. 416.

25. Kudus, K.A.; Ahmad, M.I.; Lapongan, J. Nonlinear regression approach to estimating Johnson SB parameters for diameter data. *Can. J. For. Res.* **1999**, *29*, 310–314. [CrossRef]

26. De Moraes e Silva, V.S.; Soares, T.S.; Colpini, C.; Travagin, D.P.; Hosokawa, R.T.; Scolforo, J.R.S. *Eucalyptus camaldulensis* Dehnh. yield projection using johnson S$_B$ distribution. *Rev. Árvore* **2009**, *33*, 853–863.

27. Palahí, M.; Pukkala, T.; Blasco, E.; Trasobares, A. Comparison of beta, Johnson's SB, Weibull and truncated Weibull functions for modeling the diameter distribution of forest stands in Catalonia (north-east of Spain). *Eur. J. For. Res.* **2007**, *126*, 563–571. [CrossRef]

28. Parresol, B.R. *Recovering parameters of Johnson's S$_B$ distribution*; U.S. Department of Agriculture (USDA) Forest Service, Southern Research Station: Asheville, NC, USA, 2003.

29. Rennolls, K.; Wang, M. A new parameterization of Johnson's S$_B$ distribution with application to fitting forest tree diameter data. *Can. J. For. Res.* **2005**, *35*, 575–579. [CrossRef]

30. Zhou, B.; McTague, J.P. Comparison and evaluation of five methods of estimation of the Johnson system parameters. *Can. J. For. Res.* **1996**, *26*, 928–935. [CrossRef]

31. Mateus, A.; Tomé, M. Modelling the diameter distribution of eucalyptus plantations with Johnson's S$_B$ probability density function: Parameters recovery from a compatible system of equations to predict stand variables. *Ann. For. Sci.* **2011**, *68*, 325–335. [CrossRef]

32. Ferraz, A.; Mallet, C.; Jacquemoud, S.; Goncalves, G.R.; Tome, M.; Soares, P.; Pereira, L.G.; Bretar, F. Canopy density model: A new ALS-derived product to generate multilayer crown cover maps. *IEEE Trans. Geosci. Remote Sens.* **2015**, *53*, 6776–6790. [CrossRef]

33. Gonçalves, G.R.; Pereira, L.G. A thorough accuracy estimation of DTM produced from airborne full-waveform laser scanning data of unmanaged eucalypt plantations. *IEEE Trans. Geosci. Remote Sens.* **2012**, *50*, 3256–3266. [CrossRef]

34. Arias-Rodil, M.; Diéguez-Aranda, U.; Álvarez-González, J.G.; Pérez-Cruzado, C.; Castedo-Dorado, F.; González-Ferreiro, E. Modeling diameter distributions in radiata pine plantations in Spain with existing countrywide LiDAR data. *Ann. For. Sci.* **2018**, *75*, 36. [CrossRef]

35. Castedo-Dorado, F.; Gómez-Vázquez, I.; Fernandes, P.M.; Crecente-Campo, F. Shrub fuel characteristics estimated from overstory variables in NW Spain pine stands. *For. Ecol. Manage.* **2012**, *275*, 130–141. [CrossRef]

36. Autoridade Florestal Nacional. *Instruções para o Trabalho de Campo do Inventário Florestal Nacional—IFN 2005/2006*; Direção de Unidade de Gestão Florestal, Divisão para a Intervenção Florestal: Lisboa, Portugal, 2009.

37. Prodan, M. *Holzmesslehre*; Sauerländer's Verlag: Frankfurt, Germany, 1965.

38. Ferraz, A.; Bretar, F.; Jacquemoud, S.; Gonçalves, G.; Pereira, L.; Tomé, M.; Soares, P. 3-D mapping of a multi-layered Mediterranean forest using ALS data. *Remote Sens. Environ.* **2012**, *121*, 210–223. [CrossRef]

39. Castedo-Dorado, F.; Diéguez-Aranda, U.; Álvarez-González, J.G. A growth model for *Pinus radiata* D. Don stands in north-western Spain. *Ann. For. Sci.* **2007**, *64*, 453–465. [CrossRef]

40. Gómez-Vázquez, I.; Crecente-Campo, F.; Diéguez-Aranda, U.; Castedo-Dorado, F. Modelling canopy fuel variables in *Pinus pinaster* Ait. and *Pinus radiata* D. Don stands in northwestern Spain. *Ann. For. Sci.* **2013**, *70*, 161–172. [CrossRef]

41. Tomé, M.; Tomé, J.; Ribeiro, F.; Faias, S. Equações de volume total, volume percentual e de perfil do tronco para *Eucalyptus globulus* Labill. em Portugal. *Silva Lusit.* **2007**, *15*, 25–39.

42. Diéguez-Aranda, U.; Alboreca, A.R.; Castedo-Dorado, F.; González, J.G.Á.; Barrio-Anta, M.; Crecente-Campo, F.; González, J.M.G.; Pérez-Cruzado, C.; Soalleiro, R.R.; López-Sánchez, C.A.; et al. *Herramientas selvícolas para la gestión forestal sostenible en Galicia*; Dirección Xeral de Montes, Xunta de Galicia; Tórculo Artes Gráficas, S.A: Lugo, Spain, 2009.

43. McGaughey, R. FUSION/LDV: Software for LIDAR data analysis and visualization, v3.60+. *United States Dep. Agric. For. Serv. Pacific Northwest Res. Stn.* **2018**, 211.

44. Kraus, K.; Pfeifer, N. Determination of terrain models in wooded areas with airborne laser scanner data. *ISPRS J. Photogramm. Remote Sens.* **1998**, *53*, 193–203. [CrossRef]

45. Wang, Q.J. Direct sample estimators of L moments. *Water Resour. Res.* **1996**, *32*, 3617–3619. [CrossRef]

46. Siipilehto, J.; Sarkkola, S.; Mehtätalo, L. Comparing regression estimation techniques when predicting diameter distributions of scots pine on drained peatlands. *Silva Fenn.* **2007**, *41*, 333–349. [CrossRef]

47. Scolforo, J.R.S.; Tabai, F.C.V.; de Macedo, R.L.G.; Acerbi, F.W.; de Assis, A.L. SB distribution's accuracy to represent the diameter distribution of *Pinus taeda*, through five fitting methods. *For. Ecol. Manage.* **2003**, *175*, 489–496. [CrossRef]

48. Knoebel, B.; Burkhart, H. A bivariate distribution approach to modeling forest diameter distributions at two points in time. *Biometrics* **1991**, *47*, 241–253. [CrossRef]

49. Parresol, B.R.; Fonseca, T.; Marques, C. *Numerical details and SAS programs for parameter recovery of the SB distribution*; Res. Pap. SRS–122; U.S. Department of Agriculture (USDA) Forest Service, Southern Research Station: Asheville, NC, USA, 2010.

50. R Core Team R: A Language and Environment for Statistical Computing. Available online: https://www.r-project.org/ (accessed on 12 September 2019).

51. Elzhov, T.V.; Mullen, K.M.; Spiess, A.-N.; Bolker, B. minpack.lm: R Interface to the Levenberg-Marquardt Nonlinear Least-squares Algorithm Found in MINPACK, Plus Support for Bounds. Available online: https://cran.r-project.org/package=minpack.lm (accessed on 12 September 2019).

52. Bailey, R.L.; Dell, R. Quantifying diameter distributions with the weibull function. *For. Sci.* **1972**, *19*, 97–104.

53. Newby, M.J. The properties of moment estimators for the weibull distribution based on the sample Coefficient of Variation. *Technometrics* **1980**, *22*, 187. [CrossRef]

54. Burk, T.E.; Newberry, J.D. Notes: A simple algorithm for moment-based recovery of weibull distribution parameters. *For. Sci.* **1984**, *30*, 329–332.

55. Myers, R.H. *Classical and Modern Regression with Applications*; Duxbury Press: Boston, MA, USA, 1989.

56. Fox, J.; Weisberg, S. An R Companion to Applied Regression. Available online: https://socialsciences.mcmaster.ca/jfox/Books/Companion/ (accessed on 12 September 2019).

57. Zellner, A.; Theil, H. Three-stage least squares: Simultaneous estimation of simultaneous equations. *Econometrica.* **1962**, *30*, 54–78. [CrossRef]

58. Henningsen, A.; Hamann, J.D. Systemfit: A package for estimating systems of simultaneous equations in R. *J. Stat. Softw.* **2007**, *23*, 1–40. [CrossRef]

59. Lilliefors, H.W. On the Kolmogorov-Smirnov test for normality with mean and variance unknown. *J. Am. Stat. Assoc.* **1967**, *62*, 399–402. [CrossRef]

60. Siipilehto, J. A comparison of two parameter prediction methods for stand structure in Finland. *Silva Fenn.* **2000**, *34*, 331–349. [CrossRef]

61. Reynolds, M.R.; Burk, T.E.; Huang, W.-C. Goodness-of-fit tests and model selection procedures for diameter distribution models. *For. Sci.* **1988**, *34*, 373–399.

62. Kotivuori, E.; Korhonen, L.; Packalen, P. Nationwide airborne laser scanning based models for volume, biomass and dominant height in Finland. *Silva Fenn.* **2016**, *50*, 1–28. [CrossRef]

63. Kotivuori, E.; Maltamo, M.; Korhonen, L.; Packalen, P. Calibration of nationwide airborne laser scanning based stem volume models. *Remote Sens. Environ.* **2018**, *210*, 179–192. [CrossRef]

64.　Nilsson, M.; Nordkvist, K.; Jonzén, J.; Lindgren, N.; Axensten, P.; Wallerman, J.; Egberth, M.; Larsson, S.; Nilsson, L.; Eriksson, J. A nationwide forest attribute map of Sweden predicted using airborne laser scanning data and field data from the National Forest Inventory. *Remote Sens. Environ.* **2017**, *194*, 447–454. [CrossRef]

65.　Nord-Larsen, T.; Riis-Nielsen, T. Developing an airborne laser scanning dominant height model from a countrywide scanning survey and national forest inventory data. *Scand. J. For. Res.* **2010**, *25*, 262–272. [CrossRef]

66.　Guerra-Hernández, J.; Tomé, M.; González-Ferreiro, E. Using low density LiDAR data to map Mediterranean forest characteristics by means of an area-based approach and height threshold analysis. *Rev. Teledetección* **2016**, 103–107.

67.　González-Ferreiro, E.; Arellano-Pérez, S.; Castedo-Dorado, F.; Hevia, A.; Vega, J.A.; Vega-Nieva, D.; Álvarez-González, J.G.; Ruiz-González, A.D. Modelling the vertical distribution of canopy fuel load using national forest inventory and low-density airbone laser scanning data. *PLoS ONE* **2017**, *12*, e0176114. [CrossRef]

68.　Montealegre, A.L.; Lamelas, M.T.; de la Riva, J.; García-Martín, A.; Escribano, F. Use of low point density ALS data to estimate stand-level structural variables in Mediterranean Aleppo pine forest. *Forestry* **2016**, *89*, 373–382. [CrossRef]

69.　Montealegre, A.; Lamelas, M.; Tanase, M.; de la Riva, J. Forest fire severity assessment using ALS data in a mediterranean environment. *Remote Sens.* **2014**, *6*, 4240–4265. [CrossRef]

70.　González-Ferreiro, E.; Diéguez-Aranda, U.; Crecente-Campo, F.; Barreiro-Fernández, L.; Miranda, D.; Castedo-Dorado, F. Modelling canopy fuel variables for *Pinus radiata* D. Don in NW Spain with low-density LiDAR data. *Int. J. Wildl. Fire* **2014**, *23*, 350–362. [CrossRef]

71.　Ahokas, E.; Yu, X.; Oksanen, J.; Kaartinen, H.; Model, D.T. Optimization of the Scanning Angle for Countrywide. In Proceedings of the Laser Scanning; Vosselman, G., Brenner, C., Hyyppä, J., Eds.; International Society for Photogrammetry and Remote Sensing (ISPRS): Enschede, The Netherlands, 2005; pp. 115–119.

72.　Jakubowski, M.K.; Guo, Q.; Kelly, M. Tradeoffs between lidar pulse density and forest measurement accuracy. *Remote Sens. Environ.* **2013**, *130*, 245–253. [CrossRef]

73.　Hansen, E.H.; Gobakken, T.; Næsset, E. Effects of pulse density on digital terrain models and canopy metrics using airborne laser scanning in a tropical rainforest. *Remote Sens.* **2015**, *7*, 8453–8468. [CrossRef]

74.　Stereńczak, K.; Ciesielski, M.; Bałazy, R.; Zawiła-Niedźwiecki, T. Comparison of various algorithms for DTM interpolation from LIDAR data in dense mountain forests. *Eur. J. Remote Sens.* **2016**, *49*, 599–621. [CrossRef]

75.　Liu, X. Airborne LiDAR for DEM generation: Some critical issues. *Prog. Phys. Geogr. Earth Environ.* **2008**, *32*, 31–49.

76.　Corona, P.; Cartisano, R.; Salvati, R.; Chirici, G.; Floris, A.; di Martino, P.; Marchetti, M.; Scrinzi, G.; Clementel, F.; Travaglini, D. Airborne laser scanning to support forest resource management under alpine, temperate and mediterranean environments in Italy. *Eur. J. Remote Sens.* **2012**, *45*, 27–37. [CrossRef]

77.　Tompalski, P.; White, J.C.; Coops, N.C.; Wulder, M.A. Demonstrating the transferability of forest inventory attribute models derived using airborne laser scanning data. *Remote Sens. Environ.* **2019**, *227*, 110–124. [CrossRef]

78.　Thomas, V.; Oliver, R.D.; Lim, K.; Woods, M. LiDAR and Weibull modeling of diameter and basal area. *For. Chron.* **2008**, *84*, 866–875. [CrossRef]

79.　Gonçalves-Seco, L.; González-Ferreiro, E.; Diéguez-Aranda, U.; Fraga-Bugallo, B.; Crecente, R.; Miranda, D. Assessing the attributes of high-density *Eucalyptus globulus* stands using airborne laser scanner data. *Int. J. Remote Sens.* **2011**, *32*, 9821–9841. [CrossRef]

80.　Woods, M.; Lim, K.; Treitz, P. Predicting forest stand variables from LiDAR data in the Great Lakes—St. Lawrence forest of Ontario. *For. Chron.* **2008**, *84*, 827–839. [CrossRef]

4   Paper 3: Comparison of linear regression, k-nearest neighbor, and random forest methods in airborne laser scanning-based prediction of growing stock

This chapter has been published as an original, **closed-access** paper in Forestry, whose copyedited version (also known as "Version of Record") is referred to:

Cosenza, D.N., Korhonen, L., Maltamo, M., Packalen, P., Strunk, J.L., Næsset, E., Gobakken, T., Soares, P., Tomé, M. 2020. Comparison of linear regression, k-nearest neighbor, and random forest methods in airborne laser scanning-based prediction of growing stock. Forestry. 93(5), 1-13. https://doi.org/10.1093/forestry/cpaa034

The publicity rights of the Version of Record belong to the Oxford University Press. Thus, this thesis brings the "Accepted Manuscript", which is the final draft author manuscript as accepted for publication by the journal, including modifications based on referees' suggestions, before it has undergone copyediting, typesetting and proof correction.

Comparison of linear regression, k-nearest neighbor, and random forest methods in airborne laser scanning-based prediction of growing stock

Diogo N. Cosenza[1,*], Lauri Korhonen[2], Matti Maltamo[2], Petteri Packalen[2], Jacob L. Strunk[3], Erik Næsset[4], Terje Gobakken[4], Paula Soares[1], Margarida Tomé[1]

[1] Forest Research Centre, School of Agriculture, University of Lisbon, Tapada da Ajuda, 1349-017 Lisbon, Portugal. paulasoares@isa.ulisboa.pt; magatome@isa.ulisboa.pt

[2] School of Forest Sciences, University of Eastern Finland P.O. Box 111, 80101, Joensuu, Finland. lauri.korhonen@uef.fi; matti.maltamo@uef.fi; petteri.packalen@uef.fi

[3] USDA Forest Service, Pacific Northwest Research Station, 3625 93rd Ave SW Olympia, WA 98512. jstrunk@fs.fed.us

[4] Faculty of Environmental Sciences and Natural Resource Management, Norwegian University of Life Sciences, P.O. Box 5044, NO-1432, Ås, Norway. erik.naesset@nmbu.no; terje.gobakken@nmbu.no

* Corresponding author: dncosenza@gmail.com; dncosenza@isa.ulisboa.pt Tel.: +351 213 653 309

Abstract

In this study, for five sites around the world we look at the effects of different model types and variable selection approaches on forest yield modeling performances in an Area-Based Approach (ABA). We compared ordinary least squares regression (OLS), k-nearest neighbors (kNN), and random forest (RF). Our objective was to test if there are systematic differences in accuracy between OLS, kNN and RF in ABA predictions of growing stock volume. The analyses are based on a 5-fold cross-validation at five study sites: an eucalyptus plantation, a temperate forest, and three different boreal forests. Two completely independent validation datasets were also available for two of the boreal sites. For the kNN, we evaluated multiple measures of distance including Euclidean, Mahalanobis, Most Similar Neighbor (MSN), and an RF-based distance metric. The variable selection approaches we examined included a heuristic approach (for OLS, kNN, and RF), exhaustive search among all combinations (OLS only), and all variables together (RF only). Performances varied by model type and variable selection approaches among sites. OLS and RF had similar accuracies and were more efficient than any of the kNN variants. Variable selection did not affect RF performance. Heuristic and exhaustive variable selection performed similarly for OLS. kNN fared the poorest amongst model types and kNN with RF distance was prone to overfitting when compared to a validation dataset. Additional caution is therefore required when building kNN models for volume prediction though ABA, being preferable instead to opt for models based on OLS with some variable selection, or RF with all variables together.

Keywords: machine learning; lidar; remote sensing; forest attribute estimation; benchmarking

1. Introduction

The Area-Based Approach (ABA) is commonly used in applications of forest yield modeling with Airborne Laser Scanning (ALS). In this approach field measured observations on plots are related to remotely sensed observations for the same plots using a model. Ordinary least squares regression (OLS) was predominately used in early studies (e.g. Næsset, 2002, 2004), but machine learning techniques such as k-nearest neighbor (kNN; Dudani, 1976) and random forest (RF; Breiman, 2001) have also been used (Maltamo et al., 2006; Packalén and Maltamo, 2006, 2007). These methods increased in popularity recently (e.g. Pascual et al., 2019; Silva et al., 2017). An advantage of the kNN and RF techniques is that they require less expertise to implement than linear modeling approaches or other more complex machine learning approaches such as neural networks and support vector regression (see Hastie et al., 2009; Haykin, 2009). While being straightforward to implement for practitioners, they are also efficient in handling high-dimensional data, which is often useful in remote sensing applications, and their requirement for more computational time is less of an issue today due to the increase in computing power.

kNN and RF methods have been used for prediction of both individual tree attributes (Gleason and Im, 2012; Maltamo et al., 2009; Vauhkonen et al., 2010; Yu et al., 2011) and plot level attributes (Maltamo et al. 2006b; Packalén and Maltamo 2007; Shataee et al. 2011; Latifi and Koch 2012). The principle of kNN is to predict the target variable based on the closest observations in the training dataset (Dudani 1976; Hastie et al. 2009). In kNN, a distance metric is used to determine which k training observations are nearest to the target value in terms of the predictor variables. Parameters that the modeler must decide for kNN include the number of nearest neighbors to impute, how to measure distance, and the weighting scheme employed to average imputed values. The RF algorithm is based on decision trees formed from resamples of the input data. Each decision tree uses a randomly selected subset of both the available predictors and observations. After training the model, the average of the "forest" of decision trees is used to predict new observations.

OLS and machine learning models typically require a number of decision and inspections which we will lump together as "parameter tuning" steps. Correct specification of tuning parameters for OLS and machine learning methods requires specialized expertise. For regression analysis (OLS), for example, the analyst must select variables, fit the model, and perform various diagnostics. kNN models also benefit from careful variable selection (Packalén et al. 2012) and the user must choose the number of neighbors and the distance metric. RF, on the other hand, has been shown to be less sensitive to variable selection (Belgiu and Drăgu 2016). There are a number of RF parameters than can be tuned, although it is common for analysts to use the defaults.

According to a review of kNN methods by Chirici et al. (2016), k=5 is the most frequent number of neighbors used in remote sensing applications, although values in the range 1–10 are common. Euclidean and Mahalanobis distance are often applied as distance metrics as they perform well relative to other methods, and do not depend on response attributes which makes them simple and fast to compute. Canonical correlation analysis (Most Similar Neighbor–MSN; Moeur and Stage, 1995) and RF-based distance metrics (Lin and Jeon 2002) are also frequently used. The weighting scheme used for prediction from multiple neighbors (k > 1) is usually the inverse of the distances to the k nearest neighbors.

In the case of the RF, Belgiu and Drăgu (2016) stated that the number of trees used to train the models is usually 500 since it is the default value of the most popular RF implementation, the *randomForest* package in R (see Liaw and Wiener, 2002). Furthermore, an exploratory study by Lawrence et al. (2006) showed that the error rates become stable when the number of trees is close to 500. The other parameters are normally set to the default values of the software, which are similar to those proposed by Breiman (2001). Thus, it is common practice to train the RF model by not allowing to split the trees with less than five nodes and applying one-third of the available predictor variables in the inner bootstrap.

The kNN and RF algorithms have some operational advantages. They are multivariate, non-parametric and quick to implement; however, they also have several limitations. Since kNN and RF predictions are weighted averages of the training data, the algorithms cannot extrapolate beyond the range of the training data. kNN and RF methods also typically require a greater number of training observations than parametric regression to perform well. These methods work best if the training dataset is large (e.g. thousands of observations) such that the full range of population values is represented. The demand for training observations also increases with the number of predictors due to the "curse of dimensionality" (Bellman 1961). This issue is very important for kNN, to which increasing the dimensionality can cause the distance to the nearest neighbor to be barely distinguishable from that of a distant neighbor, generating a loss of "contrast" among the distances (Beyer et al. 1999). This problem can be further accentuated if the kNN model uses "irrelevant variables", which are redundant or have a low correlation with the response variable (Blum and Langley 1997). Besides, irrelevant variables can also cause problems in the inversion of positive definite matrixes, a required step in computations of Mahalanobis and MSN distances (McRoberts et al. 2017).

To reduce problems associated with high-dimensional data, studies have used various strategies to select a subset of ALS metrics in RF and kNN models. Many approaches can be applied for this purpose (see Saeys et al., 2007), but it is common to see implementations based on stepwise variable selection (Breidenbach et al., 2010; Hudak et al., 2008; Maltamo et al., 2006), correlation feature selection (García-Gutiérrez et al., 2015), genetic algorithm (Latifi et al. 2010; Latifi and Koch 2012; McRoberts et al. 2015), or simulated annealing (Packalén et al. 2012). Some researchers have suggested that RF may result in overfitting in cases of irrelevant variables (Segal 2004), so it is common to see implementations of some form of variable selection for RF in an ABA context (see Genuer et al., 2010). To reduce dimensionality for RF applications, variables are often selected based on their importance (Silva et al. 2017; Shi et al. 2018).

OLS, kNN, and RF are common methods for ABA forest yield modeling in the literature, but there has not been a systematic evaluation of the differences in accuracies between these methods, especially when considering differences in tuning strategies. The studies that we are aware of performed comparisons with at most three datasets (e.g. Fassnacht et al., 2014; Latifi and Koch, 2012; McRoberts et al., 2017), and most of them focused on boreal or temperate forests (e.g. Maltamo et al., 2006; Packalén et al., 2012; Packalén and Maltamo, 2007; Shataeea et al., 2011). Additionally, each study employed its own tuning approach so that comparisons among them are difficult.

Our objective for this study is to identify whether there are modeling and tuning strategies which are optimal across a broad range of conditions, including sites in North America, South America, and

Europe, and to identify similarities and differences in OLS, RF, and kNN predictions among these datasets. To pursue this objective, we fit models for growing stock volume (V, m³ ha⁻¹) from lidar data for each of these datasets using OLS, kNN, and RF using multiple tuning strategies. We then cross-validated model performances using 5-fold cross-validation. We also evaluated performances using independent validation datasets which were available for two boreal forest sites in Europe.

2. Material and methods
2.1. Study areas and material

This work was conducted using datasets collected at five locations on 3 continents: a eucalyptus plantation in Brazil, boreal forests in eastern Finland (Kolari) and northern Finland (Liperi), a boreal forest in southern Norway, and a mixed temperate forest in South Carolina in the USA. The sites in Finland are referred to by their municipality, Kolari and Liperi, while the other sites are referred to by their country. Independent validation datasets were available for the two sites Liperi (Finland) and Norway (see section 2.4 for additional details). A summary of characteristics for each dataset is provided in Table 1. All of the sites have also been used for previous studies; comprehensive descriptions of study areas can be found in the primary articles cited below.

The site in Brazil is a commercial plantation of hybrid eucalyptus located in the state of Bahia (Packalén et al. 2011a, 2011b). At the time of the lidar acquisition, the plantation was composed of several even-aged stands, planted with the same spacing. The tree ages were between 2 and 12 years, the tree heights varied from 17 m to 41 m, and growing stock varied from 111 to 656 m³ ha⁻¹.

The Kolari site is located north of the Arctic Circle, where the forests mainly consisted of sparsely spaced Scots pines, although Norway spruce and deciduous trees were also present (Kotivuori et al. 2016). Tree heights ranged from 3 m to only 25 m, and the growing stock were between 4 and 462 m³ ha⁻¹, the lowest range of volume per hectare of any of the sites.

The other Finnish site, Liperi, was located in eastern Finland, where the forests were denser than Kolari and the trees achieved heights greater than 30 m (Kukkonen et al. 2019). The amount of spruce and pine stands was relatively similar with a minority of deciduous stands. The tree heights ranged from 6 m to 41 m, while the growing stock varied from 20 to 797 m³ ha⁻¹ in this dataset.

The Norwegian boreal site is located further south than the Finnish sites and had considerably larger differences in elevation than the two sites in Finland (Gobakken et al. 2013). The forests were dominated by Norway spruce due to the better fertility of the soils. The tree heights ranged from 4 m to 37 m, while the growing stock varied from 4 to 692 m³ ha⁻¹.

The site in the USA was a mix of pine plantations and mixed native hardwoods with a total of 62 different species present on the plots (Strunk et al. 2017). Tree heights for this site ranged from 5 m to 38 m and the growing stock in this dataset had the greatest range, from 2 to 1227 m³ ha⁻¹.

The ALS metrics used for each dataset were prepared for previous studies (referred to in Table 1) using different data processing software and therefore differ between the sites. However, the available ALS metrics were comparable among all sites, representing the vertical return distributions, density metrics, return intensity, and return numbers. All of them are described in Appendix 1.

Table 1. Summary of the field and ALS data.

Region	Forest type	Dominant species	No of plots	Plot radius	Point density (pt m^{-2})	Volume* (m³ há$^{-1}$)	Reference
Brazil	Clonal hybrid plantation	*E. urophilla* x *E. grandis*	195	13 m	1.5	376.1 (132.8)	(Packalén et al., 2011a, 2011b)
Kolari (Finland)	Boreal	*Pinus sylvestris*; *Picea abies*; *Betula pendula*	534	9 m; 12.62 m; 12.65 m	0.6	100.9 (64.2)	(Kotivuori et al., 2016)
Liperi (Finland)	Boreal	*Pinus sylvestris*; *Picea abies*; *Betula pendula*	Training: 578 Testing: 444	9 m; 12.6 m	4.8	Training: 186.4 (100.4) Testing: 205.6 (94.6)	(Kukkonen et al., 2019)
Norway	Boreal	*Pinus sylvestris*; *Picea abies*; *Betula pendula*	Training: 499 Testing: 78	8.92 m 17.84 m	0.7	Training: 211.4 (119.7) Testing: 230.7 (119.3)	(Gobakken et al., 2013)
USA	Temperate	62 species dominated by *Pinus taeda* (30.2%) and *Pinus palustris* (15.6%); all other species represent less than 10% of dominant species	194	11.3 m; 22.6 m	6	228.3 (160.7)	(Strunk et al., 2017)

*Plot mean growing stock volume with its respective standard deviation (in parenthesis)

2.2. Growing stock modeling

The same variable selection and modeling protocols were used for each of the five datasets (Brazil, Kolari, Liperi, Norway, USA). For simplification, we use the term "training" hereafter to refer to both OLS model fitting and the construction of non-parametric models. Each of these approaches was paired with variable selection schemes that were applied every time a model was trained. The same heuristic selection of five predictor variables was used for OLS, kNN and RF (Section 2.3), while other variable selection approaches differed by model type. The choice of five predictors was a compromise between not overfitting the OLS models and having an adequate number of predictors for the nonparametric methods. The specifics of each variable selection approach and modeling scheme are described in greater detail in the following sections.

2.2.1. OLS modeling

The OLS models were based on Formula 1, in which the square root transformation of the response variable was applied to avoid problems of heteroscedasticity. Because of this transformation, the back-transformed value requires a correction for bias. According to Gregoire et al. (2008), the residual variance of the models was added as described in Formula 2.

$$\sqrt{V_i} = \beta_{i0} + \beta_{i1}x_{i1} + \cdots + \beta_{im}x_{im} + \varepsilon_i \qquad (1)$$

$$\widehat{V_i} = \left(\widehat{\sqrt{V_i}}\right)^2 + \sigma^2 \qquad (2)$$

where V_i and $\widehat{V_i}$ are the observed and the predicted timber volume (m³ ha⁻¹) of the plot i=1, 2,…, n; β_{ij} is the model parameter j=0, 1, …, m of the plot i; x_{ij} is the predictive variable j=1, 2, …, m for the plot i; ε_i is the random error for plot i; and σ² is the residual variance of the model (m³ ha⁻¹).

Two approaches were used for variable selection for OLS. The first was a machine-learning based **He**uristic approach (OLS_He), which means that the derived models are just for prediction purposes since statistical assumptions related to the linear models were ignored. In this approach, we used a five-predictor model (m=5, see Formula 1) and the predictors were defined by the heuristic variable selection algorithm (detailed in Section 2.3). The second variable selection approach used for OLS was an all combinations **Exh**austive search algorithm (OLS_**Exh**) implemented in the R statistical environment (R Core Team 2020). The best model met the following three criteria: smallest relative root mean squared error (RMSE%, Formula 3), considering the constraints that estimated parameters are significantly different from zero (t-test, α=5%), and variance inflation factors (VIF) are less than ten (Myers 1989). A three-predictor model (m=3, see Formula 1) was used in OLS_Exh due to computational limitations. RMSE% was computed as

$$\text{RMSE } (\%) = 100 * \bar{V}^{-1} \sqrt{\frac{\sum_{i=1}^{n}(V_i - \widehat{V}_i)^2}{n}} \qquad (3)$$

where V_i and $\widehat{V}_i$ are, respectively, the observed and predicted timber volume (m³ ha⁻¹) for plot i=1, 2, …, n; $\bar{V}$ is the observed mean volume (m³ ha⁻¹).

2.2.2. kNN modeling

As shown by Packalén et al. (2012) and McRoberts et al. (2015), the prediction accuracy of kNN is sensitive to the choice of distance metric. For this reason, we tested four commonly used distance metrics: **Euc**lidean distance (kNN_**Euc**), **Mah**alanobis distance (kNN_**Mah**), **M**ost **S**imilar **N**eighbor (kNN_**MSN**), and a distance metric based on the **R**andom **F**orest proximity matrix (kNN_**RF**). All the approaches were trained using k=5. The predicted values were obtained as weighted means of the k neighbors where the weights

were $1/(1+d)$, d being the distance between a neighbor and the target. kNN models were trained using the *yaImpute* package (Crookston and Finley 2015) with the default parameters besides distance metric and k. Given the large number of potential ALS-derived auxiliary variables, we used a heuristic variable selection routine (detailed in Section 2.3) to choose five "good" ALS metrics for each kNN model.

2.2.3. RF modeling

RF modeling was performed using the *randomForest* package (Liaw and Wiener 2002) with all training parameters set to their default values, since they are well established in the literature (Breiman 2001; Belgiu and Drăgu 2016). The default number of random trees was 500, the default number of predictors randomly selected to grow a tree from each node was one-third of the available predictors, and the default minimum number of nodes was five for each tree. Latifi and Koch (2012) reported that having a large number of predictor variables is not an issue in RF. To confirm this finding, RF was used both with a **He**uristic variable selection with five variables (RF_**He**; detailed in Section 2.3) and using **all** the available predictor variables (RF_**All**).

2.3. Heuristic variable selection

Heuristic variable selection was performed with the simulated annealing metaheuristic (Kirkpatrick et al., 1983) adapted by Packalén et al. (2012) for kNN modelling. We also use the same variable selection algorithm (Algorithm 1) for kNN, OLS and RF. The idea behind a metaheuristic strategy is to find a "good" solution for a given "cost function" iteratively, by making changes in a given initial solution (see Talbi, 2009). In our case, a solution (S) is any set of five variables used to train a model, and the cost function (f_{cost}) is the RMSE% obtained by computing the residuals of the trained model respective to a given solution (Formula 3).

1. $n \leftarrow 500$
   $T_0 \leftarrow 0.2$
   $T \leftarrow T_0$
   $S \leftarrow S_0$
   $c \leftarrow f_{cost}(S)$
   $c_{best} \leftarrow c$
   $S_{best} \leftarrow S$
   $i \leftarrow 0$
2. **While** $i < n$ **do:**
   $S' \leftarrow f_{neighbor}(S, \frac{i}{n})$
   $c' \leftarrow f_{cost}(S')$
   $\Delta \leftarrow (c' - c) + 0.001$
   #Evaluation
   If $exp(-\Delta/T) >$ random(from:0, until:1), **then:**
      $c \leftarrow c'; S \leftarrow S'$
   #Recording the best solution found
   If $c' < c_{best}$, **then:**
      $c_{best} \leftarrow c'; S_{best} \leftarrow S'$
   #Cooling temperature
   $T \leftarrow max\left[0.001, \ T_0\left(1 - \frac{i}{0.8\,n}\right)\right]$
   $i \leftarrow i + 1$
3. **Return:** S_{best}

Algorithm 1- Variable selection by simulated annealing, where n is the number of iterations, i is the number of the current iteration ($i = 1, 2,…, n$), T0 is the initial temperature, T is the current temperature, S0 is the initial random solution, S is a temporary solution, S' is a neighbor solution of S, Sbest is the best solution found until the iteration i, fneighbor is the neighbor function, fcost is the cost function, c is the associated cost of S, c' is the cost associate of S', cbest is the associated cost of Sbest.

The changes to the solution are induced by the neighborhood function ($f_{neighbor}$), which produces an alternative solution ("neighbor solution", S') based on the current solution and the proportion of iterations (i) that were performed (i/n, being i= 1, 2, …, n, and n the total number of iterations). Initially, the algorithm randomly replaces two-thirds of the variables in the current solution with different variables. The number of variables replaced in each iteration is reduced over the duration of the variable selection until only one variable at a time is replaced after achieving 80% of the iterations. The parameter temperature (T) controls the probability of accepting non-improving solutions, where this probability decreases with the temperature. The initial temperature is high to allow exploring different solutions, and then decreases throughout the iterations in a process known as "cooling". In our adaptation, it decreased linearly until achieving 80% of the iterations, where the temperature was set to a very small positive value. With this configuration, the solution with the lowest error found is exploited in the last 20% of the iterations to produce a better neighbor solution so that temporary solutions with higher errors are no longer allowed. The initial temperature (T_0) and the number of iterations (n) were set to 0.2 and 500 respectively. The routine was implemented in the R environment.

2.4 Accuracy assessment

The combinations of modeling type and variable selection approaches resulted in a total of eight approaches including OLS_Exh, OLS_He, kNN_Euc, kNN_Mah, kNN_MSN, kNN_RF, RF_All, and RF_He. The performances of these approaches were assessed for each study area using cross-validation, and for two sites an independent validation. The relative RMSE (RMSE%, Formula 3) and squared Pearson's correlation computed from validation predictions were used to evaluate performances.

Cross-validation was implemented using a 5-fold approach in which a given dataset is randomly split into five evenly sized disjoint sets ("folds"). In each iteration, one of these folds was omitted and a new model was trained with the remaining data to predict the volume of the omitted fold. The five folds were combined after the five iterations, and the RMSE% was computed. The entire 5-fold cross-validation was performed 100 times for each site, and the Mean RMSE% was used as a final measure to obtain a better view of the real accuracy, as the randomness involved in the variable selection process is decreased. The intervals containing 95% of the RMSE% values were also used for comparison.

Independent test datasets that were available for two sites (Liperi and Norway) were used for additional validation. For each site, a new model was first trained using the full dataset previously used in their respective cross-validations, and the resultant models were used to predict volume to the testing datasets. Finally, RMSE% was computed both for training and testing datasets. This process was repeated 100 times. The Mean RMSE% and the intervals containing 95% of the errors were also used for accuracy assessment.

As a final assessment for each approach, we used the training dataset one more time to train a showcase model to predict volumes to the testing dataset so that we could provide figures with observed versus predicted values and compute squared Pearson correlation (r^2). For the approaches where the heuristic variable selection was used, we also provide the progress of the cost function during the optimization, where the temporary solutions were applied to predict volume to the training and testing dataset and compute their respective RMSE% in each iteration.

3. Results

Overall, all eight modeling approaches demonstrated relatively similar accuracies for most of the datasets in the 5-fold cross-validation (Figure 1). We saw increasing Mean RMSE% values for forest conditions

with greater heterogeneity in forest composition (see Section 2.1). For example, the greatest relative errors were observed for the temperate forest conditions in the USA dataset (RMSE = 34-46%) which also had the greatest observed variation in structure and species. The Brazil site is very homogeneous, especially in contrast to the USA, and had the smallest RMSE% values, ranging from 9 to 14%. The complexity of the boreal forests (Kolari, Liperi, and Norway) fell between Brazil and the USA; they had RMSE% values ranging from 19 to 30%. Additionally, the 95% intervals for RMSE% for all prediction methods overlapped for the USA dataset. This means that inferences about the relative performances of the tested prediction approaches are less certain for this site, although the trends in performances generally supported the inferences we made from other datasets.

The patterns in performance relative to modeling approach varied by dataset, but there were consistent patterns observed across datasets. Our results suggest that Mean RMSE% varied little amongst modeling approaches examined. The greatest variation in performance was amongst methods for the USA where kNN_RF and RF_He had a difference of approximately 5% in Mean RMSE%. This was consistent with other sites in that kNN models almost exclusively performed poorer (had larger RMSE% values) than OLS and RF, and that OLS and RF generally performed similarly. There was only one exception where kNN performed better than other methods: for the USA, kNN_Euc performed better than OLS methods, while other kNN models performed worse than OLS for the USA. kNN_Euc consistently had the best performances amongst kNN distance metrics across all sites. Other kNN distance metrics did not demonstrate obvious trends, and their relative performances amongst kNN methods varied by site.
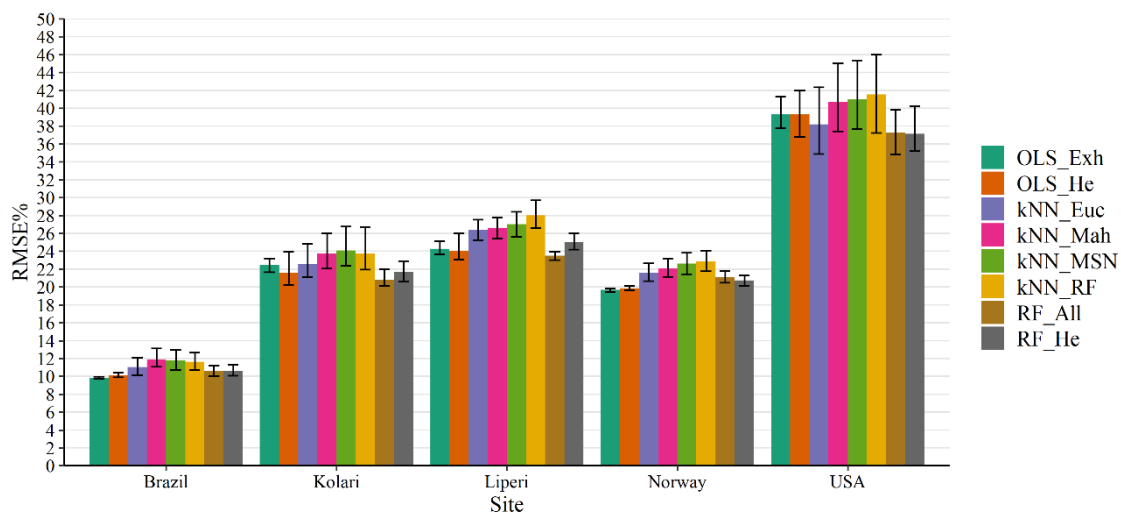

Figure 1. Mean accuracy of the modeling approaches by forest sites assessed through 5-fold cross-validation repeated 100 times. Each bar represents the mean of the relative root mean squared error (RMSE%) values obtained at the end of the 5-fold cross-validations for a given modeling approach. The whiskers represent intervals containing 95% of the RMSE%.

OLS and RF generally performed similarly across all sites (RMSE%). OLS performed better for Brazil and Norway, RF performed better for Kolari and the USA, and the result for Liperi was mixed. However, differences amongst OLS and RF were very small, with a maximum of 3 percentage points difference (USA), and most differences were less than 2 percentage points. The difference within methods (OLS_Exh versus OLS_He, and RF_ALL versus RF_He) were generally also very small (< 2 percentage points). The validation at Liperi's and Norway's external datasets had RMSE% values ranging from 24 to 34% (Figure 2). These errors were greater (3 to 5 percentage points) than the cross-validation errors. In Liperi,

validation on independent data demonstrated a similar pattern in performance to cross-validation (see Figure 1), where the best RF and OLS methods had nearly identical performances, kNN had the largest errors, and kNN_Euc performed best amongst kNN distances. Independent validation for Norway differed slightly in that kNN_Euc and kNN_RF performed similarly to OLS and RF models. Interestingly, the relative performance of RF_He clearly differed between the two sites, performing better than all other methods in Norway, and performing worst amongst OLS and RF methods for Liperi. Furthermore, most of the testing errors followed a similar pattern as the training ones. The greatest difference was observed for kNN_RF, which had notably smaller RMSE% values for the training than for the testing datasets, showing that RF distance metric in kNN had a clear tendency for overfitting.
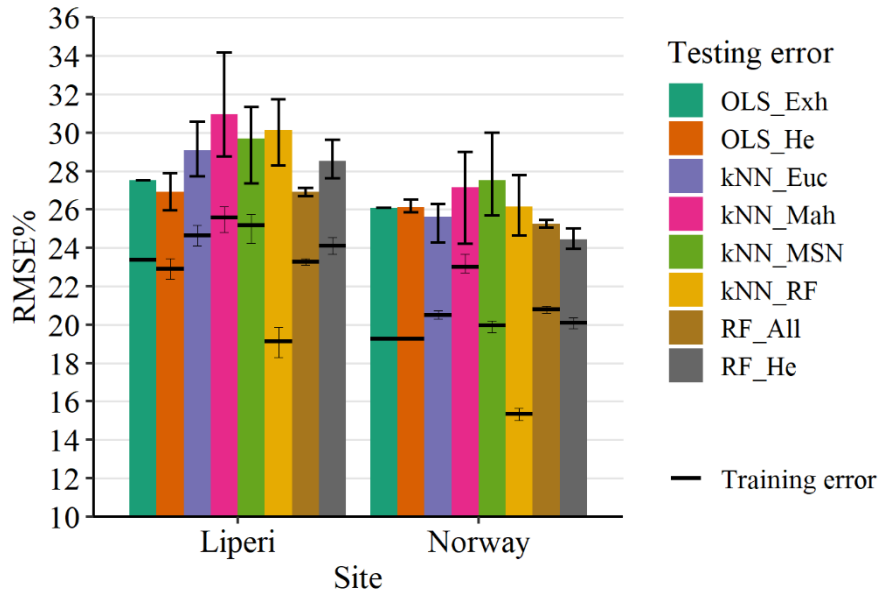

Figure 2. Mean accuracy of the modeling approaches by forest sites assessed through validation repeated 100 times. Each bold line and bar represent, respectively, the mean of the relative root mean squared error (RMSE%) values obtained at the end of the validation with the application of a trained model to the training and testing dataset. The whiskers represent intervals containing 95% of the RMSE%.

The relative agreement between observed and predicted values of the showcase models can be see for training and validation sets in Figure 3 (Liperi) and Figure 4 (Norway). As might be expected, the agreement between predicted (x-axis) and observed (y-axis) values was better for the training dataset than for the validation dataset. The r^2 values for the training datasets ranged from 0.89 to 0.96 and for independent validation datasets ranged from 0.82 to 0.89. As was observed with RMSE%, OLS and RF methods generally perform the best, and there is evidence that kNN_RF has a tendency to overfit the training dataset. For Liperi, kNN_RF performed the best for the training dataset (r^2=0.94), but performed among the worst with respect to the validation dataset (r^2=0.82). In Norway, a similar decline for kNN_RF was observed where the agreement (r^2) between predicted and observed values was greater than for any other methods at 0.96 in the training dataset, but dropped to 0.88 for the validation dataset, which is in the middle amongst other methods for the Norway validation dataset. According to the testing correlation, the best approaches for the Liperi dataset were the OLS and RF models with OLS_He and RF_All reaching r^2=0.87 and r^2=0.86, respectively. Most approaches had comparable performance for the Norway dataset where the best performances were achieved for RF_All and RF_He, both having r^2=0.89.
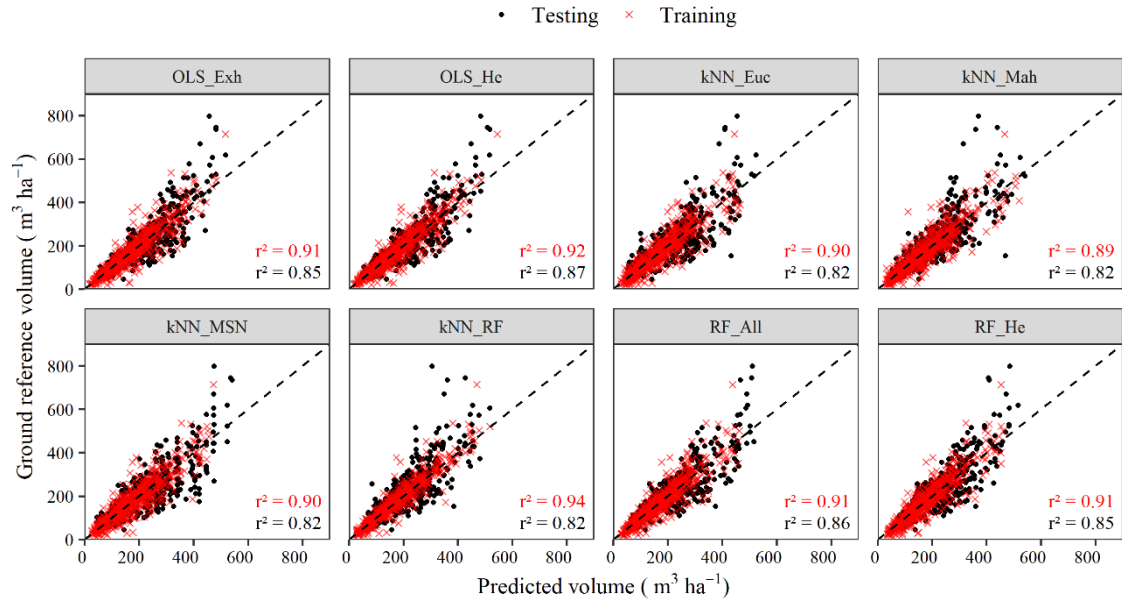
Figure 3. Observed and predicted values for testing and training dataset from Liperi.
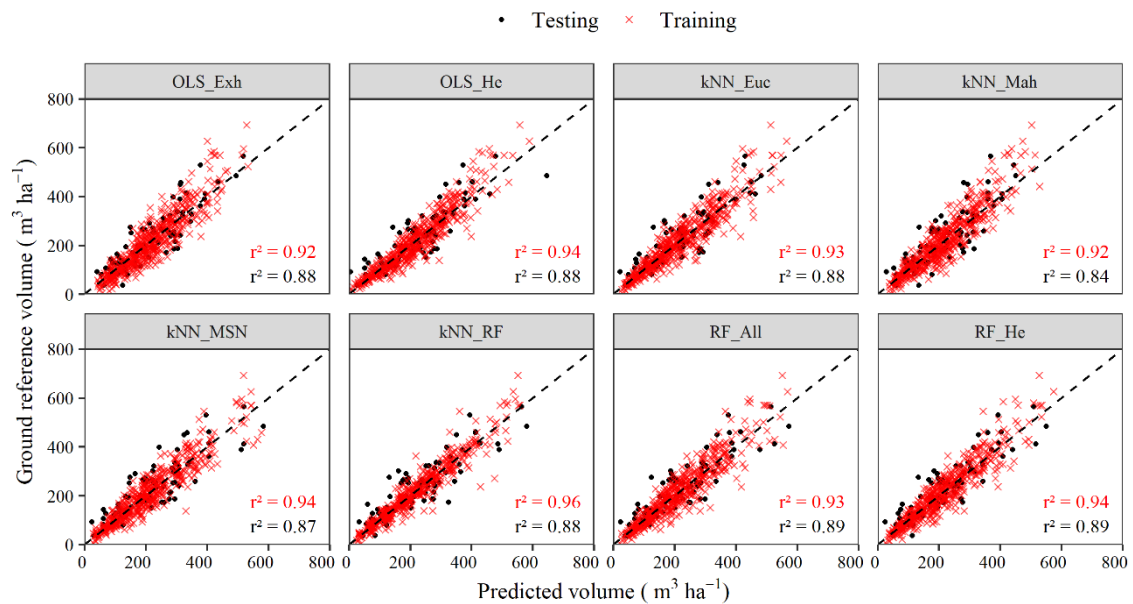

Figure 4. Observed and predicted values for testing and training datasets from Norway.

Figures 5 and 6 show the RMSE% values during the heuristic variable selection progresses for the Liperi and Norway datasets, respectively. As a general pattern, the error values for the training datasets (black) decrease monotonically with the number of iterations. However, RMSE% values for the testing datasets (grey) are erratic and do not necessarily improve with number of iterations, which suggests that heuristic variable selection may not be suitable for some modeling approaches.
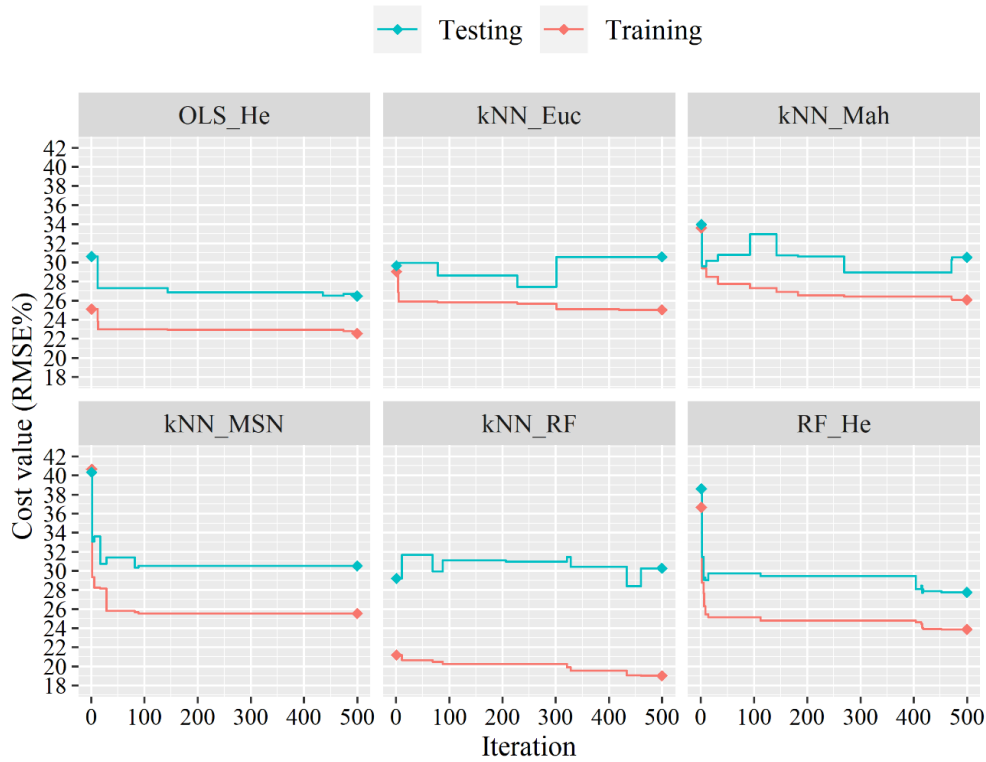
Figure 5. Optimization progress for the variable selection during the model training with the Liperi dataset. The errors were computed with the temporary solutions applied to the training and testing datasets.
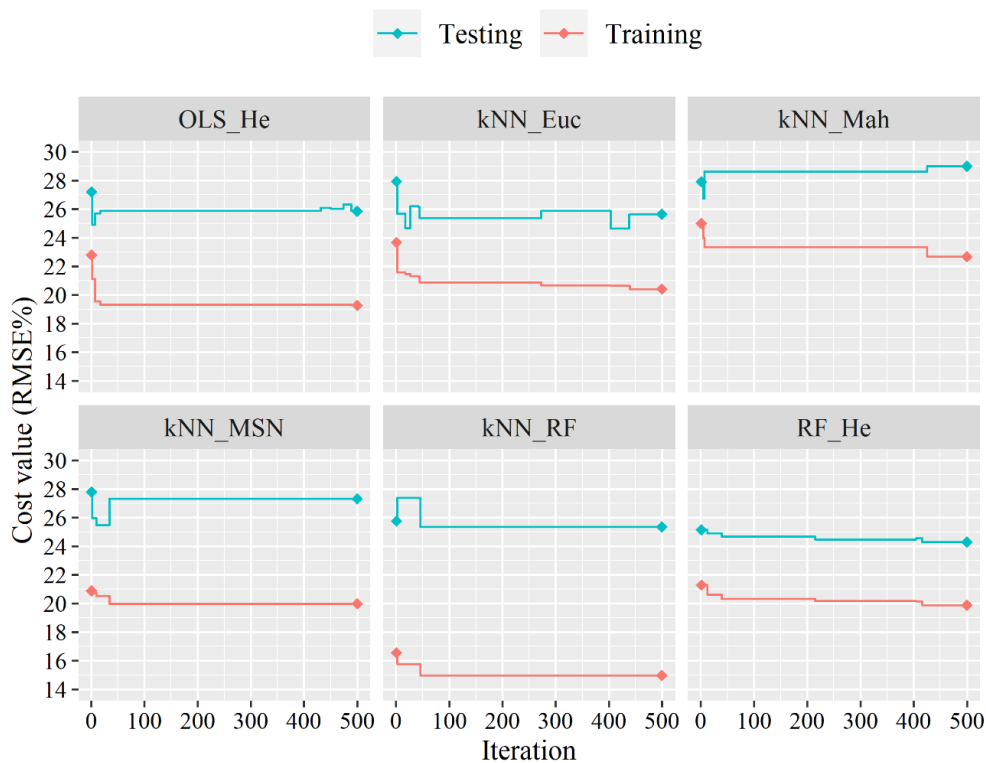

Figure 6. Optimization progress for the variable selection during the model training with the Norway dataset. The errors computed with the temporary solutions applied to the training and testing datasets.

Despite the kNN_RF having the smallest final RMSE% for the training dataset for both Liperi and Norway, it had the largest differences between testing and training errors. The pattern of kNN performances for test datasets was highly erratic relative to their testing error progress and did not show the desired systematic

improvement. OLS_He and RF_He showed systematic improvements in testing error as a result of each iteration of this variable selection and had a less erratic progress than kNN-based models. These two approaches also had the smallest final RMSE% values for the testing datasets. The differences between the initial and final RMSE% values were larger for the Liperi dataset than for the Norway dataset. The latter also had fewer steep decays. The exact patterns in Figures 5 and 6 vary each time that models are trained because the heuristic variable selection approach is stochastic in nature.

4. Discussion

This work demonstrates similarities and differences in ABA volume prediction performances between OLS, kNN, and RF methods for datasets collected around the world (northern Europe, North America, and South America). While the results differ among datasets, it was possible to distinguish some patterns which should prove helpful to researchers and practitioners.

Our first inference is that kNN methods were generally systematically less precise than OLS and RF. Better performance for RF relative to kNN has also been demonstrated in previous studies (Latifi and Koch 2012; Fassnacht et al. 2014; Tompalski et al. 2019). Possible explanations are that kNN has many parameters which need tuning, that kNN is more sensitive to correct tuning, and that the default kNN tuning parameters are less generic than those for RF. RF default parameters, in contrast, seem to work well across a wide variety of datasets. For example, Shataee (2013) demonstrated that exhaustive tuning of kNN parameters led to smaller errors for a Euclidean-based kNN than for an RF model. McRoberts et al. (2017) showed that kNN performance improves greatly through parameter tuning, which also reduced the variation in performances among kNN distance metrics. In contrast, studies which tune RF parameters are less common in the ALS literature (Shataee et al. 2011; Shataee 2013; Shi et al. 2018), and the results with respect to specific tuning parameters and their effects on performances are still unclear. Therefore it is common to use the RF with the parameters set to default, since they appear to produce sufficiently robust models (Belgiu and Drăgu 2016). However, it is important to highlight that the parameter tuning by itself cannot guarantee a reasonable performance since many factors influence a model's accuracy, such as the inherent properties of the dataset (Fassnacht et al. 2014). Besides, the full parameter tuning is time-consuming and considerably increases the computational complexity of the analysis as well as the required technical capacity of the analyst.

Establishing a comparison between our results and the ones available in existing literature was not a straightforward task since all of the studies had procedural differences in their implementation. Our results concerning the performance of kNN distance metrics disagree with some other studies. We found that kNN_Euc performed best under cross-validation, while kNN_RF was among the worst and with a clear indication of overfitting. Other studies found that kNN_Euc was outperformed by other techniques like kNN_MSN and, especially, kNN_RF (Hudak et al. 2008; Latifi et al. 2010; McRoberts et al. 2017). Both of them were considered the most robust distance metrics in some studies (Vauhkonen et al. 2010; Shataee et al. 2011; Packalén et al. 2012).

The first reason for this difference in findings may be related to differences in the model performance assessment. Earlier studies often applied leave-one-out cross-validation (LOOCV) (e.g. Latifi et al. 2010; Packalén et al. 2012; McRoberts et al. 2017), which is a specific type of cross-validation in which a single observation is omitted each time. The use of a 5-fold cross-validation, in contrast, may provide a more robust set of validation data for detection of model overfitting. A related factor is that more complex models have a greater tendency to overfit the data (Hastie et al. 2009). Since kNN_MSN and kNN_RF are more complex than

the kNN_Euc, it may be that studies using LOOCV reported performances resulting from overfit models. Lastly, kNN_MSN models are usually applied for simultaneous prediction of several response variables, such as species-specific volume prediction (e.g. Packalén and Maltamo 2007; Vauhkonen et al. 2010). In such scenario the kNN approaches would probably perform better, as the predictions are guaranteed to remain logical.

Another inference from our results relates to practical considerations of heuristic and exhaustive variable selection procedures for OLS. Our results showed that OLS models for both heuristic and exhaustive variable selection have similar performances, but they differ in some respects. A heuristic approach to variable selection can handle a much greater number of explanatory variables, and is more flexible with respect to model formulations including handling non-linear forms, and can be easily optimized for a wide range of loss functions. On the other hand, the stochastic process involved in the simulated annealing caused higher variation in the OLS_He errors. The exhaustive variable selection, although having smaller error ranges, quickly becomes computationally infeasible for large numbers of explanatory variables. The computational cost of training OLS_Exh increases factorially with the number of explanatory variables and with the number of variables to search for, and may hence be infeasible for high dimensional datasets.

Among RF methods, RF_He had comparable results to RF_All in most situations. This confirms that, to a degree, RF is robust to overfit when dealing with high dimensional data (Belgiu and Drăgu 2016). Our findings suggest that variable selection may not be needed for some applications of RF.

The cross-validation and validation with independent data are traditionally focused on the performance of a specific model, where a model with the same predictors is trained and used to predict values to the holdout folds or testing dataset. Differently, our assessment was focused on the modeling approach itself wherein the variable selection was also repeated before predicting the next holdout fold or testing dataset. The fact that these processes were repeated 100 times increased the robustness of inferences regarding the comparisons of modeling approaches and their efficiency. This methodology is therefore strongly recommended for future works that intend to test or compare modeling approaches, even if it is more computationally intensive.

This study demonstrates the importance of validation, especially independent validation. Even with a fairly intensive cross-validation scheme that uses 20% of the data for holdout validation, the results suggest that our approach still over-estimates model performances. Part of this difference may be the result of differences in the conditions as the training and validation sites, but the divergence in reported performances deserves further investigation. While the use of an independent validation dataset is the ideal way to assess model performance, it is rarely available in practice (Araújo et al. 2005). Despite the divergence between cross-validation and independent validation, our study suggests that the cross-validation can generally still provide information on the relative performances amongst methods, although we were not able to identify overfit by the kNN_RF method. Other assessment approaches which can provide reliable errors when validation datasets are not available include block cross-validation (see Roberts et al. 2017) or leaving out spatial clumps of observations, instead of choosing holdout data at random from across the study areas (e.g. Kotivuori et al. 2016, 2018). Despite that, Roberts et al. (2017) showed that a cross-validation with random folds can provide fair error estimates when a model is developed only to predict to a dataset with the same structure, which is a situation that fits to our assessment.

Our findings agree with the results of Fassnacht et al. (2014), who found that the accuracy of ABA-based predictions is influenced by the modeling approach. Therefore, our results are of great importance to remote sensing experts that need to construct accurate ABA maps of the growing stock volume or above-

ground biomass. The main results were consistent regardless of variations in ALS metrics computed for the different study sites, as the metrics still represented similar variations in vertical and horizontal canopy structure despite differences in computational methods. The differences between methods are considerably smaller than the differences between datasets, but we showed that they are systematic, and some methods are slightly better in ABA applications than others. For example, the RF_All with default parameters is robust across multiple forest types and can be reliably applied to high-dimensional datasets without time-consuming variable selection processes. OLS methods can provide similar accuracy and might be preferred over RF_all in situations where it is important to interpret how individual predictors influence the predicted values. We did not test the effects of number of training observations in this study, but it is known that OLS tends to be more reliable for small data sets (e.g. < 100 observations). Finally, we showed that kNN methods are suboptimal in situations where there is only a single response variable.

5. Conclusion

This study compared OLS, kNN, and RF modeling strategies in combination with multiple variable selection strategies for the prediction of growing stock volume in five forests around the globe. RF and OLS models performed better than kNN models, although the maximum difference was about 4 percentage points, and generally less. These results suggest that RF or OLS are preferable for estimating volume from ALS data. In addition, kNN based on RF distance was especially problematic due to its strong tendency to overfit which was not detected with a 5-fold cross-validation, but became clear during the validation with an independent test data. kNN based on Euclidean metrics outperformed other kNN approaches across all study areas.

In the case of the OLS methods the heuristic variable selection was shown to perform as well as the more time-consuming exhaustive search, which is especially advantageous in the case of high-dimensional data where the exhaustive search algorithm may not be feasible. We did not observe an improvement to RF from using variable selection, which suggest that RF is a robust approach for practical applications.

8. References

Aldred, A., and Bonnor, G. 1985. Application of airborne lasers to forest surveys. *In* Information Report PI-X-51. Chalk River, Ontario.

Araújo, M., Pearson, R., Thuiller, W., and Erhard, M. 2005. Validation of species-climate impact models under climate change. *Global Change Biology* 11(9): 1504–1513. doi:10.1111/j.1365-2486.2005.001000.x.

Axelsson, P. 2000. DEM generation from laser scanner data using adaptive TIN models. *In* International Archives of Photogrammetry and Remote Sensing. Vol. XXXIII, Part B4. Amsterdam, The Netherlands. pp. 110–117.

Balenović, I., Alberti, G., and Marjanović, H. 2013. Airborne laser scanning - the status and perspectives for the application in the South-East European forestry. *South-east European forestry* 4(2): 59–79. doi:10.15177/seefor.13-07.

Baltsavias, E.P. 1999. A comparison between photogrammetry and laser scanning. *ISPRS Journal of Photogrammetry and Remote Sensing* 54(2–3): 83–94. doi:10.1016/S0924-2716(99)00014-3.

Belgiu, M., and Drăgu, L. 2016. Random forest in remote sensing: a review of applications and future directions. *ISPRS Journal of Photogrammetry and Remote Sensing* 114: 24–31. doi:10.1016/j.isprsjprs.2016.01.011.

Bellman, R. 1961. Adaptive control processes: a guided tour. Princeton University Press, Princeton, NJ, USA.

Beyer, K., Goldstein, J., Ramakrishnan, R., and Shaft, U. 1999. When is "nearest neighbor" meaningful? *In* Lecture notes in computer science. *Edited by* G. Goos, J. Hartmanis, and J. van Leeuwen. Springer-Verlag, Berlin, Germany. pp. 217–235.

Blum, A.L., and Langley, P. 1997. Selection of relevant features and examples in machine learning. *Artificial Intelligence* 97(1–2): 245–271. doi:10.1016/s0004-3702(97)00063-5.

Bollandsås, O.M., and Næsset, E. 2007. Estimating percentile-based diameter distributions in uneven-sized Norway spruce stands using airborne laser scanner data. *Scandinavian Journal of Forest Research* 22(1): 33–47. doi:10.1080/02827580601138264.

Bonnet, S., Lisein, J., and Lejeune, P. 2017. Comparison of UAS photogrammetric products for tree detection and characterization of coniferous stands. *International Journal of Remote Sensing* 38(19): 5310–5337. Taylor & Francis. doi:10.1080/01431161.2017.1338839.

Breidenbach, J., Næsset, E., Lien, V., Gobakken, T., and Solberg, S. 2010. Prediction of species specific forest inventory attributes using a nonparametric semi-individual tree crown approach based on fused airborne laser scanning and multispectral data. *Remote Sensing of Environment* 114(4): 911–924. Elsevier Inc. doi:10.1016/j.rse.2009.12.004.

Breiman, L. 2001. Random Forests. *Machine Learning* 45(1): 5–32.

Burkhart, H.E., and Tomé, M. 2012. Modeling forest trees and stands. Springer Netherlands, Dordrecht. doi:10.1007/978-90-481-3170-9.

Cao, Q. V., and Dean, T.J. 2013. State-of-the-art: DTM generation using airborne LIDAR data. *In* Proceedings of the 15th biennial southern silvicultural research conference. e-Gen. Tech. Rep. SRS-GTR-175. *Edited by* S.R.S. U.S. Department of Agriculture, Forest Service. Asheville, USA. pp. 201–205. Available from http://www.treesearch.fs.fed.us/pubs/43592.

Chen, Q., Gong, P., Baldocchi, D., and Tian, Y.Q. 2007. Estimating basal area and stem volume for

individual trees from lidar data. *Photogrammetric Engineering & Remote Sensing* 73(12): 1355–1365. doi:10.14358/PERS.73.12.1355.

Chen, Z., Gao, B., and Devereux, B. 2017. State-of-the-Art: DTM Generation Using Airborne LIDAR Data. *Sensors* 17(12): 150. doi:10.3390/s17010150.

Chirici, G., Mura, M., McInerney, D., Py, N., Tomppo, E.O., Waser, L.T., Travaglini, D., and McRoberts, R.E. 2016. A meta-analysis and review of the literature on the k-Nearest Neighbors technique for forestry applications that use remotely sensed data. *Remote Sensing of Environment* 176: 282–294. Elsevier Inc. doi:10.1016/j.rse.2016.02.001.

Colomina, I., and Molina, P. 2014. Unmanned aerial systems for photogrammetry and remote sensing: a review. *ISPRS Journal of Photogrammetry and Remote Sensing* 92: 79–97. International Society for Photogrammetry and Remote Sensing, Inc. (ISPRS). doi:10.1016/j.isprsjprs.2014.02.013.

Crookston, N.L., and Finley, A.O. 2015. yaImpute : an R package for kNN imputation. *Journal of Statistical Software* 23(10). doi:10.18637/jss.v023.i10.

Dandois, J., Olano, M., and Ellis, E. 2015. Optimal sltitude, overlap, and weather conditions for computer vision UAV estimates of forest structure. *Remote Sensing* 7(10): 13895–13920. doi:10.3390/rs71013895.

Dash, J., Pont, D., Watt, M.S., Dash, J., Pont, D., Brownlie, R., Dunningham, A., Watt, M., and Pearse, G. 2016. Remote sensing for precision forestry. *NZ Journal of Forestry* (June): 15–24.

Dubayah, R.O., and Drake, J.B. 2000. Lidar remote sensing for forestry. *Journal of Forestry* 98(6): 44–46. doi:10.1093/jof/98.6.44.

Dudani, S.A. 1976. The distance-weighted k-nearest-neighbor rule. *IEEE Transactions on Systems, Man, and Cybernetics* (4): 325–327. doi:10.1109/TSMC.1976.5408784.

Eitel, J.U.H., Höfle, B., Vierling, L.A., Abellán, A., Asner, G.P., Deems, J.S., Glennie, C.L., Joerg, P.C., LeWinter, A.L., Magney, T.S., Mandlburger, G., Morton, D.C., Müller, J., and Vierling, K.T. 2016. Beyond 3-D: the new spectrum of lidar applications for earth and ecological sciences. *Remote Sensing of Environment* 186: 372–392. doi:10.1016/j.rse.2016.08.018.

Eltner, A., Kaiser, A., Castillo, C., Rock, G., Neugirg, F., and Abellán, A. 2016. Image-based surface reconstruction in geomorphometry - merits, limits and developments. *Earth Surface Dynamics* 4(2): 359–389. doi:10.5194/esurf-4-359-2016.

Evans, J.S., and Hudak, A.T. 2007. A multiscale curvature algorithm for classifying discrete return LiDAR in forested environments. *IEEE Transactions on Geoscience and Remote Sensing* 45(4): 1029–1038. doi:10.1109/TGRS.2006.890412.

Fassnacht, F.E.E., Hartig, F., Latifi, H., Berger, C., Hernández, J., Corvalán, P., and Koch, B. 2014. Importance of sample size, data type and prediction method for remote sensing-based estimations of aboveground forest biomass. *Remote Sensing of Environment* 154(1): 102–114. doi:10.1016/j.rse.2014.07.028.

Fonseca, T.F., Marques, C.P., and Parresol, B.R. 2009. Describing maritime pine diameter distributions with Johnson's SB distribution using a new all-parameter recovery approach. *Forest Science* 55(4): 367–373.

García-Gutiérrez, J., Martínez-Álvarez, F., Troncoso, A., and Riquelme, J.C. 2015. A comparison of machine learning regression techniques for LiDAR-derived estimation of forest variables. *Neurocomputing* 167: 24–31. Elsevier. doi:10.1016/j.neucom.2014.09.091.

Genuer, R., Poggi, J.-M., and Tuleau-Malot, C. 2010. Variable selection using random forests. *Pattern Recognition Letters* 31(14): 2225–2236. Elsevier B.V. doi:10.1016/j.patrec.2010.03.014.

Gleason, C.J., and Im, J. 2012. Forest biomass estimation from airborne LiDAR data using machine learning approaches. *Remote Sensing of Environment* 125: 80–91. Elsevier Inc. doi:10.1016/j.rse.2012.07.006.

Gobakken, T., Korhonen, L., and Næsset, E. 2013. Laser-assisted selection of field plots for an area-based forest inventory. *Silva Fennica* 47(5): 1–20. doi:10.14214/sf.943.

Gobakken, T., and Næsset, E. 2005. Weibull and percentile models for lidar-based estimation of basal area distribution. *Scandinavian Journal of Forest Research* 20(6): 490–502. doi:10.1080/02827580500373186.

Goodbody, T.R.H., Coops, N.C., and White, J.C. 2019. Digital aerial photogrammetry for updating area-based forest inventories: a review of opportunities, challenges, and future directions. *Current Forestry Reports* 5(2): 55–75. Current Forestry Reports. doi:10.1007/s40725-019-00087-2.

Goodwin, N.R., Coops, N.C., and Culvenor, D.S. 2006. Assessment of forest structure with airborne LiDAR and the effects of platform altitude. *Remote Sensing of Environment* 103(2): 140–152. doi:10.1016/j.rse.2006.03.003.

Graham, A., Coops, N.C., Wilcox, M., and Plowright, A. 2019. Evaluation of ground surface models derived from unmanned aerial systems with digital aerial photogrammetry in a disturbed conifer forest. *Remote Sensing* 11(1): 1–21. doi:10.3390/rs11010084.

Gregoire, T.G., Lin, Q.F., Boudreau, J., and Nelson, R. 2008. Regression estimation following the square-root transformation of the response. *Forest Science* 54(6): 597–606. doi:doi.org/10.1093/forestscience/54.6.597.

Guerra-Hernández, J., Cosenza, D.N., Rodriguez, L.C.E., Silva, M., Tomé, M., Díaz-Varela, R.A., and González-Ferreiro, E. 2018. Comparison of ALS- and UAV(SfM)-derived high-density point clouds for individual tree detection in Eucalyptus plantations. *International Journal of Remote Sensing* 39(15–16): 5211–5235. Taylor & Francis. doi:10.1080/01431161.2018.1486519.

Guimarães, N., Pádua, L., Marques, P., Silva, N., Peres, E., and Sousa, J.J. 2020. Forestry remote sensing from unmanned aerial vehicles: a review focusing on the data, processing and potentialities. *Remote Sensing* 12(6): 1046. doi:10.3390/rs12061046.

Hastie, T., Tibshirani, R., and Friedman, J. 2009. The elements of statistical learning: data mining, inference, and prediction. *In* 2nd edition. Springer Netherlands.

Haykin, S.O. 2009. Neural networks and learning machines. *In* 3rd edition. Pearson education, Inc., Upper Saddle River, USA.

Hollaus, M. 2015. 3D point clouds for forestry applications. *Österreichische Z. Vermess. Geoinf. VGI* 103: 138–150.

Holopainen, M., Vastaranta, M., and Hyyppä, J. 2014. Outlook for the next generation's precision forestry in Finland. *Forests* 5(7): 1682–1694. doi:10.3390/f5071682.

Hudak, A.T., Crookston, N.L., Evans, J.S., Hall, D.E., and Falkowski, M.J. 2008. Nearest neighbor imputation of species-level, plot-scale forest structure attributes from LiDAR data. *Remote Sensing of Environment* 112(5): 2232–2245. doi:10.1016/j.rse.2007.10.009.

Hudak, A.T., Evans, J.S., and Stuart Smith, A.M. 2009. LiDAR utility for natural resource managers. *Remote Sensing* 1(4): 934–951. doi:10.3390/rs1040934.

Iglhaut, J., Cabo, C., Puliti, S., Piermattei, L., O'Connor, J., and Rosette, J. 2019. Structure from motion

photogrammetry in forestry: a review. *Current Forestry Reports* 5(3): 155–168. Current Forestry Reports. doi:10.1007/s40725-019-00094-3.

Iqbal, I.A., Musk, R.A., Osborn, J., Stone, C., and Lucieer, A. 2019. A comparison of area-based forest attributes derived from airborne laser scanner, small-format and medium-format digital aerial photography. *International Journal of Applied Earth Observation and Geoinformation* 76(August 2018): 231–241. Elsevier. doi:10.1016/j.jag.2018.12.002.

Johnson, N.L. 1949. Systems of frequency curves generated by methods of translation. *Biometrika* 36(1/2): 149. doi:10.2307/2332539.

Kaartinen, H., Hyyppä, J., Yu, X., Vastaranta, M., Hyyppä, H., Kukko, A., Holopainen, M., Heipke, C., Hirschmugl, M., Morsdorf, F., Næsset, E., Pitkänen, J., Popescu, S., Solberg, S., Wolf, B.M., and Wu, J.-C. 2012. An international comparison of individual tree detection and extraction using airborne laser scanning. *Remote Sensing* 4(4): 950–974. doi:10.3390/rs4040950.

Kirkpatrick, S., Gelatt, C.D., and Vecchi, M.P. 1983. Optimization by simulated annealing. *Science* 220(4598): 671–680. doi:10.1126/science.220.4598.671.

Kotivuori, E., Korhonen, L., and Packalen, P. 2016. Nationwide airborne laser scanning based models for volume, biomass and dominant height in Finland. *Silva Fennica* 50(4): 1–28. doi:10.14214/sf.1567.

Kotivuori, E., Maltamo, M., Korhonen, L., and Packalen, P. 2018. Calibration of nationwide airborne laser scanning based stem volume models. *Remote Sensing of Environment* 210(October 2017): 179–192. Elsevier. doi:10.1016/j.rse.2018.02.069.

Kraus, K., and Pfeifer, N. 1998. Determination of terrain models in wooded areas with airborne laser scanner data. *ISPRS Journal of Photogrammetry and Remote Sensing* 53(4): 193–203. doi:10.1016/S0924-2716(98)00009-4.

Kukkonen, M., Maltamo, M., Korhonen, L., and Packalen, P. 2019. Multispectral airborne LiDAR data in the prediction of boreal tree species composition. *IEEE Transactions on Geoscience and Remote Sensing* 57(6): 3462–3471. IEEE. doi:10.1109/TGRS.2018.2885057.

Latifi, H., Fassnacht, F., and Koch, B. 2012. Forest structure modeling with combined airborne hyperspectral and LiDAR data. *Remote Sensing of Environment* 121: 10–25. doi:10.1016/j.rse.2012.01.015.

Latifi, H., and Koch, B. 2012. Evaluation of most similar neighbour and random forest methods for imputing forest inventory variables using data from target and auxiliary stands. *International Journal of Remote Sensing* 33(21): 6668–6694. doi:10.1080/01431161.2012.693969.

Latifi, H., Nothdurft, A., and Koch, B. 2010. Non-parametric prediction and mapping of standing timber volume and biomass in a temperate forest: application of multiple optical/LiDAR-derived predictors. *Forestry* 83(4): 395–407. doi:10.1093/forestry/cpq022.

Lawrence, R.L., Wood, S.D., and Sheley, R.L. 2006. Mapping invasive plants using hyperspectral imagery and Breiman Cutler classifications (randomForest). *Remote Sensing of Environment* 100(3): 356–362. doi:10.1016/j.rse.2005.10.014.

Lefsky, M. a., Cohen, W.B., Parker, G.G., and Harding, D.J.D. 2002. Lidar remote sensing for ecosystem studies. *BioScience* 52(1): 19. doi:10.1641/0006-3568(2002)052[0019:LRSFES]2.0.CO;2.

Liaw, A., and Wiener, M. 2002. Classification and regression by randomForest. *R news* 2(December): 18–22. doi:10.1177/154405910408300516.

Lim, K., Treitz, P., Wulder, M., St-Onge, B., and Flood, M. 2003. LiDAR remote sensing of forest structure. *Progress in Physical Geography: Earth and Environment* 27(1): 88–106.

doi:10.1191/0309133303pp360ra.

Lin, Y., and Jeon, Y. 2002. Random forests and adaptive nearest neighbors. *In* Technical report nº 1055. Madison, Wisconsin, USA.

Lindberg, E., and Holmgren, J. 2017. Individual tree crown methods for 3D data from remote sensing. *Current Forestry Reports* 3(1): 19–31. Current Forestry Reports. doi:10.1007/s40725-017-0051-6.

Liu, X. 2008. Airborne LiDAR for DEM generation: some critical issues. *Progress in Physical Geography: Earth and Environment* 32(1): 31–49. doi:10.1177/0309133308089496.

Maclean, G.A., and Krabill, W.B. 1986. Gross-merchantable timber volume estimation using an airborne lidar system. *Canadian Journal of Remote Sensing* 12(1): 7–18. doi:10.1080/07038992.1986.10855092.

Maltamo, M., Eerikäinen, K., Packalén, P., and Hyyppä, J. 2006a. Estimation of stem volume using laser scanning-based canopy height metrics. *Forestry: An International Journal of Forest Research* 79(2): 217–229. doi:10.1093/forestry/cpl007.

Maltamo, M., and Gobakken, T. 2014. Predicting tree diameter distributions. *In* Forestry applycations of airborne laser scanning: concepts and case studies. *Edited by* M. Maltamo, E. Næsset, and J. Vauhkonen. Springer Netherlands, Dordrecht. pp. 177–191. doi:10.1007/978-94-017-8663-8_9.

Maltamo, M., Malinen, J., Packalén, P., Suvanto, A., and Kangas, J. 2006b. Nonparametric estimation of stem volume using airborne laser scanning, aerial photography, and stand-register data. *Canadian Journal of Forest Research* 36(2): 426–436. doi:10.1139/x05-246.

Maltamo, M., Mehtätalo, L., Valbuena, R., Vauhkonen, J., and Packalen, P. 2018. Airborne laser scanning for tree diameter distribution modelling: a comparison of different modelling alternatives in a tropical single-species plantation. *Forestry: An International Journal of Forest Research* 91(1): 121–131. doi:10.1093/forestry/cpx041.

Maltamo, M., Peuhkurinen, J., Malinen, J., Vauhkonen, J., Packalén, P., and Tokola, T. 2009. Predicting tree attributes and quality characteristics of scots pine using airborne laser scanning data. *Silva Fennica* 43(3): 507–521. doi:10.14214/sf.203.

Mateus, A., and Tomé, M. 2011. Modelling the diameter distribution of Eucalyptus plantations with Johnson's SBprobability density function: Parameters recovery from a compatible system of equations to predict stand variables. *Annals of Forest Science* 68(2): 325–335. doi:10.1007/s13595-011-0037-7.

McRoberts, R.E., Chen, Q., Domke, G.M., Næsset, E., Gobakken, T., Chirici, G., and Mura, M. 2017. Optimizing nearest neighbour configurations for airborne laser scanning-assisted estimation of forest volume and biomass. *Forestry* 90(1): 99–111. doi:10.1093/forestry/cpw035.

McRoberts, R.E., Næsset, E., and Gobakken, T. 2013. Inference for lidar-assisted estimation of forest growing stock volume. *Remote Sensing of Environment* 128: 268–275. Elsevier B.V. doi:10.1016/j.rse.2012.10.007.

McRoberts, R.E., Næsset, E., and Gobakken, T. 2015. Optimizing the k-nearest neighbors technique for estimating forest aboveground biomass using airborne laser scanning data. *Remote Sensing of Environment* 163(August): 13–22. doi:10.1016/j.rse.2015.02.026.

Meng, X., Currit, N., and Zhao, K. 2010. Ground filtering algorithms for airborne LiDAR data: A review of critical issues. *Remote Sensing* 2(3): 833–860. doi:10.3390/rs2030833.

Moeur, M., and Stage, A.R. 1995. Most Similar Neighbor: an improved sampling inference procedure for natural resource planning. *Forest Science* 41(2): 337–359.

Mohan, M., Silva, C.A., Klauberg, C., Jat, P., Catts, G., Cardil, A., Hudak, A.T., and Dia, M. 2017. Individual tree detection from Unmanned Aerial Vehicle (UAV) derived Canopy Height Model in an open canopy mixed conifer forest. *Forests* 8(9): 340. doi:10.3390/f8090340.

Myers, R.H. 1989. Classical and modern regression with applications. Duxbury Press, Boston, Massachusetts.

Næsset, E. 2002. Predicting forest stand characteristics with airborne scanning laser using a practical two-stage procedure and field data. *Remote Sensing of Environment* 80(1): 88–99. doi:10.1016/S0034-4257(01)00290-5.

Næsset, E. 2004. Practical large-scale forest stand inventory using a small-footprint airborne scanning laser. *Scandinavian Journal of Forest Research* 19(2): 164–179. doi:10.1080/02827580310019257.

Næsset, E. 2014. Area-based inventory in Norway – from innovation to an operational reality. *In* Forestry Applications of Airborne Laser Scanning. *Edited by* M. Maltamo, E. Næsset, and J. Vauhkonen. Springer, Dordrecht. pp. 215–240. doi:10.1007/978-94-017-8663-8_11.

Nelson, R. 2013. How did we get here? An early history of forestry lidar 1. *Canadian Journal of Remote Sensing* 39(sup1): S6–S17. Taylor & Francis. doi:10.5589/m13-011.

Nelson, R., Krabill, W., and Tonelli, J. 1988. Estimating forest biomass and volume using airborne laser data. *Remote Sensing of Environment* 267(2): 247–267. doi:10.1016/0034-4257(88)90028-4.

Nex, F., and Remondino, F. 2014. UAV for 3D mapping applications: a review. *Applied Geomatics* 6(1): 1–15. doi:10.1007/s12518-013-0120-x.

Nilsson, M., Nordkvist, K., Jonzén, J., Lindgren, N., Axensten, P., Wallerman, J., Egberth, M., Larsson, S., Nilsson, L., Eriksson, J., and Olsson, H. 2017. A nationwide forest attribute map of Sweden predicted using airborne laser scanning data and field data from the National Forest Inventory. *Remote Sensing of Environment* 194: 447–454. Elsevier Inc. doi:10.1016/j.rse.2016.10.022.

Nord-Larsen, T., and Riis-Nielsen, T. 2010. Developing an airborne laser scanning dominant height model from a countrywide scanning survey and national forest inventory data. *Scandinavian Journal of Forest Research* 25(3): 262–272. doi:10.1080/02827581.2010.486000.

de Oliveira, L.T., Ferreira, M.Z., de Carvalho, L.M.T., Filho, A.C.F., Oliveira, T.C. de A., Silveira, E.M. de O., and Junior, F.W.A. 2014. Determining timber volume of eucalyptus stands by airborne laser scanning [In Portuguese]. *Pesquisa Agropecuaria Brasileira* 49(9): 692–700. doi:10.1590/S0100-204X2014000900005.

Packalén, P., Heinonen, T., Pukkala, T., Vauhkonen, J., and Maltamo, M. 2011a. Dynamic treatment units in eucalyptus plantation. *Forest Science* 57(5): 416–426.

Packalén, P., and Maltamo, M. 2006. Predicting the plot volume by tree species using airborne laser scanning and aerial photographs. *Forest Science* 52(6): 611–622. doi:10.109352.6.611.

Packalén, P., and Maltamo, M. 2007. The k-MSN method for the prediction of species-specific stand attributes using airborne laser scanning and aerial photographs. *Remote Sensing of Environment* 109(3): 328–341. doi:10.1016/j.rse.2007.01.005.

Packalén, P., Mehtätalo, L., and Maltamo, M. 2011b. ALS-based estimation of plot volume and site index in a eucalyptus plantation with a nonlinear mixed-effect model that accounts for the clone effect. *Annals of Forest Science* 68(6): 1085–1092. doi:10.1007/s13595-011-0124-9.

Packalén, P., Temesgen, H., and Maltamo, M. 2012. Variable selection strategies for nearest neighbor imputation methods used in remote sensing based forest inventory. *Canadian Journal of Remote*

Sensing 38(5): 557–569. doi:10.5589/m12-046.

Parresol, B.R. 2003. Recovering parameters of Johnson's SB distribution. *In* Research Paper SRS-31. U.S. Department of Agriculture (USDA) Forest Service, Southern Research Station, Asheville, NC. Available from http://www.treesearch.fs.fed.us/pubs/5455.

Pascual, A., Bravo, F., and Ordoñez, C. 2019. Assessing the robustness of variable selection methods when accounting for co-registration errors in the estimation of forest biophysical and ecological attributes. *Ecological Modelling* 403(February): 11–19. Elsevier. doi:10.1016/j.ecolmodel.2019.04.018.

Picos, J., Bastos, G., Míguez, D., Alonso, L., and Armesto, J. 2020. Individual tree detection in a eucalyptus plantation using unmanned aerial vehicle (UAV)-LiDAR. *Remote Sensing* 12(5): 885. doi:10.3390/rs12050885.

Popescu, S.C. 2007. Estimating biomass of individual pine trees using airborne lidar. *Biomass and Bioenergy* 31(9): 646–655. doi:10.1016/j.biombioe.2007.06.022.

R Core Team. 2020. R: a language and environment for statistical computing (v4.0.0). R Foundation for Statistical Computing, Vienna, Austria. Available from https://www.r-project.org/ [accessed 5 July 2021].

Reutebuch, S.E., Andersen, H.E., and McGaughey, R.J. 2005. Light detection and ranging (LIDAR): an emerging tool for multiple resource inventory. *Journal Of Forestry* 103(6): 286–292. doi:10.1080/01431160500396493.

Roberts, D.R., Bahn, V., Ciuti, S., Boyce, M.S., Elith, J., Guillera-Arroita, G., Hauenstein, S., Lahoz-Monfort, J.J., Schröder, B., Thuiller, W., Warton, D.I., Wintle, B.A., Hartig, F., and Dormann, C.F. 2017. Cross-validation strategies for data with temporal, spatial, hierarchical, or phylogenetic structure. *Ecography* 40(8): 913–929. doi:10.1111/ecog.02881.

Saeys, Y., Inza, I., and Larrañaga, P. 2007. A review of feature selection techniques in bioinformatics. *Bioinformatics* 23(19): 2507–2517. doi:10.1093/bioinformatics/btm344.

Segal, M.R. 2004. Machine Learning Benchmarks and Random Forest Regression. *Biostatistics*: 1–14. Center for Bioinformatics & Molecular Biostatistic, San Francisco, CA. Available from http://escholarship.org/uc/item/35x3v9t4.pdf.

Shataee, S. 2013. Forest attributes estimation using aerial laser scanner and TM data. *Forest Systems* 22(3): 484. doi:10.5424/fs/2013223-03874.

Shataee, S., Weinaker, H., and Babanejad, M. 2011. Plot-level forest volume estimation using airborne laser scanner and TM data, comparison of boosting and random forest tree regression algorithms. *Procedia Environmental Sciences* 7: 68–73. doi:10.1016/j.proenv.2011.07.013.

Shi, Y., Wang, T., Skidmore, A.K., and Heurich, M. 2018. Important LiDAR metrics for discriminating forest tree species in Central Europe. *ISPRS Journal of Photogrammetry and Remote Sensing* 137: 163–174. International Society for Photogrammetry and Remote Sensing, Inc. (ISPRS). doi:10.1016/j.isprsjprs.2018.02.002.

Silva, C., Klauberg, C., Hudak, A., Vierling, L., Jaafar, W., Mohan, M., Garcia, M., Ferraz, A., Cardil, A., and Saatchi, S. 2017. Predicting stem total and assortment volumes in an industrial Pinus taeda L. forest plantation using airborne laser scanning data and random forest. *Forests* 8(7): 254. doi:10.3390/f8070254.

Sithole, G., and Vosselman, G. 2004. Experimental comparison of filter algorithms for bare-Earth extraction from airborne laser scanning point clouds. *ISPRS Journal of Photogrammetry and Remote Sensing*

59(1–2): 85–101. doi:10.1016/j.isprsjprs.2004.05.004.

Strunk, J., Gould, P., Packalen, P., Poudel, K., Andersen, H.-E., and Temesgen, H. 2017. An examination of diameter density prediction with k-NN and airborne lidar. *Forests* 8(11): 444. doi:10.3390/f8110444.

Talbi, E.-G. 2009. Metaheuristics: from design to implementation. John Wiley & Sons, Hoboken, NJ.

Tesfamichael, S.G., Ahmed, F.B., and van Aardt, J.A.N. 2010. Investigating the impact of discrete-return lidar point density on estimations of mean and dominant plot-level tree height in Eucalyptus grandis plantations. *International Journal of Remote Sensing* 31(11): 2925–2940. doi:10.1080/01431160903144086.

Tompalski, P., White, J.C., Coops, N.C., and Wulder, M.A. 2019. Demonstrating the transferability of forest inventory attribute models derived using airborne laser scanning data. *Remote Sensing of Environment* 227(September 2018): 110–124. Elsevier. doi:10.1016/j.rse.2019.04.006.

Vauhkonen, J., Ene, L., Gupta, S., Heinzel, J., Holmgren, J., Pitkänen, J., Solberg, S., Wang, Y., Weinacker, H., Hauglin, K.M., Lien, V., Packalén, P., Gobakken, T., Koch, B., Næsset, E., Tokola, T., and Maltamo, M. 2012. Comparative testing of single-tree detection algorithms under different types of forest. *Forestry* 85(1): 27–40. doi:10.1093/forestry/cpr051.

Vauhkonen, J., Korpela, I., Maltamo, M., and Tokola, T. 2010. Imputation of single-tree attributes using airborne laser scanning-based height, intensity, and alpha shape metrics. *Remote Sensing of Environment* 114(6): 1263–1276. Elsevier Inc. doi:10.1016/j.rse.2010.01.016.

Vauhkonen, J., Maltamo, M., Mcroberts, R.E., and Næsset, E. 2014. Forestry applications of airborne laser scanning. *Edited By* M. Maltamo, E. Næsset, and J. Vauhkonen. Springer Netherlands, Dordrecht. doi:10.1007/978-94-017-8663-8.

Wang, Y., Hyyppa, J., Liang, X., Kaartinen, H., Yu, X., Lindberg, E., Holmgren, J., Qin, Y., Mallet, C., Ferraz, A., Torabzadeh, H., Morsdorf, F., Zhu, L., Liu, J., and Alho, P. 2016. International benchmarking of the individual tree detection methods for modeling 3-D canopy structure for silviculture and forest ecology using airborne laser scanning. *IEEE Transactions on Geoscience and Remote Sensing* 54(9): 5011–5027. doi:10.1109/TGRS.2016.2543225.

Wehr, A., and Lohr, U. 1999. Airborne laser scanning—an introduction and overview. *ISPRS Journal of Photogrammetry and Remote Sensing* 54(2–3): 68–82. doi:10.1016/S0924-2716(99)00011-8.

Wulder, M.A., Bater, C.W., Coops, N.C., Hilker, T., and White, J.C. 2008. The role of LiDAR in sustainable forest management. *Forestry Chronicle* 84(6): 807–826. doi:10.5558/tfc84807-6.

Wulder, M.A., White, J.C., Nelson, R.F., Næsset, E., Ørka, H.O., Coops, N.C., Hilker, T., Bater, C.W., and Gobakken, T. 2012. Lidar sampling for large-area forest characterization: A review. *Remote Sensing of Environment* 121: 196–209. Elsevier B.V. doi:10.1016/j.rse.2012.02.001.

Yu, X., Hyyppä, J., Vastaranta, M., Holopainen, M., and Viitala, R. 2011. Predicting individual tree attributes from airborne laser point clouds based on the random forests technique. *ISPRS Journal of Photogrammetry and Remote Sensing* 66(1): 28–37. Elsevier B.V. doi:10.1016/j.isprsjprs.2010.08.003.

Zhang, K., Chen, S.C., Whitman, D., Shyu, M.L., Yan, J., and Zhang, C. 2003. A progressive morphological filter for removing nonground measurements from airborne LIDAR data. *IEEE Transactions on Geoscience and Remote Sensing* 41(4 PART I): 872–882. doi:10.1109/TGRS.2003.810682.

Appendix 1. A list of the ALS metrics by data set. The abbreviations consist of a prefix that specifies the metric type, a statistic indicator, and a suffix showing the return type. The prefixes are the height (H), intensity (I), percentage of below fractional height bin (B), and return percentage above fixed height (D). The statistic indicators for height and intensity metrics are the minimum (min), mean (mean), maximum (max), standard deviation (std), median (med), skewness (skew), kurtosis (kurt), variance (var), mode (mode), coefficient of variation (cv), interquartile distance (iqd), average absolute deviation (aad), the n-th L-moments (mom), and the number x related to the x-th height percentile. The subscripted suffixes indicate that the metric is computed from first and single return (F), or last and single returns (L), while no suffix refers to all returns.

Dataset	No. of metrics	Metrics
Brazil	18	$H10_F$ $H30_F$ $H50_F$ $H70_F$ $H90_F$ $H95_F$ $Hmean_F$ $Hstd_F$ $D10_F$ $D30_F$ $H10_L$ $H30_L$ $H50_L$ $H70_L$ $H90_L$ $H95_L$ $Hmean_L$ $Hstd_L$
Kolari	84	$D1_F$ $D2_F$ $D3_F$ $D4_F$ $D5_F$ $D6_F$ $D7_F$ $D8_F$ $D9_F$ $D10_F$ $D11_F$ $D12_F$ $D13_F$ $D14_F$ $D15_F$ $D16_F$ $D17_F$ $D18_F$ $D19_F$ $D20_F$ $D21_F$ $D22_F$ $D23_F$ $D24_F$ $H5_F$ $H10_F$ $H15_F$ $H20_F$ $H25_F$ $H30_F$ $H35_F$ $H40_F$ $H45_F$ $H50_F$ $H55_F$ $H60_F$ $H65_F$ $H70_F$ $H75_F$ $H80_F$ $H85_F$ $H90_F$ $H95_F$ $H99_F$ $Hmax_F$ $Hmean_F$ $Hstd_F$ $D1_L$ $D2_L$ $D3_L$ $D4_L$ $D5_L$ $D6_L$ $D7_L$ $D8_L$ $D9_L$ $D10_L$ $D11_L$ $D12_L$ $D13_L$ $D14_L$ $D15_L$ $D16_L$ $D17_L$ $D18_L$ $D19_L$ $D20_L$ $D21_L$ $D22_L$ $D23_L$ $H50_L$ $H55_L$ $H60_L$ $H65_L$ $H70_L$ $H75_L$ $H80_L$ $H85_L$ $H90_L$ $H95_L$ $H99_L$ $Hmax_L$ $Hmean_L$ $Hstd_L$
Liperi	58	$Hmax_F$ $Hmin_F$ $Hstd_F$ $Hmed_F$ $Hmean_F$ $Hskew_F$ $Hkurt_F$ $Imax_F$ $Istd_F$ $Imed_F$ $Imean_F$ $Iskew_F$ $Ikurt_F$ $H10_F$ $H30_F$ $H50_F$ $H70_F$ $H90_F$ $I10_F$ $I30_F$ $I50_F$ $I70_F$ $I90_F$ $D0.5_F$ $D2_F$ $D5_F$ $D10_F$ $D15_F$ $D20_F$ $Hmax_L$ $Hmin_L$ $Hstd_L$ $Hmed_L$ $Hmean_L$ $Hskew_L$ $Hkurt_L$ $Imax_L$ $Imin_L$ $Istd_L$ $Imed_L$ $Imean_L$ $Iskew_L$ $Ikurt_L$ $H10_L$ $H30_L$ $H50_L$ $H70_L$ $H90_L$ $I10_L$ $I30_L$ $I50_L$ $I70_L$ $I90_L$ $D0.5_L$ $D2_L$ $D5_L$ $D10_L$ $D15_L$
Norway	23	Hcv_F $Hmax_F$ $Hmean_F$ $H0_F$ $H10_F$ $H20_F$ $H30_F$ $H40_F$ $H50_F$ $H60_F$ $H70_F$ $H80_F$ $H90_F$ $B0_F$ $B10_F$ $B20_F$ $B30_F$ $B40_F$ $B50_F$ $B60_F$ $B70_F$ $B80_F$ $B90_F$
USA	53	$Hmax$ $Hmean$ $Hmode$ $Hstd$ $Hvar$ Hcv $Hiqd$ $Hsquew$ $Hkurt$ $Haad$ $Hmom1$ $Hmom2$ $Hmom3$ $Hmom4$ $H1$ $H5$ $H10$ $H20$ $H25$ $H30$ $H40$ $H50$ $H60$ $H70$ $H75$ $H80$ $H90$ $H95$ $H99$ $B1$ $B5$ $B10$ $B20$ $B25$ $B30$ $B40$ $B50$ $B60$ $B70$ Others: *Percentage of first returns above 1.5 m* *Percentage of all returns above 1.5 m* *Ration between all returns above 1.5 m and the total of first returns* *Number of first returns above 1.5 m* *Number of All returns above 1.5 m* *Percentage of first return above Hmean* *Percentage of first return above Hmode* *Percentage of all return above Hmean* *Percentage of all return above Hmode* *Ratio between all returns above Hmean and the total of first returns* *Ratio between all returns above Hmode and the total of first returns* *Ratio between first returns and all returns* *Ratio between first and all returns* *Ratio between second and all returns*

5 Paper 4: Predicting growing stock volume of eucalyptus plantations using 3-D point clouds derived from UAV imagery and ALS data

This chapter has been published as an original, **<u>open-access</u>** paper in Forests:

Predicting Growing Stock Volume of *Eucalyptus* Plantations Using 3-D Point Clouds Derived from UAV Imagery and ALS Data

Juan Guerra-Hernández [1,2,*], Diogo N. Cosenza [1], Adrian Cardil [3], Carlos Alberto Silva [4,5], Brigite Botequim [1], Paula Soares [1], Margarida Silva [6], Eduardo González-Ferreiro [7] and Ramón A. Díaz-Varela [8]

[1] Forest Research Centre, School of Agriculture, University of Lisbon, Instituto Superior de Agronomia (ISA), Tapada da Ajuda, 1349-017 Lisboa, Portugal; dncosenza@gmail.com (D.N.C.); bbotequim@isa.ulisboa.pt (B.B.); paulasoares@isa.ulisboa.pt (P.S.)

[2] 3edata. Centro de iniciativas empresariais. Fundación CEL. O Palomar s/n, 27004 Lugo, Spain

[3] Tecnosylva. Parque Tecnológico de León. 24009 León, Spain; adriancardil@gmail.com

[4] Biosciences Laboratory, NASA Goddard Space Flight Center, Greenbelt, MD 20707, USA; carlos_engflorestal@outlook.com

[5] Department of Geographical Sciences, University of Maryland, College Park, Maryland, MD 20740, USA

[6] RAIZ (Forest and Paper Research Institute), The Navigator Company, Rua José Estevão, 3800-783 Eixo, Portugal; margarida.silva@thenavigatorcompany.com

[7] Departamento de Tecnología Minera, Topografía y de Estructuras, Grupo de Investigación en Geomática e Ingeniería Cartográfica GI-202-GEOINCA, Escuela Superior y Técnica de Ingenieros de Minas, Universidad de León, Av. de Astorga s/n, Campus de Ponferrada, 24401 Ponferrada, Spain; egonf@unileon.es

[8] Biodiversity and Applied Botany Unit (GI BIOAPLIC 1809), Department of Botany, University of Santiago de Compostela, Escuela Politécnica Superior, R/Benigno Ledo, Campus Universitario, 27002 Lugo, Spain; ramon.diaz@usc.es

[*] Correspondence: juanguerra@isa.ulisboa.pt or juan.guerra@3edata.es; Tel.: +351-21-365-3356

Abstract: Estimating forest inventory variables is important in monitoring forest resources and mitigating climate change. In this respect, forest managers require flexible, non-destructive methods for estimating volume and biomass. High-resolution and low-cost remote sensing data are increasingly available to measure three-dimensional (3D) canopy structure and to model forest structural attributes. The main objective of this study was to evaluate and compare the individual tree volume estimates derived from high-density point clouds obtained from airborne laser scanning (ALS) and digital aerial photogrammetry (DAP) in *Eucalyptus* spp. plantations. Object-based image analysis (OBIA) techniques were applied for individual tree crown (ITC) delineation. The ITC algorithm applied correctly detected and delineated 199 trees from ALS-derived data, while 192 trees were correctly identified using DAP-based point clouds acquired from Unmanned Aerial Vehicles (UAV), representing accuracy levels of respectively 62% and 60%. Addressing volume modelling, non-linear regression fit based on individual tree height and individual crown area derived from the ITC provided the following results: Model Efficiency (Mef) = 0.43 and 0.46, Root Mean Square Error (RMSE) = 0.030 m^3 and 0.026 m^3, rRMSE = 20.31% and 19.97%, and an approximately unbiased results (0.025 m^3 and 0.0004 m^3) using DAP and ALS-based estimations, respectively. No significant difference was found between the observed value (field data) and volume estimation from ALS and DAP (*p*-value from *t*-test statistic = 0.99 and 0.98, respectively). The proposed approaches could also be used to estimate basal area or biomass stocks in *Eucalyptus* spp. plantations.

Keywords: unmanned aerial vehicles (UAV); forest inventory; volume; canopy height model (CHM); object based image analysis (OBIA); structure from motion (SfM)

1. Introduction

Sustainable forest management demands accurate information that can be obtained efficiently and rapidly [1] in order to describe forest structure and quantify forest resources [2]. However, although accurate, traditional forest inventory is resource- and time-consuming, indicating the need for either alternative or complementary methods that may overcome the drawbacks of field data acquisition [3]. In addition, although field-measured data are commonly assumed to be ground truth values for remote sensing estimations, the associated errors tend to be large [3–6].

A number of alternatives to traditional field-based measurement of morphological parameters for characterizing three-dimensional (3D) structure of trees and canopies have emerged [4,7]. Airborne Laser Scanning (ALS), Digital Aerial Photogrammetry (DAP) and Terrestrial Laser Scanning (TLS) have become widely established as forest mapping and monitoring methods [8–11]. In the last two decades, DAP, ALS (e.g., [12–14]) or a combination of these methods (e.g., [15–17]) have been increasingly used to support forest inventories at different scales.

ALS has been the primary source of 3D data on forest vertical structure since the 1990s [18,19]. There has been an abundance of research demonstrating the utility of ALS for predicting forest biophysical variables to support forest inventories at individual tree- and stand-level [20,21]. Since the late 2000s DAP has provided a promising alternative, as the accuracy of stand-based estimates has been found to be similar to that achieved through ALS, at much lower cost [17,22,23].

Baltsavias [12] provided a comprehensive comparison of DAP and ALS data, highlighting the advantages and disadvantages of both technologies with regards to acquisition, accuracy, maturity and costs. Although ALS data have many advantages (e.g., direct measurement of height, higher penetration through the vegetation), DAP still represents an essential source of data for the forest inventory analyses. In fact, photogrammetric software has developed rapidly in the past 15–20 years. Since the first studies [24], advances in computer vision, image matching algorithms and computing power have promoted the use of aerial images for generating high-resolution 3D data by image matching [25]. Many photogrammetric software packages (proprietary and open-source) have been developed, offering unparalleled opportunities to produce 3D data from 2D image collections with high overlap.

Recent advances in sensors and in image processing –particularly Structure from Motion (SfM) technology– have also enabled the extraction of dense point clouds obtained by DAP [16,24,26–29]. In this sense, DAP derived from SfM is an emerging source of 3D data, reaching quality standards close to those provided by ALS [25,30]. works by [26,31–33] pointed out the potential of DAP for forest applications. During the past five years in particular, there has been an increasing interest in the use of DAP to generate 3D data analogous to ALS data, in order to support forest inventories [17,22,25,34–39]. This interest can be attributed to the need to optimize costs while improving the temporal resolution.

Unmanned Aerial Vehicles (UAVs), also known as drones or Unmanned Aerial Systems (UAS), have emerged as a cost-effective alternative to conventional methods based on manned fixed-wing aircraft or helicopters for DAP imagery and ALS data collection [40–43]. Since the first studies in which UAV-derived data was used for forest inventory purposes [44,45], UAV-based forestry applications of both ALS and DAP have increased substantially [40,46–52]. Indeed, ALS and Red-Green-Blue (RGB) sensors mounted on UAV platforms are becoming cost-effective tools for monitoring forest structure because of their high spatial and temporal resolution, achieved by the low flight height, operational flexibility and relatively low cost of the flight surveys, which meet most of forest managers requirements [53]. In particular, light UAVs equipped with inexpensive consumer grade cameras have recently appeared as a feasible option for monitoring 3D forest structure [54]. In addition, multi-temporal UAV-acquired data can also be used for rapid, accurate and cost-effective tree growth assessment, providing up-to-date information to support decision-making in forest management [48,54–58].

Two main strategies have been adopted for DAP and ALS-based analysis in forestry inventories: (i) the Area-Based Approach (ABA), a distribution-based technique which typically provides data at stand level, and (ii) the individual tree crown (ITC) delineation, in which individual tree crowns,

heights and positions are the basic units of assessment. ABA has been used with ALS and DAP to estimate forest attributes over a wide range of forest types including Temperate (e.g., [59]), Boreal (e.g., [13,14,17,34,60]), Atlantic (e.g., [61,62]), Tropical (e.g., [37]), Alpine (e.g., [63,64]), Mediterranean forests (e.g., [65–69]) and plantations [70]. At the stand level, results from recent research on small- to medium-sized boreal and tropical forests have demonstrated the potential use of UAV-based DAP data for estimating forest biomass [53,71]. On the other hand, ITC has also been applied to DAP point clouds [72] and to ALS clouds [73,74]. ITC presents several advantages over ABA for estimation of above-ground biomass because it can be used to derive biomass when an allometric model is available at individual tree level [75]. At the same time, it is particularly well suited for precision forestry, which usually requires information about individual trees.

Finally, ALS and SfM approaches to tree height estimation tend to underestimate tree height [73,74,76,77]. Recent studies [77] have presented a model that explains the observed bias using probability theory, developing methods for correcting several ALS metrics used for ABA prediction of stand structure. However, few studies have evaluated the influence of this bias at individual-tree level. In this respect, further research is needed in order to analyze the influence of this bias in the individual-tree biomass and volume models for both technologies.

The objectives of this study were as follows: (i) to investigate the combined use of ALS- and SfM-derived individual-tree measurements (height and crown area) with non-linear regression models to estimate individual tree diameter and volume; and (ii) to compare the estimation of ALS- and SfM-derived individual-tree volume models to estimate growing stock volume in relation to field data.

2. Materials and Methods

2.1. Study Area

The study area is located in the municipality of Valongo (41.213° N, −8.496° W) in the district of Porto, Portugal (Figure 1). The site consists of a seven year old plantation of *Eucalyptus spp.* clonal material (G74), covering an area of 26 ha. Tree spacing was 3.70×2.5 m, yielding a density of one tree per 9.25 m^{-2}. The elevation ranges from 163 to 294 m above the WGS84 reference ellipsoid. The terrain is topographically complex, with steep slopes (mean slope = 24.2%), and of elevation up to 131 m. The mean annual rainfall is 1568 mm, and 42.1% of the precipitation occurs between November and January. The mean annual temperature is 14.2 °C, ranging from 8.6 °C in the coldest months (December to February) to 20.1 °C in the warmest months (July to September). The study site is characterized by evenly planted trees of superior genetic material with a low mortality rate.
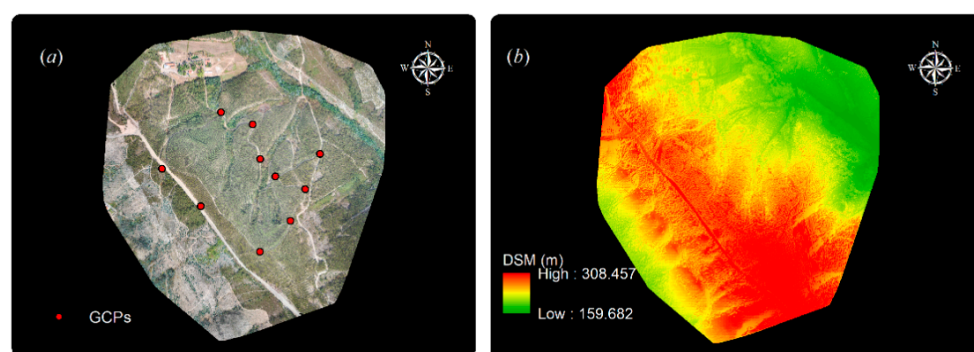
Figure 1. (**a**) UAV-derived RGB-orthomosaic image of the study area and 10 ground control points (GCPs) (red dots) (**b**) UAV-derived Digital Surface Model (DSM) generated using Pix4d$^{\circledR}$ software.

2.2. Field Measurements and Field Volume Estimation

The field data were collected in December 2016 (to correspond to the date of acquisition of ALS data) from 6 square plots, each of approximately 400 m^2 (Table 1). A total of 323 reference trees were

measured and located in 6 square plots (400 m^2). The height of each tree (*h*, m) within the plots was measured with a Haglof Vertex IV hypsometer equipped with a T3 transponder. The diameter at breast height (1.30 m above the ground – *d*, cm) was measured with a steel diameter measuring tape. Field plots were remeasured using the same methods in September 2017 (matching with UAV-based DAP acquisition).

Table 1. Statistical description of the field data within six field plots for a total of 323 reference trees

Plot	*d*		*h*		$\hat{v}$	
	Mean		**Mean**		**Mean**	
	Dec 2016	Sep 2017	Dec 2016	Sep 2017	Dec 2016	Sep 2017
P1	13.2	13.4	19.4	20.9	0.13	0.14
P2	12.9	13.3	18.8	19.9	0.12	0.15
P3	13.4	13.8	18.6	20.0	0.13	0.15
P4	13.8	14.1	18.8	19.8	0.13	0.15
P5	13.7	14.0	18.3	19.7	0.13	0.15
P6	13.8	14.2	17.6	19.1	0.13	0.14
Min.	5.3	5.4	9.9	10.3	0.01	0.01
Mean	13.5	13.8	18.6	19.9	0.13	0.14
Max.	17.3	17.8	22.8	23.5	0.24	0.26
SD	1.7	1.7	1.5	1.6	0.03	0.04

Average (Mean), minimum (Min), maximum (Max) and standard deviation (SD), values of the individual tree diameter (*d*, cm), height (*h*, m) and field data volume estimation ($\hat{v}$, m^3).

In order to obtain accurate positions of the trees, topographic surveys were conducted to determine the position of the center of each tree within the plots. A Trimble® TSC3 GPS controller with Trimble® R8s Integrate GNSS System Antenna (Trimble, Sunnyvale, CA, USA) (dual-frequency real-time kinematic receiver –RTK) was used to determine the coordinates of a densified geodetic network for the study area by applying real time kinematic (RTK). Based on the network established with GPS, a topographic survey of the plots was conducted using a Trimble® M3 Robotic Total Station (Trimble, Sunnyvale, CA, USA). Observations on the position of each tree within the plot were made during the survey.

Field-derived volumes were estimated using the Equation (1), provided by [78].

$$\hat{v} = 0.2105 \left(\frac{d}{100}\right)^{1.8191} h^{1.0703} \tag{1}$$

where $\hat{v}$ is the estimated volume (m^3), *d* is the diameter (cm) at the breast height (1.30 m) and *h* is the tree height (m).

2.3. ALS Acquisition

The airborne surveys were conducted on 17 December 2016, covering an area of 100 ha. The data were captured with Leica ALS80-HP laser scanner operating at pulse rate of 704 kHz, field of view of 6.5° and scan rate of 73.5 Hz, which was mounted on a Cessna airplane that flew the area at an approximately flight altitude of 2750 m.a.s.l and an average speed of 250 km.h^{-1}. The overlap between sweeps was 30%, achieving an average laser pulse density of 43.33 pulses m^{-2}.

2.4. UAV Data Acquisition and Use

The airborne surveys were conducted on 6 September 2017. An RGB S.O.D.A. 10.2 (20 MP) camera (senseFly Co, Cheseaux-Lausanne, Switzerland) was mounted, with nadir view, on a fixed-wing UAV (SenseFly eBee) (Figure 2). The camera, which was equipped with a 12.75 × 8.5 mm sensor

and 5472×3648 pixels detector, was used in manual mode. Exposure settings (ISO 150 and shutter speed of 1/1000 s) were set before each take-off according to the light conditions. This provided ~6 cm pixel^{-1} resolution for a variable altitude above ground level, which is especially useful in areas of diverse elevation range such as mountainous regions. Atmospheric conditions during the airborne surveys were characterized by calm winds, clear lighting at the flight time (between 11.30 am and 12.15 pm) to minimize the effect of shadowing. Flight parameters were determined using eMotion V. 3.2.4 flight planning and monitoring software. The flight plan covered the entire study area with longitudinal and lateral overlaps of 85% in both cases. The flight line spacing was 25 m (Figure 2). In total, 744 images were used to generate orthomosaics and Digital Surface Models (DSMs) by the SfM image reconstruction process. Two-block flights were required to capture the entire forest study area (the orthomosaic covered an area 103.70 ha with average Ground Sample Distance (GSD) of 5.95 cm).
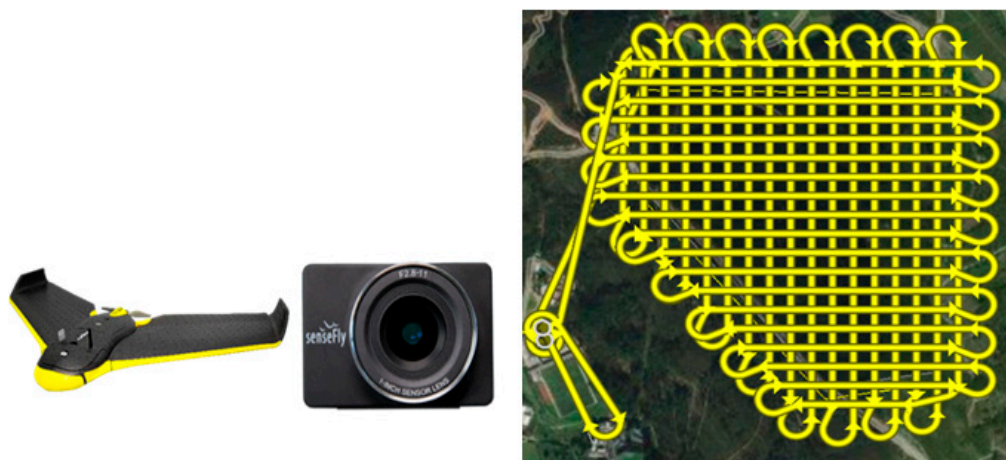

Figure 2. UAV Camera (left) and flight design (right).

2.5. 3D Model Generation and Preprocessing Point Clouds

The absolute orientation of the aerial photos was determined using aerotriangulation techniques implemented in pix4D 3.3.29 (pix4D®, Ecublens, Switzerland). A set of 10 ground control points (GCPs) measured in the field with topographic methods was used to georeference the SfM mosaics to a projected coordinate system for both datasets. The ground control photogrammetric points (GCPs) were captured with a Trimble TSC3 controller and a Trimble R8s GNSS antenna (RTK precision 8 mm + 1 ppm Horizontal/15 mm + 0.5 ppm Vertical) mounted on a pole. The GCPs markers comprised a set of 1×1 m cross-shaped white painted timber planks with some black and white 50×50 cm painted checkerboards. For reliable accuracy of GPS measurement, all GCPs were located in open areas with no canopy cover. At each point, GPS signals were logged in RTK–global navigation satellite system (GNSS) mode. The recordings were processed with real-time correction data retrieved from the fixed base station in Gaia (Porto) (latitude: 41°06′21.67048″ N, longitude: 8°35′20.73434″ W, and ellipsoidal elevation: 287.63 m above the WGS84 reference ellipsoid).

Photogrammetric point clouds were computed using SfM techniques, implemented in Pix4D 3.3.29. The matching parameters for point cloud densification were set as follows: multiscale, image scale = 1/2 (half image size) and point density = 'optimal'. The minimum number of matched images was also set to 3. DEM$_{SfM}$ was generated from the ground points by using a natural neighbor interpolation technique implemented in Pix4D (additional details of the algorithms are proprietary and were not disclosed by Pix4D).

The ALS and SfM point clouds preprocessed using FUSION/LDV 3.60 software [79] and LasTools [80]. For more details of point cloud processing see details in [74]. Finally, two CHMs (CHM$_{SfM}$ and CHM$_{ALS}$) were obtained by subtracting the DEMs (DEM$_{ALS}$ and DEM$_{SfM}$) from the DSMs (DSM$_{ALS}$ and DSM$_{SfM}$) in the FUSION LiDAR Toolkit [79].

2.6. ITC Process to Derive ALS- and SfM-Variables

Individual tree position (*X* and *Y* coordinates), height (h_{SfM}, h_{ALS}) and crown area (ca_{SfM}, ca_{ALS}) were retrieved from the respective CHM_{SfM} and CHM_{ALS} (Figure 2). Resampling of the CHMs to 20 cm resolution and subsequent smoothing with mean filter (5 × 5 window) in the case of ALS and median filters (3 × 3 window) for SfM were conducted using the FUSION LiDAR Toolkit [79]. Crown delineation followed the procedure detailed in [81]. The process is divided into three main phases: segmentation, classification and iterative watershed segmentation The *Chessboard Segmentation* algorithm was used to split the image into square image objects. In the second phase, a *Classification* algorithm was used to classify image objects from the smoothed CHM. Objects with an elevation value of less than 5 m were classified as gaps. The threshold was established empirically from field observations and by trial-and-error tests. The remaining objects were assigned to the 'temporary canopy' class. These objects were used to locate tree tops and delineate tree crowns in the following iterative watershed segmentation processes. In the iteration, the *Find Local Extrema algorithm* was used to classify the image objects of the 'temporary canopy' class, which fulfills a local extreme condition according to image object features within a search domain in their neighborhoods. However, because of the forest stand and tree species characteristics, the initial maximum search domain used in the iterative process (see Figure 3 in [81]) to detect top trees was changed from 5 to 3, and 4 interactions were applied. A search with a variable square window enables detection of apices of trees with a large variety of crown sizes. Objects less than 3 m away from any detected tree top were retained in the 'temporary canopy' class (candidates for watershed) and any other objects were disregarded. This distance was the maximum observed crown width in the plots, which was considered the limit for crown growing in the next step. Then, the crown delineation results (Figure 3) and tree top positions were exported in ESRI^TM shapefiles as vector polygons and points respectively, for subsequent analysis.
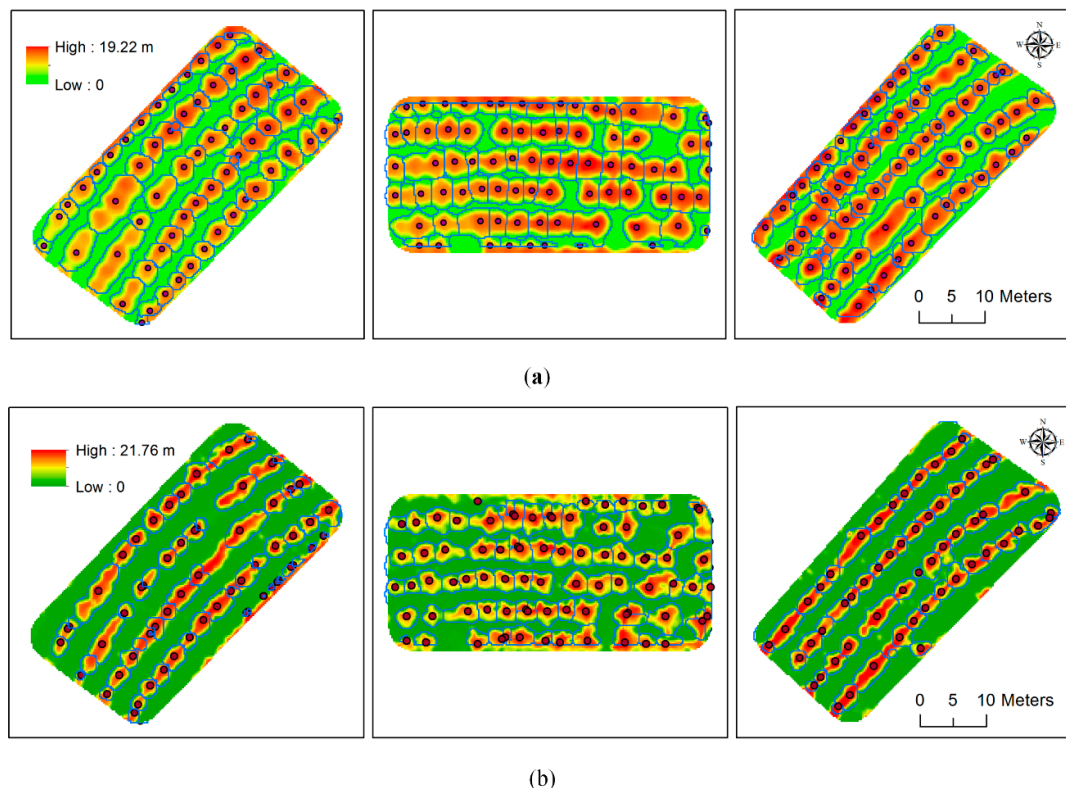

(**a**)

(b)

Figure 3. Examples of the canopy height models (cool to warm colors representing low to high heights), crown delineation (blue lines), and tree top positions (red dots) within example plots using airborne laser scanning (ALS) (**a**) and Structure from Motion (SfM) (**b**).

2.7. Individual Tree Volume Estimation

Volume equation (Equation (1)) requires the measurement of tree diameter or circumference, which is not available from UAV imagery. We therefore tested two approaches for estimating ALS- and SfM-derived individual-tree volumes (v_{SfM} and v_{ALS}) (Figure 4). In the first approach, the multiplicative (power function) model in Equation (2) was fitted using d (from field data) as the dependent variable and the pairs of explanatory variables h_{SfM}, ca_{SfM} for SfM, or h_{ALS}, ca_{ALS} for ALS. The predicted diameter obtained by each method (d_{SfM} and d_{ALS}) and their respective height estimates (h_{SfM} and h_{ALS}) were then included as independent variables in Equation (1) to predict the individual volumes for the subset of 192 trees for ALS and 199 for SfM (v_{SfM} and v_{ALS}, respectively). In the second approach, the multiplicative (power function) model in Equation (3) was also fitted to predict v_{SfM} and v_{ALS} for the 192 and 199 trees respectively, but v was considered a dependent variable (estimated using the field-measured d and h in Equation (1)), and the pairs h_{SfM}, ca_{SfM} (from SfM) or h_{ALS}, ca_{ALS} (from ALS) were considered explanatory variables, without the need to estimate the diameters.

$$\hat{d} = h^{\beta_0} ca^{\beta_1} + \varepsilon \tag{2}$$

$$\hat{v} = h^{\beta_0} ca^{\beta_1} + \varepsilon \tag{3}$$

where $\hat{v}$ is the estimated volume (m^3), $\hat{d}$ is the estimated tree diameter (cm), h is the tree height (m), ca is the canopy area (m), generated from ALS or SfM, β_0, β_1, are the exponential parameters to be estimated by non-linear regression analysis; and ε is the additive random error. The models were fitted using the Non-linear Least Squares *nls* function implemented in the *BASE* package of R software (R Core Team, 2018).

Finally, the Model Efficiency (Mef, Equation (4)), the overall root mean square error (RMSE, Equation (5)), the relative root mean square error (rRMSE, Equation (6)) and the Bias (Equation (7)) were computed in order to determine the accuracy of ALS and SfM models for estimating diameter and volume with the second approach. Mef compares predictions directly with observed data using a statistic analogous to R^2 [82]. This statistic provides a simple index of performance on a relative scale, where 1 indicates a 'perfect' fit, 0 reveals that the model is no better than a simple average, and negative values indicate a poor model.

$$Mef = 1 - \left(\frac{(n-1) \sum_{i=1}^{n} (y_i - \hat{y}_i)^2}{(n-p) \sum_{i=1}^{n} \left(y_i - \overline{y}\right)^2} \right) \tag{4}$$

$$RMSE = \sqrt{\frac{\sum_{i=1}^{n} (y_i - \hat{y}_i)^2}{n}} \tag{5}$$

$$rRMSE = \frac{RMSE}{\overline{y}} * 100 \tag{6}$$

$$Bias = \frac{\sum_{i=1}^{n} (\hat{y}_i - y_i)}{n} \tag{7}$$

where n is the number of trees; y_i is the field-measured tree diameter i; $\overline{y}$ is the the mean observed value for the field-measured diameters; $\hat{y}_i$ is the estimated value of diameter derived from the non-linear regression model and p is the number of parameters in the models.

Finally, using the correctly detected and delineated trees, d was compared with d_{SfM}, d_{ALS} and v with v_{SfM}, v_{ALS} in the subsample of 192 trees for SfM and 199 for ALS, respectively. Estimated and observed values were plotted and visually examined. A paired *t*-test was conducted to compare ALS- and SfM-predicted variables (d_{SfM}, d_{ALS}, v_{SfM}, *and* v_{ALS}) to verify the significance of the deviations between the observed and estimated values. However, these deviations were previously checked using

the Shapiro-Wilk test [83], which indicated that the distributions meet the assumption of normality. The tests were conducted at a 5%significance level.
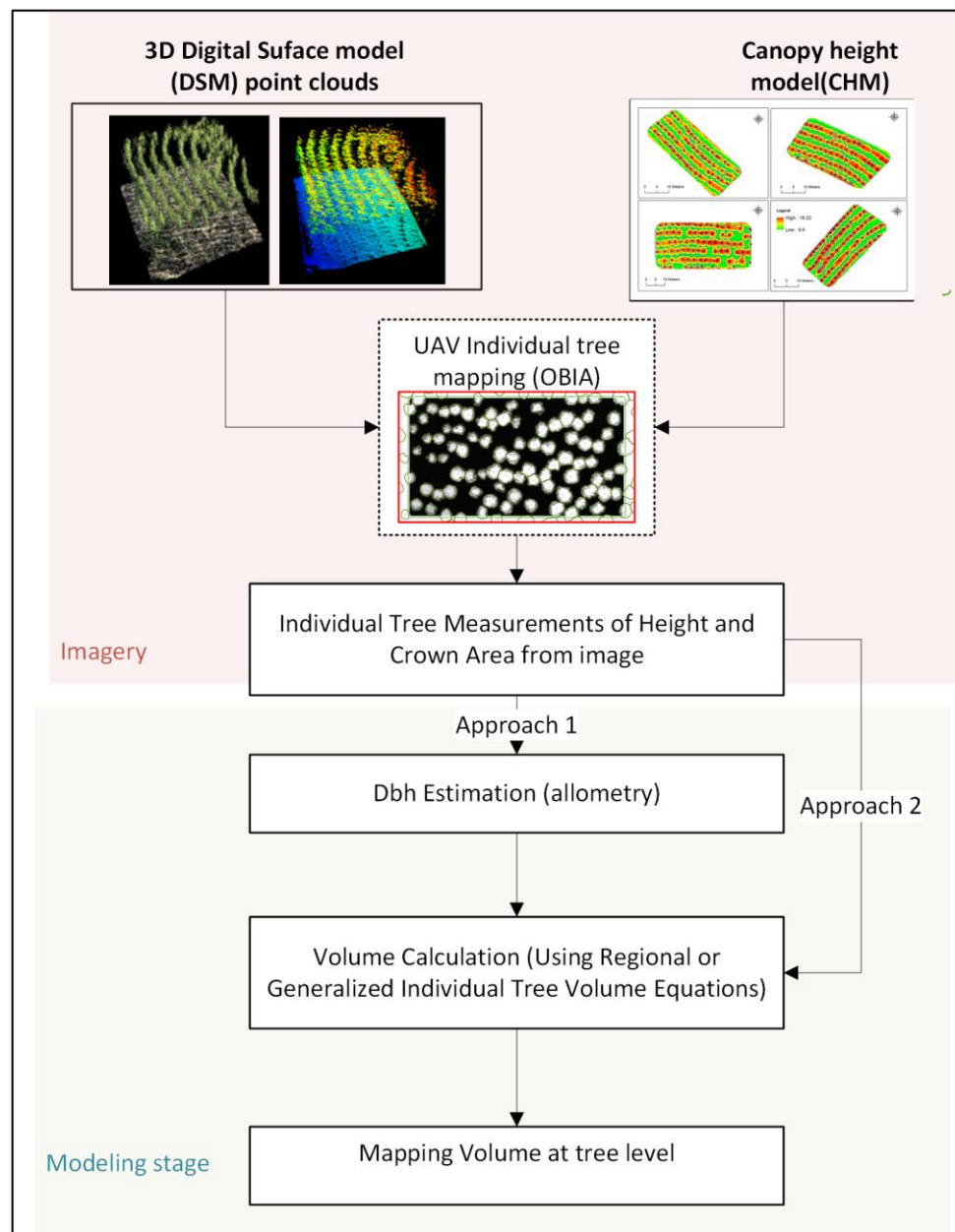

Figure 4. Summary steps of individual tree crown (ITC) to map volume.

3. Results

Field, ALS and SfM Volume Estimation

Table 2 shows the parameter estimates and goodness-of-fit statistics for the models used to predict *d* (cm) in the first approach, and *v* directly estimated by SfM- and ALS-variables in the second approach.

In the first approach, non-linear regression yielded an Mef value of 0.45 for the SfM-estimated diameter and 0.47 for ALS-estimated diameter (RMSE = 1.17 and 1.12 cm, rRMSE of 8.49 % and 8.31%, respectively). Although the UAV-based DAP method tends to underestimate tree height relative to field measurements (hypsometers), there was no appreciable bias throughout the observed diameter (Figure 5a,b). The bias values (0.38 and 0.35 cm) indicated a slight tendency to overestimate the initial diameter values from field data (Figure 5a,b). On the other hand, although *d* was not directly measured

in CHMs derived from UAV and ALS, h_{SfM} and h_{ALS} were, and these variables were significant in the SfM and ALS equations. For d_{SfM} and d_{ALS} modelling, the crown area (ca_{SfM} and ca_{ALS}) was also statistically significant ($p < 0.05$ and $p < 0.001$, respectively).

Table 2. Models selected for estimating SfM and ALS derived individual tree diameter and volume.

Approach	Dependent variable	Predictors	Parameter estimate	Standard error	*p*-value	Mef	RMSE (cm)	rRMSE (%)	bias (cm)
1st	d_{SfM}	Constant	0.863	1.170	< 0.001	0.45	1.17	8.49	0.38
		h_{SfM}	0.907	0.108	< 0.001				
		ca_{SfM}	0.037	0.037	0.013				
	d_{ALS}	Constant	0.564	0.151	< 0.001	0.47	1.12	8.31	0.35
		h_{ALS}	1.042	0.090	< 0.001				
		ca_{ALS}	0.062	0.015	< 0.001				

Approach	Dependent variable	Predictors	Parameter estimate	Standard error	*p*-value	Mef	RMSE (m^3)	rRMSE (%)	bias (m^3)
2nd	v_{SfM}	Constant	0.004	0.002	0.082	0.43	0.030	20.31	0.0016
		h_{SfM}	1.192	0.201	< 0.001				
		ca_{SfM}	0.151	0.035	< 0.001				
	v_{ALS}	Constant	0.001	0.000	0.106	0.46	0.026	19.97	0.0004
		h_{ALS}	1.828	0.224	< 0.001				
		ca_{ALS}	0.024	0.037	< 0.001				

h_{SfM} and h_{ALS} are the SfM and ALS-derived tree height (m), ca_{SfM} and ca_{ALS} are the SfM and ALS-derived individual crown area (m^2), Mef is the model efficiency statistic, RMSE is the root mean squared error and rRMSE is the relative root mean square error.
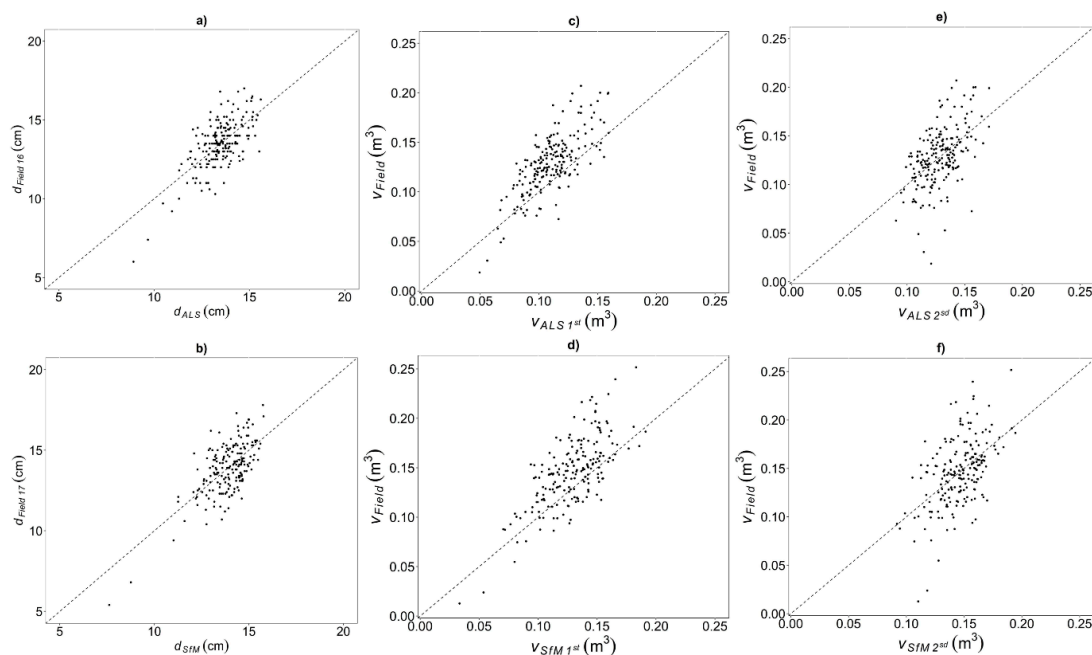

Figure 5. Scatter plots of ALS and SfM-derived variables against field-derived variables: (**a**) field-measured tree diameter (*d*) against ALS-estimated tree diameter (d_{ALS}); (**b**) field-measured tree diameter (*d*) against SfM-estimated tree diameter (d_{SfM}); (**c**) field-estimated volume (v_{field}) against ALS-estimated volume (v_{ALS}) using the first approach; (**d**) field-estimated volume (v_{field}) against SfM-estimated volume (v_{SfM}) using the first approach; (**e**) field-estimated volume (v_{field}) against ALS-estimated volume (v_{ALS}) using the second approach; (**f**) field-estimated volume (v_{field}) against SfM -estimated volume (v_{SfM}) using the second approach.

In the case of v_{ALS} modelling, the second approach yielded an Mef value of 0.56. The mean rRMSE of v estimation was 20.31% (0.030 m^3) when calculated on the basis of the SfM cloud, and 19.97% (0.026 m^3) when based on the ALS cloud. There were no appreciable biases from the models throughout the observed volume range using both approaches (Figure 5c–f). However, the tendency of ALS and SfM to underestimate h may be the main reason for the slight underestimation of v in the first approach (Figure 5c,d). In the case of the second approach, a slightly positive bias (0.0004 and 0.0016 m^3) indicated slight overestimation when volume was modeled directly form ALS- and SfM-variables (Figure 5e,f).

The *t*-test (Table 3) showed that there were no evidence of significant differences between observed and estimated values of diameter (*p*-values of 0.98 for both approaches in the subsample of 192 trees for SfM and 199 for ALS, respectively) and volume using the second approach (*p*-values of 0.99 for ALS and 0.98 for SfM, Figure 6b). However, there were significant differences using the 1st approach between the observed values and estimated value at the tree level (Table 3, Figure 6b). It is important to note that the mean values of field data for diameter and volume computed for ALS and SfM in the subsample were similar that the values considering the 6 field plots for the total of 323 reference trees, except for the mean volume values for volume in 2017 (Table 3).

Table 3. Field, ALS and SfM diameter and volume estimations from both approaches with their minimum (Min.), mean (Mean), maximum (Max.) and standard deviation (SD) values and the results for the *t*-test in the subsample of 192 trees for SfM and 199 for ALS, respectively. Field 16 and Field 17 are the field data acquisition years for ALS (Dec 2016) and SfM (Sep 2017), respectively.

| Plot | d_{ALS} (cm) | | d_{SfM} (cm) | | v_{ALS} (m^3) | | | v_{SfM} (m^3) | | |
	ALS	Field 16	SfM	Field 17	ALS 1st	ALS 2^{sd}	Field 16	SfM 1st	SfM 2^{sd}	Field 17
P1	14.1	13.3	14.3	13.4	0.13	0.15	0.13	0.15	0.15	0.14
P2	13.4	12.5	14.0	13.4	0.11	0.14	0.11	0.13	0.15	0.14
P3	13.1	13.3	13.9	14.0	0.10	0.13	0.12	0.12	0.14	0.15
P4	13.4	13.8	13.8	14.3	0.11	0.14	0.13	0.12	0.14	0.15
P5	13.5	13.8	14.0	14.2	0.11	0.14	0.13	0.13	0.15	0.15
P6	13.2	14.2	13.1	14.0	0.11	0.16	0.14	0.12	0.14	0.14
Min.	8.9	6.0	7.6	5.4	0.05	0.05	0.02	0.03	0.09	0.01
Mean	13.5	13.5	13.9	13.9	0.11	0.15	0.13	0.13	0.15	0.15
Max.	15.6	17.0	15.8	17.8	0.16	0.20	0.21	0.19	0.19	0.25
SD	1.0	1.5	1.1	1.6	0.02	0.02	0.03	0.02	0.02	0.03
t-test *p*-value	0.98		0.98		<0.001	0.99		<0.001	0.98	
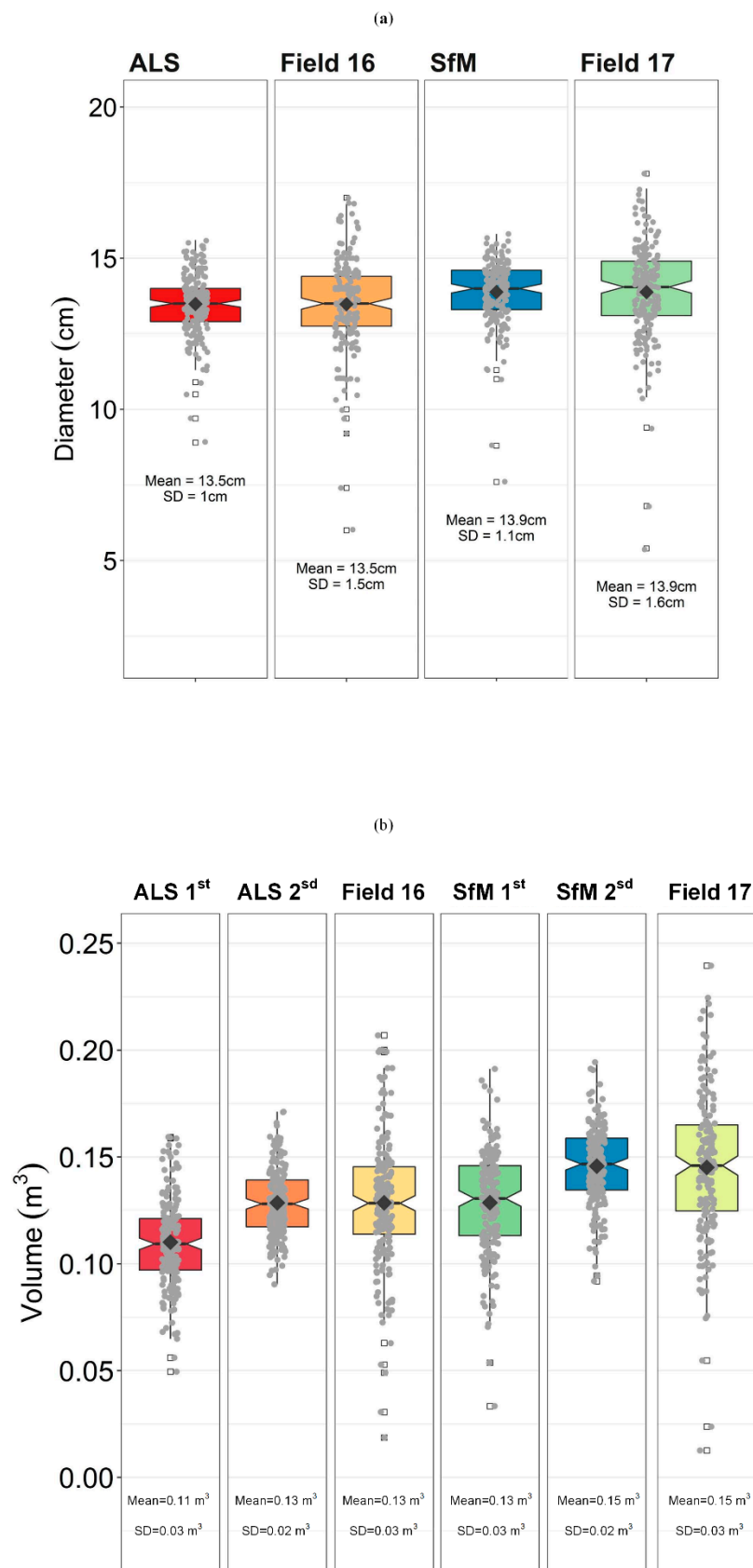
Figure 6. Box plot of field-measured and remotely sensed estimated values of diameter (**a**) and volume using the 1st approach and 2nd approach (**b**). The lower and upper areas of the boxes represent the 5th and 75th percentiles and the horizontal band represents the median. The upper and lower whiskers extend from to the highest and lowest value respectively within the 1.5 times the interquartile range.

4. Discussion

Both v_{SfM} and v_{ALS} were accurately estimated from UAV photograph and ALS-based 3-D point clouds using SfM- and ALS-variables extracted automatically from their respective CHMs. Although ALS-based methods and UAV-based DAP methods tend to underestimate tree height [73,74,77], relative to field measurements (hypsometers), no appreciable biases in the observed diameter and volume range estimations occurred with either technologies in the 2nd approach.

Variables derived from the automated processing of ALS and UAV-based DAP with ITC delineation (h_{SfM}, h_{ALS}, ca_{SfM}, and ca_{ALS}) were found to be significant explanatory variables for predicting d and v in both approaches; however, the Mef and RMSE values for diameter models indicate poorer fits than reported in some recent studies in *P. pinea* plantations [57] (Mef = 0.79, rRMSE = 4.99%, n = 50 trees) and Japanese Cypress (*Chamaecyparis obtusa*) [84] (R^2 = 0.79, n = 51 individual trees where d ranged from 11 to 58 cm) using UAV-based DAP point clouds.

In the case of ALS-based diameter models, our results were similar in terms of R^2 to those reported by Chisholm et al. [85], who extracted forest below-canopy information using UAV-based LiDAR and developed post-processing software to detect trees and to estimate their diameters (R^2 = 0.45, rRMSE = 25.1%). Finally, the results were also similar in terms of rRMSE to those reported by Cosenza et al. [86] in a eucalyptus plantation in Brazil (rRMSE = 9%), for an exponential equation with h as explanatory variable. Cosenza et al. [86] also observed a slight tendency to overestimate the initial diameter values (bias = 0.12 cm).

Studies conducted in *Picea abies* (L.) H. Karst. and *Pinus sylvestris* L. stands in Sweden and in *Pinus taeda* L. stands in the SE United States found that ALS-derived h and crown diameter (*cd*) explained up to 87% and 91% of the variance associated with the estimation of d, with RMSE of 3.8 and 4.9 cm, respectively [87,88]. Zhao et al. [89] reported an R^2 value of 0.87 and a RMSE value of 5.2 cm for ALS-derived tree dimension variables including h, *cd* and crown base height in *P. taeda* stands. In this study, the diameter equation based on ALS-derived variables performed well, although the values of Mef were slightly lower than some of those reported for other species [87,88].

Regarding volume modelling, the performance of the v_{ALS} and v_{SfM} estimates for predicting tree volume directly from ALS- and SfM-derived variables (the second approach, R^2 = 0.46, R^2 = 0.43; RMSE = 0.026 m^3, RMSE = 0.030 m^3; respectively) was lower than that obtained in different conifer species (R^2 = 0.88) [88], as well as in *P. taeda* (R^2 = 0.80) [89] and *P. pinea* (Mef = 0.84 − 0.85) [57]. The mean differences between the deviations of field volume and the ALS- or SfM-derived volume were statistically significant using the 1st approach. The tendency of ALS and UAV-based DAP technologies to underestimate h may be the main reason for the underestimation of v with 1st approach. It should be also borne in mind that the ALS and UAV-based DAP, as a tree height estimation technique, tends to underestimate tree height (e.g., DAP [39,90,91], UAV-based DAP [47,74,76,92] and ALS [73,77,93–95] point cloud data). However, our volume modelling results suggest that this bias may not influence in volume estimations using the 2nd approach, leaving open the question as to when and where specific models should be developed for correcting the bias at tree level depending on particular species or forest structure [77]. The results of this study are consistent with the approaches used by other authors [57,73], in which the use of linear regression improved the accuracy of tree height estimations from DAP-ALS data in terms of RMSE and bias, instead of using tree height extracted directly from the CHM to calculate the RMSEs and bias [74], as also occurred with modelling volume in the present study.

There are three possible reasons for the differences in performance for diameter models using SfM- and ALS-variables relative to other species: (i) First, broadleaved trees trees in particular are more challenging for both local maxima detection and delineation compared to conifer trees. (ii) Second, crown delineation remains difficult because the crowns of neighboring trees often overlap due to the high density of trees per unit area. (iii) Third, the low density of leaves in the crowns and the small size of the crowns of mature trees prevent a considerable number of laser pulses from hitting the crown (thus hampering crown delineation). As expected, the ALS cloud contributed to yielding

slightly better results for diameter and volume estimation, but we did not observe differences in terms of volume estimations. As with previous studies using DAP, ITC delineation is more affected than ALS crown delineation as UAV-based DAP has several limitations: (i) ALS is insensitive to shadows made by clouds [15], (ii) the images are strongly influenced by atmospheric conditions (e.g., wind swaying can cause problems building point clouds), solar illumination and view angles (sun, surface and sensor geometry), occlusions caused by shadows are particular problematic for generation of image-based point clouds in dense forest canopies [45,96–98]. In addition, seasonality (timing) influences underestimation of tree heights but can improve detection accuracy [99]. The allometric relationship between volume and ALS or SfM crown-derived variables could be also refined through improvements in UAV imagery acquisition and processing.

Finally, a more comprehensive examination of the effects of varying the conditions of UAV-based DAP acquisition and their implications for estimating forest inventory variables in different types of forest should be carried out using these techniques [100–102]. Many facets have not been explored with current state-of-the-art techniques. Several effects related to flight configuration (i.e., flight speed, wind effect, illumination effect), post-processing pipelines (i.e., comparing different SfM algorithms), field data collection (i.e., number of field plots) and environmental variables (i.e., effect of aspect or slope when using different DEM approaches or the DEM-independent approach) must be analyzed. Future research must also explore how the type of platform (fixed-wing versus multirotor), sensors or the type of forest (e.g., temperate, deciduous, evergreen needleleaf, and tropical forest) influence the ability of UAV-based DAP methods to accurately characterize biometric tree variables at the tree level.

5. Conclusions

The study findings showed that UAV-based DAP methods are useful and comparable to ALS for forest inventory and sustainable forest management in planted forests, by providing accurate estimations of forest structural attributes at the tree level. The results suggested that object-based image analysis (OBIA) provides more accurate predictive models for individual volumes of *Eucalyptus* trees based on ALS-derived and SfM-derived variables from the 3D point clouds than those obtained using indirect approaches to estimate diameter.

Author Contributions: Conceptualization, J.G.-H., D.N.C., A.C. and C.A.S.; Methodology, D.N.C., J.G.-H., B.B., and P.S.; Data Analysis, J.G.-H., D.N.C., and B.B.; Investigation, J.G.-H., D.N.C., B.B., E.G.-F. and R.A.D.-V.; Resources, M.S., and P.S.; Writing—Original Draft, J.G.-H., D.N.C., B.B., A.C., C.A.S. Preparation, J.G.-H., D.N.C., B.B., A.C., C.A.S., E.G.-F., and R.A.D.-V.; Writing—Review and Editing, J.G.-H., D.N.C., B.B., A.C., C.A.S., P.S., E.G.-F. and R.A.D.-V.; Funding acquisition, M.S.; Project Administration, M.S.; Supervision, E.G.-F. and R.A.D.-V.

References

1. Burkhart, H.E.; Tomé, M. *Modeling Forest Trees and Stands*; Springer Science & Business Media: Dordrecht, The Netherlands, 2012.
2. Bauwens, S.; Bartholomeus, H.; Calders, K.; Lejeune, P. Forest Inventory with Terrestrial LiDAR: A Comparison of Static and Hand-Held Mobile Laser Scanning. *Forests* **2016**, *7*, 127. [CrossRef]
3. Williams, M.S.; Bechtold, W.A.; LaBau, V.J. Five Instruments for Measuring Tree Height: An Evaluation. *South. J. Appl. For.* **1994**, *18*, 76–82. [CrossRef]

4.   Thenkabail, P.S.; Durrieu, S.; Véga, C.; Bouvier, M.; Gosselin, F.; Renaud, J.-P.; Saint-André, L. Optical Remote Sensing of Tree and Stand Heights. In *Land Resources Monitoring, Modeling, and Mapping with Remote Sensing*; CRC Press: Boca Raton, FL, USA, 2015; pp. 449–485.

5.   Díaz-Varela, R.A.; de la Rosa, R.; León, L.; Zarco-Tejada, P.J. High-Resolution Airborne UAV Imagery to Assess Olive Tree Crown Parameters Using 3D Photo Reconstruction: Application in Breeding Trials. *Remote Sens.* **2015**, *7*, 4213–4232. [CrossRef]

6.   Panagiotidis, D.; Abdollahnejad, A.; Surový, P.; Chiteculo, V. Determining Tree Height and Crown Diameter from High-Resolution UAV Imagery. *Int. J. Remote Sens.* **2016**, 1–19. [CrossRef]

7.   White, J.C.; Coops, N.C.; Wulder, M.A.; Vastaranta, M.; Hilker, T.; Tompalski, P. Remote Sensing Technologies for Enhancing Forest Inventories: A Review. *Can. J. Remote Sens.* **2016**, 1–23. [CrossRef]

8.   Giannetti, F.; Puletti, N.; Quatrini, V.; Travaglini, D.; Bottalico, F.; Corona, P.; Chirici, G. Integrating Terrestrial and Airborne Laser Scanning for the Assessment of Single-Tree Attributes in Mediterranean Forest Stands. *Eur. J. Remote Sens.* **2018**, *51*, 795–807. [CrossRef]

9.   Liang, X.; Kankare, V.; Hyyppä, J.; Wang, Y.; Kukko, A.; Haggrén, H.; Yu, X.; Kaartinen, H.; Jaakkola, A.; Guan, F. Terrestrial Laser Scanning in Forest Inventories. *ISPRS J. Photogramm. Remote Sens.* **2016**, *115*, 63–77. [CrossRef]

10.   Abegg, M.; Kükenbrink, D.; Zell, J.; Schaepman, M.E.; Morsdorf, F. Terrestrial Laser Scanning for Forest Inventories—Tree Diameter Distribution and Scanner Location Impact on Occlusion. *Forests* **2017**, *8*, 184. [CrossRef]

11.   Liu, G.; Wang, J.; Dong, P.; Chen, Y.; Liu, Z. Estimating Individual Tree Height and Diameter at Breast Height (DBH) from Terrestrial Laser Scanning (TLS) Data at Plot Level. *Forests* **2018**, *9*, 398. [CrossRef]

12.   Baltsavias, E.P. A Comparison between Photogrammetry and Laser Scanning. *ISPRS J. Photogramm. Remote Sens.* **1999**, *54*, 83–94. [CrossRef]

13.   Næsset, E. Determination of Mean Tree Height of Forest Stands by Digital Photogrammetry. *Scand. J. For. Res.* **2002**, *17*, 446–459. [CrossRef]

14.   Næsset, E. Predicting Forest Stand Characteristics with Airborne Scanning Laser Using a Practical Two-Stage Procedure and Field Data. *Remote Sens. Environ.* **2002**, *80*, 88–99. [CrossRef]

15.   White, J.; Wulder, M.; Vastaranta, M.; Coops, N.; Pitt, D.; Woods, M. The Utility of Image-Based Point Clouds for Forest Inventory: A Comparison with Airborne Laser Scanning. *Forests* **2013**, *4*, 518–536. [CrossRef]

16.   Fritz, A.; Kattenborn, T.; Koch, B. UAV-Based Photogrammetric Point Clouds—Tree Stem Mapping in Open Stands in Comparison to Terrestrial Laser Scanner Point Clouds. *Int. Arch. Photogramm. Remote Sens. Spat. Inf. Sci.* **2013**, *40*, 141–146. [CrossRef]

17.   Gobakken, T.; Bollandsås, O.M.; Næsset, E. Comparing Biophysical Forest Characteristics Estimated from Photogrammetric Matching of Aerial Images and Airborne Laser Scanning Data. *Scand. J. For. Res.* **2015**, *30*, 73–86. [CrossRef]

18.   Maltamo, M.; Næsset, E.; Vauhkonen, J. Forestry Applications of Airborne Laser Scanning. *Concepts Case Stud. Manag. Ecosys* **2014**, *27*, 2014.

19.   Naesset, E. Estimating Timber Volume of Forest Stands Using Airborne Laser Scanner Data. *Remote Sens. Environ.* **1997**, *61*, 246–253. [CrossRef]

20.   Hyyppä, J.; Hyyppä, H.; Leckie, D.; Gougeon, F.; Yu, X.; Maltamo, M. Review of Methods of Small-Footprint Airborne Laser Scanning for Extracting Forest Inventory Data in Boreal Forests. *Int. J. Remote Sens.* **2008**, *29*, 1339–1366. [CrossRef]

21.   Van Leeuwen, M.; Nieuwenhuis, M. Retrieval of Forest Structural Parameters Using LiDAR Remote Sensing. *Eur. J. For. Res.* **2010**, *129*, 749–770. [CrossRef]

22.   Puliti, S.; Gobakken, T.; Ørka, H.O.; Næsset, E. Assessing 3D Point Clouds from Aerial Photographs for Species-Specific Forest Inventories. *Scand. J. For. Res.* **2017**, *32*, 68–79. [CrossRef]

23.   Tuominen, S.; Balazs, A.; Saari, H.; Pölönen, I.; Sarkeala, J.; Viitala, R. Unmanned Aerial System Imagery and Photogrammetric Canopy Height Data in Area-Based Estimation of Forest Variables. *Silva Fenn.* **2015**, *49*. [CrossRef]

24.   Bohlin, J.; Wallerman, J.; Fransson, J.E. Forest Variable Estimation Using Photogrammetric Matching of Digital Aerial Images in Combination with a High-Resolution DEM. *Scand. J. For. Res.* **2012**, *27*, 692–699. [CrossRef]

25.   Nurminen, K.; Karjalainen, M.; Yu, X.; Hyyppä, J.; Honkavaara, E. Performance of Dense Digital Surface Models Based on Image Matching in the Estimation of Plot-Level Forest Variables. *ISPRS J. Photogramm. Remote Sens.* **2013**, *83*, 104–115. [CrossRef]

26. St-Onge, B.; Vega, C.; Fournier, R.A.; Hu, Y. Mapping Canopy Height Using a Combination of Digital Stereo-photogrammetry and Lidar. *Int. J. Remote Sens.* **2008**, *29*, 3343–3364. [CrossRef]

27. Zarco-Tejada, P.J.; Diaz-Varela, R.; Angileri, V.; Loudjani, P. Tree Height Quantification Using Very High Resolution Imagery Acquired from an Unmanned Aerial Vehicle (UAV) and Automatic 3D Photo-Reconstruction Methods. *Eur. J. Agron.* **2014**, *55*, 89–99. [CrossRef]

28. Goodbody, T.R.; Coops, N.C.; White, J.C. Digital Aerial Photogrammetry for Updating Area-Based Forest Inventories: A Review of Opportunities, Challenges, and Future Directions. *Curr. For. Rep.* **2019**, *5*, 55–75. [CrossRef]

29. Iglhaut, J.; Cabo, C.; Puliti, S.; Piermattei, L.; O'Connor, J.; Rosette, J. Structure from Motion Photogrammetry in Forestry: A Review. *Curr. For. Rep.* **2019**, 1–14. [CrossRef]

30. White, J.C.; Stepper, C.; Tompalski, P.; Coops, N.C.; Wulder, M.A. Comparing ALS and Image-Based Point Cloud Metrics and Modelled Forest Inventory Attributes in a Complex Coastal Forest Environment. *Forests* **2015**, *6*, 3704–3732. [CrossRef]

31. Baltsavias, E.; Gruen, A.; Eisenbeiss, H.; Zhang, L.; Waser, L.T. High-quality Image Matching and Automated Generation of 3D Tree Models. *Int. J. Remote Sens.* **2008**, *29*, 1243–1259. [CrossRef]

32. Véga, C.; St-Onge, B. Height Growth Reconstruction of a Boreal Forest Canopy over a Period of 58 Years Using a Combination of Photogrammetric and Lidar Models. *Remote Sens. Environ.* **2008**, *112*, 1784–1794. [CrossRef]

33. Waser, L.T.; Baltsavias, E.; Ecker, K.; Eisenbeiss, H.; Feldmeyer-Christe, E.; Ginzler, C.; Küchler, M.; Zhang, L. Assessing Changes of Forest Area and Shrub Encroachment in a Mire Ecosystem Using Digital Surface Models and CIR Aerial Images. *Remote Sens. Environ.* **2008**, *112*, 1956–1968. [CrossRef]

34. Vastaranta, M.; Wulder, M.A.; White, J.C.; Pekkarinen, A.; Tuominen, S.; Ginzler, C.; Kankare, V.; Holopainen, M.; Hyyppä, J.; Hyyppä, H. Airborne Laser Scanning and Digital Stereo Imagery Measures of Forest Structure: Comparative Results and Implications to Forest Mapping and Inventory Update. *Can. J. Remote Sens.* **2013**, *39*, 382–395. [CrossRef]

35. Pitt, D.G.; Woods, M.; Penner, M. A Comparison of Point Clouds Derived from Stereo Imagery and Airborne Laser Scanning for the Area-Based Estimation of Forest Inventory Attributes in Boreal Ontario. *Can. J. Remote Sens.* **2014**, *40*, 214–232. [CrossRef]

36. Rahlf, J.; Breidenbach, J.; Solberg, S.; Næsset, E.; Astrup, R. Comparison of Four Types of 3D Data for Timber Volume Estimation. *Remote Sens. Environ.* **2014**, *155*, 325–333. [CrossRef]

37. Ota, T.; Ogawa, M.; Shimizu, K.; Kajisa, T.; Mizoue, N.; Yoshida, S.; Takao, G.; Hirata, Y.; Furuya, N.; Sano, T. Aboveground Biomass Estimation Using Structure from Motion Approach with Aerial Photographs in a Seasonal Tropical Forest. *Forests* **2015**, *6*, 3882–3898. [CrossRef]

38. Holopainen, M.; Vastaranta, M.; Karjalainen, M.; Karila, K.; Kaasalainen, S.; Honkavaara, E.; Hyyppä, J. Forest Inventory Attribute Estimation Using Airborne Laser Scanning, Aerial Stereo Imagery, Radargrammetry and Interferometry-Finnish Experiences of the 3D Techniques. *ISPRS Ann. Photogramm. Remote Sens. Spat. Inf. Sci.* **2015**, *2*, 63. [CrossRef]

39. Tanhuanpää, T.; Saarinen, N.; Kankare, V.; Nurminen, K.; Vastaranta, M.; Honkavaara, E.; Karjalainen, M.; Yu, X.; Holopainen, M.; Hyyppä, J. Evaluating the Performance of High-Altitude Aerial Image-Based Digital Surface Models in Detecting Individual Tree Crowns in Mature Boreal Forests. *Forests* **2016**, *7*, 143. [CrossRef]

40. Wallace, L.; Lucieer, A.; Watson, C.; Turner, C. Assessing the Feasibility of UAV-Based LiDAR for High Resolution Forest Change Detection. *Proc. ISPRS—Int. Arch. Photogramm. Remote Sens. Spat. Inf. Sci.* **2012**, *39*, B7. [CrossRef]

41. Lisein, J.; Pierrot-Deseilligny, M.; Bonnet, S.; Lejeune, P. A Photogrammetric Workflow for the Creation of a Forest Canopy Height Model from Small Unmanned Aerial System Imagery. *Forests* **2013**, *4*, 922–944. [CrossRef]

42. Wallace, L.; Lucieer, A.; Malenovský, Z.; Turner, D.; Vopěnka, P. Assessment of Forest Structure Using Two UAV Techniques: A Comparison of Airborne Laser Scanning and Structure from Motion (SfM) Point Clouds. *Forests* **2016**, *7*, 62. [CrossRef]

43. Jaakkola, A.; Hyyppä, J.; Yu, X.; Kukko, A.; Kaartinen, H.; Liang, X.; Hyyppä, H.; Wang, Y. Autonomous Collection of Forest Field Reference—The Outlook and a First Step with UAV Laser Scanning. *Remote Sens.* **2017**, *9*, 785. [CrossRef]

44. Dandois, J.P.; Ellis, E.C. Remote Sensing of Vegetation Structure Using Computer Vision. *Remote Sens.* **2010**, *2*, 1157–1176. [CrossRef]

45. Dandois, J.P.; Olano, M.; Ellis, E.C. Optimal Altitude, Overlap, and Weather Conditions for Computer Vision UAV Estimates of Forest Structure. *Remote Sens.* **2015**, *7*, 13895–13920. [CrossRef]

46. Dandois, J.P.; Ellis, E.C. High Spatial Resolution Three-Dimensional Mapping of Vegetation Spectral Dynamics Using Computer Vision. *Remote Sens. Environ.* **2013**, *136*, 259–276. [CrossRef]

47. Zahawi, R.A.; Dandois, J.P.; Holl, K.D.; Nadwodny, D.; Reid, J.L.; Ellis, E.C. Using Lightweight Unmanned Aerial Vehicles to Monitor Tropical Forest Recovery. *Biol. Conserv.* **2015**, *186*, 287–295. [CrossRef]

48. Guerra-Hérnandez, J.; González-Ferreiro, E.; Sarmento, A.; Silva, J.; Nunes, A.; Correia, A.C.; Fontes, L.; Tomé, M.; Díaz-Varela, R. Short Communication. Using High Resolution UAV Imagery to Estimate Tree Variables in Pinus Pinea Plantation in Portugal. *For. Syst.* **2016**, *25*, 9. [CrossRef]

49. Mohan, M.; Silva, C.A.; Klauberg, C.; Jat, P.; Catts, G.; Cardil, A.; Hudak, A.T.; Dia, M. Individual Tree Detection from Unmanned Aerial Vehicle (UAV) Derived Canopy Height Model in an Open Canopy Mixed Conifer Forest. *Forests* **2017**, *8*, 340. [CrossRef]

50. Thiel, C.; Schmullius, C. Comparison of UAV Photograph-Based and Airborne Lidar-Based Point Clouds over Forest from a Forestry Application Perspective. *Int. J. Remote Sens.* **2017**, *38*, 2411–2426. [CrossRef]

51. Cardil, A.; Vepakomma, U.; Brotons, L. Assessing Pine Processionary Moth Defoliation Using Unmanned Aerial Systems. *Forests* **2017**, *8*, 402. [CrossRef]

52. Navarro, J.; Algeet, N.; Fernández-Landa, A.; Esteban, J.; Rodríguez-Noriega, P.; Guillén-Climent, M. Integration of UAV, Sentinel-1, and Sentinel-2 Data for Mangrove Plantation Aboveground Biomass Monitoring in Senegal. *Remote Sens.* **2019**, *11*, 77. [CrossRef]

53. Puliti, S.; Ørka, H.O.; Gobakken, T.; Næsset, E. Inventory of Small Forest Areas Using an Unmanned Aerial System. *Remote Sens.* **2015**, *7*, 9632–9654. [CrossRef]

54. Torresan, C.; Berton, A.; Carotenuto, F.; Di Gennaro, S.F.; Gioli, B.; Matese, A.; Miglietta, F.; Vagnoli, C.; Zaldei, A.; Wallace, L. Forestry Applications of UAVs in Europe: A Review. *Int. J. Remote Sens.* **2017**, *38*, 2427–2447. [CrossRef]

55. Whitehead, K.; Hugenholtz, C.H. Remote Sensing of the Environment with Small Unmanned Aircraft Systems (UASs), Part 1: A Review of Progress and Challenges 1. *J. Unmanned Veh. Syst.* **2014**, *2*, 69–85. [CrossRef]

56. Tang, L.; Shao, G. Drone Remote Sensing for Forestry Research and Practices. *J. For. Res.* **2015**, 1–7. [CrossRef]

57. Guerra-Hernández, J.; González-Ferreiro, E.; Monleón, V.; Faias, S.; Tomé, M.; Díaz-Varela, R. Use of Multi-Temporal UAV-Derived Imagery for Estimating Individual Tree Growth in Pinus Pinea Stands. *Forests* **2017**, *8*, 300. [CrossRef]

58. Pádua, L.; Hruška, J.; Bessa, J.; Adão, T.; Martins, L.M.; Gonçalves, J.A.; Peres, E.; Sousa, A.M.; Castro, J.P.; Sousa, J.J. Multi-Temporal Analysis of Forestry and Coastal Environments Using UASs. *Remote Sens.* **2017**, *10*, 24. [CrossRef]

59. Hall, S.A.; Burke, I.C.; Box, D.O.; Kaufmann, M.R.; Stoker, J.M. Estimating Stand Structure Using Discrete-Return Lidar: An Example from Low Density, Fire Prone Ponderosa Pine Forests. *For. Ecol. Manag.* **2005**, *208*, 189–209. [CrossRef]

60. Järnstedt, J.; Pekkarinen, A.; Tuominen, S.; Ginzler, C.; Holopainen, M.; Viitala, R. Forest Variable Estimation Using a High-Resolution Digital Surface Model. *ISPRS J. Photogramm. Remote Sens.* **2012**, *74*, 78–84. [CrossRef]

61. González-Ferreiro, E.; Diéguez-Aranda, U.; Miranda, D. Estimation of Stand Variables in Pinus Radiata D. Don Plantations Using Different LiDAR Pulse Densities. *Forestry* **2012**, *85*, 281–292. [CrossRef]

62. González-Ferreiro, E.; Diéguez-Aranda, U.; Crecente-Campo, F.; Barreiro-Fernández, L.; Miranda, D.; Castedo-Dorado, F. Modelling Canopy Fuel Variables for Pinus Radiata D. Don in NW Spain with Low-Density LiDAR Data. *Int. J. Wildland Fire* **2014**, *23*, 350–362. [CrossRef]

63. Montaghi, A.; Corona, P.; Dalponte, M.; Gianelle, D.; Chirici, G.; Olsson, H. Airborne Laser Scanning of Forest Resources: An Overview of Research in Italy as a Commentary Case Study. *Int. J. Appl. Earth Obs. Geoinformation* **2013**, *23*, 288–300. [CrossRef]

64. Corona, P.; Cartisano, R.; Salvati, R.; Chirici, G.; Floris, A.; Di Martino, P.; Marchetti, M.; Scrinzi, G.; Clementel, F.; Torresan, C. Airborne Laser Scanning to Support Forest Resource Management under Alpine, Temperate and Mediterranean Environments in Italy. *Eur. J. Remote Sens.* **2012**, *45*, 27–37.

65. González-Olabarria, J.-R.; Rodríguez, F.; Fernández-Landa, A.; Mola-Yudego, B. Mapping Fire Risk in the Model Forest of Urbión (Spain) Based on Airborne LiDAR Measurements. *For. Ecol. Manag.* **2012**, *282*, 149–156. [CrossRef]

66. Guerra-Hernández, J.; Görgens, E.B.; García-Gutiérrez, J.; Rodriguez, L.C.E.; Tomé, M.; González-Ferreiro, E. Comparison of ALS Based Models for Estimating Aboveground Biomass in Three Types of Mediterranean Forest. *Eur. J. Remote Sens.* **2016**, *49*, 185–204. [CrossRef]

67. Montealegre, A.L.; Lamelas, M.T.; Tanase, M.A.; de la Riva, J. Estimación de La Severidad En Incendios Forestales a Partir de Datos LiDAR-PNOA y Valores de Composite Burn Index. *Rev. Teledetec.* **2017**, *49*, 1–16. [CrossRef]

68. Montealegre, A.L.; Lamelas, M.T.; de la Riva, J.; García-Martín, A.; Escribano, F. Use of Low Point Density ALS Data to Estimate Stand-Level Structural Variables in Mediterranean Aleppo Pine Forest. *For. Int. J. For. Res.* **2016**, *89*, 373–382. [CrossRef]

69. Domingo, D.; Alonso, R.; Lamelas, M.T.; Montealegre, A.L.; Rodríguez, F.; de la Riva, J. Temporal Transferability of Pine Forest Attributes Modeling Using Low-Density Airborne Laser Scanning Data. *Remote Sens.* **2019**, *11*, 261. [CrossRef]

70. Silva, C.A.; Klauberg, C.; Hudak, A.T.; Vierling, L.A.; Liesenberg, V.; Carvalho, S.P.E.; Rodriguez, L.C. A Principal Component Approach for Predicting the Stem Volume in Eucalyptus Plantations in Brazil Using Airborne LiDAR Data. *For. Int. J. For. Res.* **2016**, *89*, 422–433. [CrossRef]

71. Kachamba, D.J.; Ørka, H.O.; Gobakken, T.; Eid, T.; Mwase, W. Biomass Estimation Using 3D Data from Unmanned Aerial Vehicle Imagery in a Tropical Woodland. *Remote Sens.* **2016**, *8*, 968. [CrossRef]

72. St-Onge, B.; Audet, F.-A.; Bégin, J. Characterizing the Height Structure and Composition of a Boreal Forest Using an Individual Tree Crown Approach Applied to Photogrammetric Point Clouds. *Forests* **2015**, *6*, 3899–3922. [CrossRef]

73. Mielcarek, M.; Stereńczak, K.; Khosravipour, A. Testing and Evaluating Different LiDAR-Derived Canopy Height Model Generation Methods for Tree Height Estimation. *Int. J. Appl. Earth Obs. Geoinformation* **2018**, *71*, 132–143. [CrossRef]

74. Guerra-Hernández, J.; Cosenza, D.N.; Rodriguez, L.C.E.; Silva, M.; Tomé, M.; Díaz-Varela, R.A.; González-Ferreiro, E. Comparison of ALS-and UAV (SfM)-Derived High-Density Point Clouds for Individual Tree Detection in Eucalyptus Plantations. *Int. J. Remote Sens.* **2018**, *39*, 5211–5235.

75. Maltamo, M.; Eerikäinen, K.; Packalén, P.; Hyyppä, J. Estimation of Stem Volume Using Laser Scanning-Based Canopy Height Metrics. *Forestry* **2006**, *79*, 217–229. [CrossRef]

76. Hentz, Â.M.; Silva, C.A.; Dalla Corte, A.P.; Netto, S.P.; Strager, M.P.; Klauberg, C. Estimating Forest Uniformity in Eucalyptus Spp. and Pinus Taeda L. Stands Using Field Measurements and Structure from Motion Point Clouds Generated from Unmanned Aerial Vehicle (UAV) Data Collection. *For. Syst.* **2018**, *27*, 5. [CrossRef]

77. Roussel, J.-R.; Caspersen, J.; Béland, M.; Thomas, S.; Achim, A. Removing Bias from LiDAR-Based Estimates of Canopy Height: Accounting for the Effects of Pulse Density and Footprint Size. *Remote Sens. Environ.* **2017**, *198*, 1–16. [CrossRef]

78. Tomé, M.; Tomé, J.; Ribeiro, F.; Faias, S. Equações de Volume Total, Volume Percentual e de Perfil Do Tronco Para Eucalyptus Globulus Labill. Em Portugal. *Silva Lusit.* **2007**, *15*, 25–39.

79. McGaughey, R.J. *FUSION/LDV: Software for LIDAR Data Analysis and Visualization*; Version 3.60+; Pacific Northwest Research Station, United States Department of Agriculture Forest Service: Seattle, WA, USA, 2017.

80. Isenburg, M. *LAStools—Efficient Tools for LiDAR Processing*; Version 160921; Academic: Cambridge, MA, USA, 2016.

81. González-Ferreiro, E.; Diéguez-Aranda, U.; Barreiro-Fernández, L.; Buján, S.; Barbosa, M.; Suárez, J.C.; Bye, I.J.; Miranda, D. A Mixed Pixel-and Region-Based Approach for Using Airborne Laser Scanning Data for Individual Tree Crown Delineation in Pinus Radiata D. Don Plantations. *Int. J. Remote Sens.* **2013**, *34*, 7671–7690. [CrossRef]

82. Vanclay, J.K.; Skovsgaard, J.P. Evaluating Forest Growth Models. *Ecol. Model.* **1997**, *98*, 1–12. [CrossRef]

83. Shapiro, S.S.; Wilk, M.B.; Chen, H.J. A Comparative Study of Various Tests for Normality. *J. Am. Stat. Assoc.* **1968**, *63*, 1343–1372. [CrossRef]

84. Iizuka, K.; Yonehara, T.; Itoh, M.; Kosugi, Y. Estimating Tree Height and Diameter at Breast Height (DBH) from Digital Surface Models and Orthophotos Obtained with an Unmanned Aerial System for a Japanese Cypress (Chamaecyparis Obtusa) Forest. *Remote Sens.* **2017**, *10*, 13. [CrossRef]

85. Chisholm, R.A.; Cui, J.; Lum, S.K.; Chen, B.M. UAV LiDAR for Below-Canopy Forest Surveys. *J. Unmanned Veh. Syst.* **2013**, *1*, 61–68. [CrossRef]

86. Cosenza, D.N.; Soares, V.P.; Leite, H.G.; Gleriani, J.M.; do Amaral, C.H.; Gripp Júnior, J.; da Silva, A.A.L.; Soares, P.; Tomé, M. Airborne Laser Scanning Applied to Eucalyptus Stand Inventory at Individual Tree Level. *Pesqui. Agropecuária Bras.* **2018**, *53*, 1373–1382. [CrossRef]

87. Persson, A.; Holmgren, J.; Söderman, U. Detecting and Measuring Individual Trees Using an Airborne Laser Scanner. *Photogramm. Eng. Remote Sens.* **2002**, *68*, 925–932.

88. Popescu, S.C. Estimating Biomass of Individual Pine Trees Using Airborne Lidar. *Biomass Bioenergy* **2007**, *31*, 646–655. [CrossRef]

89. Zhao, K.; Popescu, S.; Nelson, R. Lidar Remote Sensing of Forest Biomass: A Scale-Invariant Estimation Approach Using Airborne Lasers. *Remote Sens. Environ.* **2009**, *113*, 182–196. [CrossRef]

90. Korpela, I. *Individual Tree Measurements by Means of Digital Aerial Photogrammetry*; Finnish Society of Forest Science: Helsinki, Finland, 2004; Volume 3.

91. St-Onge, B.; Jumelet, J.; Cobello, M.; Véga, C. Measuring Individual Tree Height Using a Combination of Stereophotogrammetry and Lidar. *Can. J. For. Res.* **2004**, *34*, 2122–2130. [CrossRef]

92. Jensen, J.L.; Mathews, A.J. Assessment of Image-Based Point Cloud Products to Generate a Bare Earth Surface and Estimate Canopy Heights in a Woodland Ecosystem. *Remote Sens.* **2016**, *8*, 50. [CrossRef]

93. Hopkinson, C.; Chasmer, L.; Hall, R.J. The Uncertainty in Conifer Plantation Growth Prediction from Multi-Temporal Lidar Datasets. *Remote Sens. Environ.* **2008**, *112*, 1168–1180. [CrossRef]

94. Yu, X.; Hyyppä, J.; Kukko, A.; Maltamo, M.; Kaartinen, H. Change Detection Techniques for Canopy Height Growth Measurements Using Airborne Laser Scanner Data. *Photogramm. Eng. Remote Sens.* **2006**, *72*, 1339–1348. [CrossRef]

95. Gatziolis, D.; Fried, J.S.; Monleon, V.S. Challenges to Estimating Tree Height via LiDAR in Closed-Canopy Forests: A Parable from Western Oregon. *For. Sci.* **2010**, *56*, 139–155.

96. Milas, A.S.; Arend, K.; Mayer, C.; Simonson, M.A.; Mackey, S. Different Colours of Shadows: Classification of UAV Images. *Int. J. Remote Sens.* **2017**, *38*, 3084–3100. [CrossRef]

97. Laliberte, A.S.; Herrick, J.E.; Rango, A.; Winters, C. Acquisition, Orthorectification, and Object-Based Classification of Unmanned Aerial Vehicle (UAV) Imagery for Rangeland Monitoring. *Photogramm. Eng. Remote Sens.* **2010**, *76*, 661–672. [CrossRef]

98. Ke, Y.; Quackenbush, L.J. A Review of Methods for Automatic Individual Tree-Crown Detection and Delineation from Passive Remote Sensing. *Int. J. Remote Sens.* **2011**, *32*, 4725–4747. [CrossRef]

99. Nuijten, R.J.; Coops, N.C.; Goodbody, T.R.; Pelletier, G. Examining the Multi-Seasonal Consistency of Individual Tree Segmentation on Deciduous Stands Using Digital Aerial Photogrammetry (DAP) and Unmanned Aerial Systems (UAS). *Remote Sens.* **2019**, *11*, 739. [CrossRef]

100. Frey, J.; Kovach, K.; Stemmler, S.; Koch, B. UAV Photogrammetry of Forests as a Vulnerable Process. A Sensitivity Analysis for a Structure from Motion RGB-Image Pipeline. *Remote Sens.* **2018**, *10*, 912. [CrossRef]

101. Fraser, B.; Congalton, R. Issues in Unmanned Aerial Systems (UAS) Data Collection of Complex Forest Environments. *Remote Sens.* **2018**, *10*, 908. [CrossRef]

102. Ni, W.; Sun, G.; Pang, Y.; Zhang, Z.; Liu, J.; Yang, A.; Wang, Y.; Zhang, D. Mapping Three-Dimensional Structures of Forest Canopy Using UAV Stereo Imagery: Evaluating Impacts of Forward Overlaps and Image Resolutions With LiDAR Data as Reference. *IEEE J. Sel. Top. Appl. Earth Obs. Remote Sens.* **2018**, *11*, 3578–3589. [CrossRef]

6   General conclusions

The general objective of this thesis was to advance knowledge in the application of aerial 3D-data in the forest characterization context. To meet this goal, it focused four cutting-edge research topics related to the forestry applications of 3D data collected by aerial platforms, namely, airborne laser scanning (ALS) and digital aerial photogrammetry (DAP). Each work approached different aspects of the 3D data workflow and expanded the understanding of its application.

Four common algorithms were deeply investigated for filtering ALS ground points and had their parameters calibrated for irregular terrain. The results showed that performing an exhaustive filter calibration is not a mandatory process to derive accurate digital terrain models (DTM), whereas applications of algorithms default allowed deriving DTM with comparable quality. Likewise, the DTM derived through calibrated filters has a significant but low improvement on the forest application when compared to the DTM derived by default parameters.

The application of the high-flexible Johnson's S_B probability density function (PDF) was adapted to the ALS data to estimate diameter distributions in two species, eucalyptus and pine. Fitting this PDF was demonstrated to be not straightforward and required many equations to predict the PDF inputs. Johnson's S_B distribution was therefore overly sensitive to errors of the predicted inputs, reasons why this function was just slightly better than Weibull distribution to estimate diameter distributions.

The ALS data from five different forest sites worldwide were used to compare three common modeling approaches used to estimate growing stock volume, ordinary least squares (OLS), random forest (RF), and k-nearest neighbor (kNN). The predictions was more accurate using OLS and RF. kNN-based models had the lest accurate prediction and may result in overfitting. Contrary to the other approaches, RF models had the advantage of performing well when trained with all available predictors so the training does not need to be associated with prior variable selection.

The point clouds derived from ALS and DAP presented comparable results when it comes to detect and estimate individual tree volumes in eucalyptus plantations, suggesting that both technologies can provide comparable results for growing stock estimation. This result benefits the DAP since it is an inexpensive approach to collect 3D forest data, especially when associated with unmanned aerial vehicles.

6.1 Final considerations

After fifteen years of studies, airborne laser scanning (ALS) is a mature technology for which there is comprehensive literature to support practitioners worldwide. Despite being younger, the digital aerial photogrammetry (DAP) can take advantage of the ALS approaches since they share similarities in the point cloud processing workflow. However, there are still factors limiting the implementation of these technologies by public and private organizations, which are associated with costs of the surveys (especially for the ALS) and, most importantly, the lack of practitioners trained to deal with this data. In this case, even with an increasing number of adepts, there are still great opportunities to develop more user-friendly devices and software to call attention of beginner forest

practitioners. Moreover, many doubts regarding the application of ALS and DAP wait to be answered, especially the ones regarding the cost of the inventories

This thesis focused on the aerial surveyed 3D data, especially with ALS, given its relevance in the forestry scenario. However, it is important to highlight that terrestrial scanning is also an alternative approach to collect 3D forest data from below canopies (see Liang et al. 2016, 2018), but its application is less common so far. However, there have been evolutions in the ALS approaches with multispectral LiDAR devices (e.g., Kukkonen et al., 2019) and spaceborne laser scanning (e.g., Margolis et al., 2015). Despite these techniques are still incipient, they can put the LiDAR-based inventories in a new level of sophistication in the future.

Finally, improving forest measurement technologies is imperative since it is crucial to diagnose forest stands and to make well-based decisions. Far from being an end-in-itself, the forest inventory has the main goal to provide quality information for forest management and planning, so each scientific contribution in this matter is a step toward forest sustainability.

6.2   References

Kukkonen, M., Maltamo, M., Korhonen, L., Packalen, P., 2019. Comparison of multispectral airborne laser scanning and stereo matching of aerial images as a single sensor solution to forest inventories by tree species. Remote Sens. Environ. 231, 111208. https://doi.org/10.1016/j.rse.2019.05.027

Liang, X., Hyyppä, J., Kaartinen, H., Lehtomäki, M., Pyörälä, J., Pfeifer, N., Holopainen, M., Brolly, G., Francesco, P., Hackenberg, J., Huang, H., Jo, H.W., Katoh, M., Liu, L., Mokroš, M., Morel, J., Olofsson, K., Poveda-Lopez, J., Trochta, J., Wang, D., Wang, J., Xi, Z., Yang, B., Zheng, G., Kankare, V., Luoma, V., Yu, X., Chen, L., Vastaranta, M., Saarinen, N., Wang, Y., 2018. International benchmarking of terrestrial laser scanning approaches for forest inventories. ISPRS J. Photogramm. Remote Sens. 144, 137–179. https://doi.org/10.1016/j.isprsjprs.2018.06.021

Liang, X., Kankare, V., Hyyppä, J., Wang, Y., Kukko, A., Haggrén, H., Yu, X., Kaartinen, H., Jaakkola, A., Guan, F., Holopainen, M., Vastaranta, M., 2016. Terrestrial laser scanning in forest inventories. ISPRS J. Photogramm. Remote Sens. 115, 63–77. https://doi.org/10.1016/j.isprsjprs.2016.01.006

Margolis, H.A., Nelson, R.F., Montesano, P.M., Beaudoin, A., Sun, G., Andersen, H.E., Wulder, M.A., 2015. Combining satellite lidar, airborne lidar, and ground plots to estimate the amount and distribution of aboveground biomass in the boreal forest of North America. Can. J. For. Res. 45, 838–855. https://doi.org/10.1139/cjfr-2015-0006